J. Micropalaeontology, 43, 383–421, 2024
https://doi.org/10.5194/jm-43-383-2024

Journal of Micropalaeontology
Open Access

Miocene Climatic Optimum and Middle Miocene Climate Transition: a foraminiferal record from the central Ross Sea, Antarctica

Samantha E. Bombard[1], R. Mark Leckie[1], Imogen M. Browne[2], Amelia E. Shevenell[2], Robert M. McKay[3], David M. Harwood[4], and the IODP Expedition 374 Scientists✚

[1]Department of Earth, Geographic, and Climate Sciences, University of Massachusetts Amherst, Amherst, MA 01003, USA
[2]College of Marine Science, University of South Florida, St. Petersburg, FL, USA
[3]Antarctic Research Centre, Victoria University of Wellington, Wellington, Aotearoa / New Zealand
[4]Department of Earth and Atmospheric Sciences, University of Nebraska-Lincoln, Lincoln, NE 68588, USA
✚A full list of authors appears at the end of the paper.

Correspondence: Samantha E. Bombard (sambombard@umass.edu)

Received: 15 January 2024 – Revised: 25 July 2024 – Accepted: 1 August 2024 – Published: 19 September 2024

Abstract. The Ross Sea record of the Miocene Climatic Optimum (MCO; ∼16.9–14.7 Ma) and the Middle Miocene Climate Transition (MMCT; ∼14.7–13.8 Ma) provides critical insights into Antarctic ocean–cryosphere interactions during a time of extreme warmth and subsequent cooling. Here we report on Lower to Middle Miocene foraminiferal assemblages from the International Ocean Discovery Program (IODP) Site U1521 on the outer shelf of the central Ross Sea to identify regional shifts in environmental and water mass conditions and trace continental shelf evolution. We identified seven benthic biofacies clusters, dominated by abundant *Globocassidulina subglobosa* (a proposed indicator of proto-Circumpolar Deep Water, pCDW), *Uvigerina* cf. *U. fueguina* (high productivity and enhanced bottom-water currents), *Nonionella* spp. (high productivity), or *Melonis* spp. (high productivity) using a Q-mode cluster analysis to develop preliminary regional paleoenvironmental interpretations. Four unique assemblages, including *Globobulimina* cf. *G. auriculata* (high productivity and low oxygen), are also identified.

Unit IV (representing the early MCO event) is a short-lived (∼80 ka), progradational, clast-poor sandy diamictite, likely deposited during deglaciation; the upper part of Unit IV is transitional with overlying Unit III. Unit IV sediments contain the most persistently abundant and diverse foraminiferal assemblages recovered at U1521 because they are mud-rich and diatom-poor, despite very high sedimentation rates. The benthic assemblages shift between *Globocassidulina* and *Uvigerina* dominance, suggesting changes in the pCDW influence relative to productivity and/or current activity. We suggest the abundance of *Uvigerina* (a shelf-edge proxy) in Unit IV records the northward progradation of the Ross continental shelf at this location during the late Early to Middle Miocene.

Unit III (MCO) was deposited in an open-marine setting, evident by the ice-rafted detritus or debris (IRD) clast-free, diatom-rich/diatom-bearing muds. The sporadic nature of foraminiferal abundances in Unit III is likely due to intervals of terrigenous mud alternating with more diatom-rich/diatom-bearing muds. As in Unit IV, the muddier lithologies (higher natural gamma ray (NGR) values) are more likely to preserve calcareous foraminifera, whereas the most diatom-rich sediments (lower NGR values) are more corrosive to carbonate. We interpret the muddier intervals as interglacials with incursions of pCDW, as indicated by increased *Globocassidulina subglobosa*, and sporadic occurrences of rare warmer-water planktic foraminifera. Collectively, these multiple incursions of warmer-water planktic foraminifera provide evidence for polar amplification in the Ross Sea during the MCO and MMCT. The diatom-rich muds are interpreted as glacials during the MCO with open-marine conditions and higher productivity. The dominance of *Globobulimina* in the upper part of Unit III corresponds with the carbon maximum of Carbon Maxima 2 (CM2) and low-oxygen conditions in the sediments at

~ 16.1 Ma. Subsequent glaciation (including Mi2, Miocene Isotope event 2), marine-based ice sheet grounding, and erosion on the shallow shelf are recorded by the widespread Ross Sea Unconformity 4 (RSU4; ~ 15.95–14.2 Ma) at Site U1521. Unit II (MMCT) likely represents sedimentation in the interval between the RSU4 and the Mi3 (Miocene Isotope event 3) glaciation at ~ 13.9–13.8 Ma. The benthic biofacies composition of Unit II shows a further increase in neritic taxa, including *Elphidium magellanicum* and *Epistominella vitrea*, suggesting continued shoaling of the continental shelf, which facilitated the growth of marine-based ice sheets during the Middle Miocene.

Our initial correlation between Site U1521 and the ANtarctic geological DRILLing Project (ANDRILL) site, AND-2A, yields similar environmental interpretations, including peak warm events 3 and 4 during the MCO, supported by the foraminifera and unit lithologies. Suspected glacial intervals during the MCO, including Mi2 at the top of Unit III, correlate well with the reconstructed deep-sea estimates of ice volume changes (seawater $\delta^{18}O_{sw}$ record) from the Ocean Drilling Program (ODP) Site 1171 on the South Tasman Rise.

1 Introduction

1.1 Why the Middle Miocene?

The Early to Middle Miocene serves as an analogue for our future climate (e.g., Shackleton and Kennett, 1975; Miller et al., 1987; Zachos et al., 2001; Shevenell and Kennett, 2004; Steinthorsdottir et al., 2021). The Miocene Climatic Optimum (MCO) was a greenhouse interval from ~ 16.9–14.7 Ma, with average global temperatures ~ 3–4 °C warmer than today and peak MCO warming of ~ 7–8 °C, leading to major changes in the global carbon cycle (Vincent and Berger, 1985; Flower and Kennett, 1993; Holbourn et al., 2015, 2022) and atmospheric CO_2 concentrations near or moderately higher than today (Steinthorsdottir et al., 2021; Hönisch et al., 2023). The MCO was followed by the Middle Miocene Climate Transition (MMCT) from ~ 14.7–13.8 Ma (Steinthorsdottir et al., 2021), defined by cooler conditions in advance of a ~ 1 ‰ increase in deep-sea benthic $\delta^{18}O_{bf}$ values that define the major Mi3 (Miocene Isotope event 3) glaciation at ~ 13.9 Ma (Kennett, 1977; Wright et al., 1991; Flower and Kennett, 1994; Shevenell et al., 2004, 2008; Holbourn et al., 2014, 2022), and related to ice sheet expansion in Antarctica (Wright et al., 1991; John et al., 2004, 2011; Shevenell et al., 2008; McKay et al., 2022). Investigations of the Ross Sea paleoenvironmental evolution (e.g., ice extent, water mass behavior, productivity, relative sea level, and paleobathymetry) during the MCO and MMCT provide invaluable insight into how Antarctica may respond to our current warming climate, including possible incursions of a precursor to Circumpolar Deep Water (CDW).

1.2 Ross Sea oceanography

The Ross Sea has a dynamic oceanography and is home to the world's largest ice shelf (Fig. 1). The Ross Ice Shelf serves as the buttress for the Antarctic Ice Sheet (AIS) and is sensitive to warming (e.g., basal melt and mass loss) (Pritchard et al., 2012; DeConto and Pollard, 2016; Shepherd et al., 2018; Smith et al., 2019). One environmental factor that plays a major role in the sensitivity of the AIS is ocean forcing. Today, there are a variety of water masses created, mixed, imported, and exported from the Ross Sea (e.g., Budillon et al., 2003; Orsi and Wiederwohl, 2009; Smith et al., 2012). For this study, we are particularly interested in a precursor to Circumpolar Deep Water (CDW or proto-CDW) and its incursions into the Ross Sea and possible role during the MCO and MMCT.

Today, CDW is a relatively warm nutrient-rich water mass that intrudes onto the Ross Sea continental shelf as modified Circumpolar Deep Water (mCDW), melting the Ross Ice Shelf at the grounding line (Jacobs et al., 1979; Ainley and Jacobs, 1981; Whitworth, 1998; Orsi and Wiederwohl, 2009; Dinniman et al., 2011; Pritchard et al., 2012; Castagno et al., 2017; Colleoni et al., 2018; Prothro et al., 2018; Majewski et al., 2018, 2020; Wang et al., 2023). There are a number of oceanographic controls that either enhance or diminish the ability of CDW to encroach onto the continental shelf. The Antarctic Circumpolar Current (ACC), Southern Ocean frontal system, and Antarctic Slope Current (ASC) can all act as barriers to CDW into the Ross Sea. Previous Miocene studies have shown that the Southern Ocean frontal system was weaker (Shevenell et al., 2004; Herold et al., 2012; Sangiorgi et al., 2018; Evangelinos et al., 2020), and the ACC was weaker during the Early and Middle Miocene (Herold et al., 2012; Hill et al., 2013; Evangelinos et al., 2020). A weaker frontal system and weaker ACC allowed low-latitude warm-surface waters and proto-CDW to be present near the Antarctic margin. In contrast to proto-CDW, High-Salinity Shelf Water (HSSW) is a dense, salty, and corrosive water mass formed from brine rejection associated with sea ice formation in the Ross Sea polynya today (Osterman and Kellogg, 1979; Melis and Salvi, 2009; Majewski et al., 2016, 2018, 2020; Prothro et al., 2018; Capotondi et al., 2018; Kim et al., 2020). Previous foraminiferal studies on the Ross continental shelf have alluded to the relationship between foraminifera and specific water masses (Kennett, 1966; Osterman and Kellogg, 1979; Majewski et al., 2018, 2020). Here we investigate Miocene foraminiferal biofacies to learn

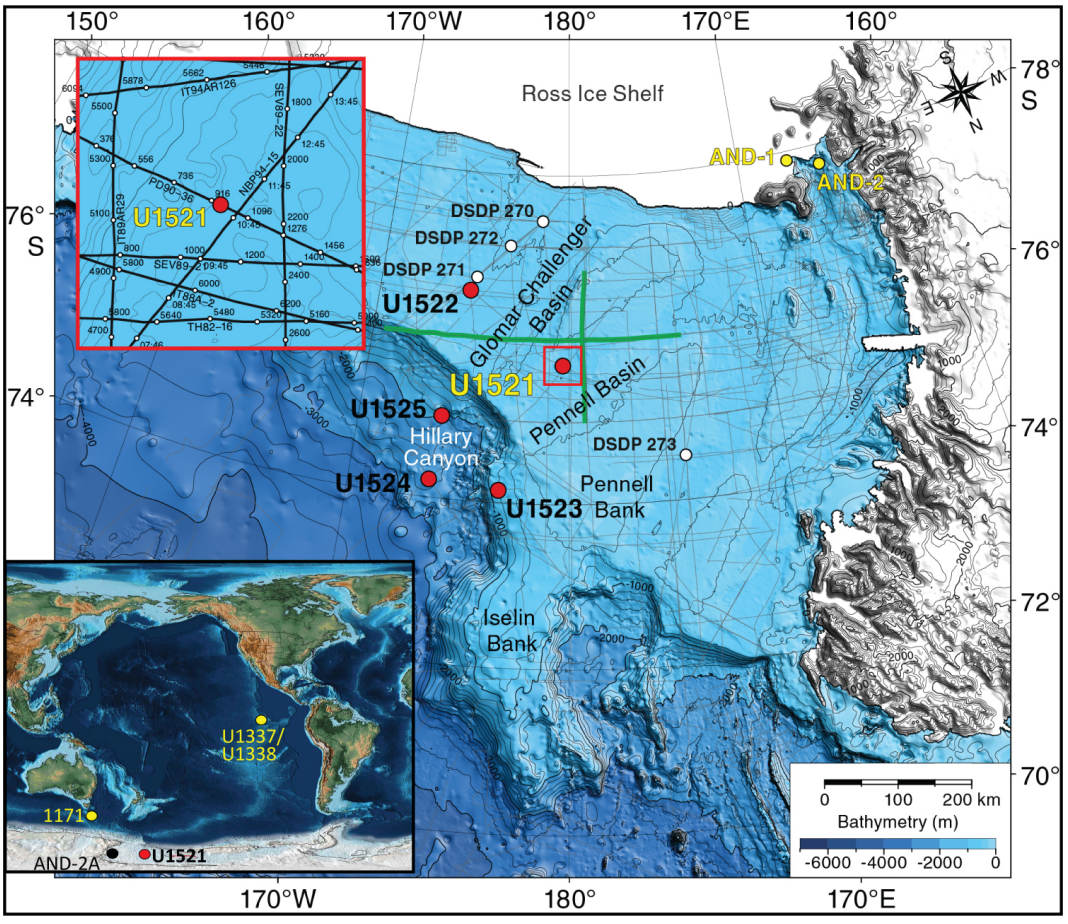

Figure 1. Map of IODP Expedition 374 drill sites (McKay et al., 2019) with an inset map modified from Scotese (2021) to show the locations of Site U1521 (this study), AND-2A (Patterson and Ishman, 2012), ODP Site 1171 (Shevenell et al., 2008), and IODP Sites U1337/U1338 (Holbourn et al., 2014, 2015).

about the water masses and other environmental characteristics during the time of the MCO and MMCT in the Ross Sea. Foraminifera had a front-row seat to the oceanographic and paleoclimatic events associated with dynamic changes in the size and extent of the Antarctic Ice Sheet during the MCO and MMCT. To date, there are no published foraminiferal studies of the MCO and MMCT interval from the Antarctic continental shelf.

1.3 Ross Sea Neogene studies: past to present

Many drilling projects have investigated Early to Middle Miocene foraminifera from the Ross Sea. Deep Sea Drilling Project (DSDP) Leg 28 (1972–1973; Hayes et al., 1975) collected sediment cores from DSDP Sites 270–273 on the continental shelf and Site 274 on the continental rise in the Ross Sea, ranging in age from the late Oligocene to the present. Upper Oligocene–Lower Miocene foraminifera from Site 270 have been documented by Leckie and Webb (1980, 1983, 1985, 1986) and Kulhanek et al. (2019), and Middle Miocene foraminifera have been reported from Site 273 (D'Agostino and Webb, 1980) and Site 272 (Steinhauff and Webb, 1987). The variable recovery of Neogene sediments has limited the ability for scientists to study the Miocene Antarctic shelf foraminiferal record until recently with International Ocean Discovery Program (IODP) Expedition 374 (McKay et al., 2019). Other more proximal Oligocene–Middle Miocene foraminiferal records were recovered on the inner shelf adjacent to the Transantarctic Mountains, including McMurdo Sound Sediment and Tectonic Studies (MSSTS) (Barrett, 1986; Webb et al., 1986) and Cenozoic Investigations in the western ROss Sea hole 1 (CIROS-1) (Barrett et al., 1991; Roberts et al., 2003; Coccioni and Galeotti, 1997; Webb, 1989). The Cape Roberts Project (CRP; 1997–1999) recovered Eocene to Miocene foraminifera (Strong and Webb, 2000, 2001; Webb and Strong, 2000, 2006). These records have revealed the dynamic nature of glacial processes on the continental shelf and adjacent to the Transantarctic Mountains since the Oligocene, but the larger perspective of AIS history has remained elusive.

The ANtarctic geological DRILLing Project, ANDRILL (2006–2007), collected Lower Miocene to recent foraminiferal bearing sediments (Patterson and Ishman, 2012). The Early to Middle Miocene record from ANDRILL core 2A (AND-2A) has been extensively examined to investigate how glacial and interglacial periods impacted the Antarctic region (McKay et al., 2022). Levy et al. (2016) interpret dynamic ice sheet behavior at AND-2A during the Early to Middle Miocene, noting the variation in environmental conditions during peak warmth events. The only published foraminiferal records of the MCO and MMCT in the Ross Sea come from ice-proximal AND-2A record (Patterson and Ishman, 2012); the glacial and oceanographic record of these climate events on the continental shelf remains unresolved.

International Ocean Discovery Program (IODP) Expedition 374 drilled five sites on the Ross Sea continental shelf, slope, and rise to understand the history of the West Antarctic Ice Sheet (McKay et al., 2019). Site U1521 (75°41.0351′ S, 179°40.3108′ W) is located within the Pennell Basin at a water depth of 562 m. The Lower to Middle Miocene interval at Site U1521 is captured from Lithologic Unit IV through the lower part of Unit II (∼ 280–65 m; CSF-A, Core Depth below Sea Floor-A). Lithologic Units IV, III, and II record three distinct lithologies. Unit IV is a diatom-bearing clast-poor sandy diamictite (sequence 4A in Marschalek et al., 2021). Unit III is a moderately to highly bioturbated olive-gray to greenish-gray diatom-bearing/diatom-rich mudstone (sequence 4B in Marschalek et al., 2021), and the lower ∼ 20 m of Unit II is comprised of a muddy diamictite, where the base is intermixed with the underlying diatomite of Unit III (McKay et al., 2019). These three lithologic units suggest that Ross Sea environmental conditions changed throughout the late Early to early Middle Miocene.

One way to investigate the Ross Sea record of the Early and Middle Miocene is by examining the benthic and planktic foraminiferal assemblages in the context of the sedimentary facies and physical properties. Since foraminifera are sensitive to changes in the environment, the foraminiferal record from Site U1521 should capture aspects of the environmental changes associated with the MCO and MMCT (e.g., water mass behavior, current activity, productivity, and paleobathymetry). Here we focused on four questions that reflect high-priority objectives of IODP Expedition 374 (McKay et al., 2019): (1) do benthic foraminiferal biofacies capture water mass and other environmental changes during the MCO and MMCT? (2) Can benthic foraminiferal biofacies inform us about the progradational and aggradational history of the Ross Sea continental shelf during the Early and Middle Miocene? (3) What might planktic foraminiferal occurrences tell us about surface-ocean circulation, relative sea surface temperatures, or polar amplification in the Ross Sea? (4) How do environmental changes at Site U1521 on the central outer shelf compare with the AND-2A record adjacent to the Transantarctic Mountains and with a deep-sea record from the Southern Ocean (ODP Site 1171)?

To investigate these questions, we examined the Early to Middle Miocene foraminiferal assemblages and used a Q-mode cluster analysis to identify benthic biofacies as proxies for changing environmental conditions. We hypothesize that *Globocassidulina subglobosa* is a proxy for the incursion of a Southern Ocean water mass, here referred to as proto-CDW (pCDW) into the Ross Sea since the late Oligocene. Planktic foraminifera are very rare in the Early to Middle Miocene of the Ross Sea, but we have identified sporadic occurrences of warmer-water planktic species, which provide clues about sea surface temperatures and perhaps the shifting position and strength of the Polar Front and/or Antarctic Circumpolar Current during the MCO and MMCT. In addition to considering our data in terms of changing water masses, circulation at the seafloor, productivity, and paleobathymetry, we use physical properties and seismic data to understand the depositional history and progradation of the continental shelf. We compare our findings with the orbitally tuned benthic foraminiferal isotopic record from Pacific IODP Sites U1337 and U1338 (Holbourn et al., 2014, 2015), with paleoenvironmental interpretations from AND-2A (Levy et al., 2016) and a seawater $\delta^{18}O_{sw}$ record, a proxy for ice volume, from the Ocean Drilling Program (ODP) Site 1171 on the South Tasman Rise (Shevenell et al., 2008).

2 Methods

2.1 Sample processing and analysis

Within the interval of interest (65.0–280.72 m; CSF-A) 135 samples of 20 cm^3 volume (including 19 larger-volume shipboard core-catcher samples) were collected. Before processing, all samples, with the exception of shipboard core-catcher samples, were weighed to obtain a bulk mass then placed in a freeze-dryer. After the freeze-dryer, each sample was soaked in a borax solution with a pH of ∼ 10, with the pH monitored closely. The nature of the sediments often required additional processing due to compaction. When samples did not break down, we tried freezing–thawing in sodium sulfate (samples from Unit III) or boiling in a weak hydrogen peroxide and borax solution for 30 min to 1 h (samples from Unit IV). Even though both methods yielded samples with foraminifera that were well preserved and not broken, boiling in hydrogen peroxide did a better job of breaking down the consolidated sediment than freezing–thawing. Each sample was washed over a > 63 µm sieve that was dipped in a methylene blue stain between samples to monitor for lab contamination. Samples were placed in a 55 °C oven to dry for 24 h before a final round of weighing. Samples examined in this study were not floated using a heavy liquid such as sodium polytungstate.

Picking methods evolved as we learned more about the nature of the lithologic units and their foraminiferal abun-

dances. Initially, 52 samples from all three units were dry-split to half, quarter, or whole pieces, and all foraminifera between 63 and 355 µm were picked. Due to the poor foraminiferal recovery of the initial 52 samples, our methodology shifted to picking foraminifera from the 125 and 250 µm size fractions. All of the 250 µm fraction was picked, whereas the 125 µm fraction was dry-split, and two trays were examined for foraminifera; if 10 or more foraminifera were found, then we picked the entirety of the > 125 µm fraction. Our final shift in picking methods was a result of rare occurrences of subpolar and temperate planktic foraminifera; we now pick everything in the > 125 µm fraction. Numerous authors studying Pleistocene and Holocene foraminifera in the Ross Sea utilize the > 125 µm fraction for counts, which we adopted here (e.g., Prothro et al., 2018; Majewski et al., 2018, 2020). Picked specimens from all methods are included in this preliminary study, focusing primarily on the genus level for benthic foraminifera and species level for planktic foraminifera. The genus-level identification of the benthic foraminifera is adopted in our analyses because each genus is typically dominated by a singular species.

Ideally, we would prefer to use at least 300 specimens for any statistical analysis, but this is not practical with these low-abundance Antarctic samples. Foraminiferal studies from the Late Pleistocene–Holocene of the Ross Sea have demonstrated the statistical significance of foraminiferal assemblages despite low abundances (e.g., Fillon, 1974; Osterman and Kellogg, 1979); we suggest the same is true for the Miocene assemblages. Given the pervasive low abundances of foraminiferal tests through the Miocene study interval at Site U1521, we ran a rarefaction analysis (number of specimens versus number of species; Sanders, 1968) on all 135 samples to define a reasonable minimum number of benthic specimens that a sample must contain to be included in a cluster analysis, which is used to identify benthic biofacies. The shape of the species abundance curve decreases at a logarithmic rate as the number of specimens in a sample increases arithmetically (e.g., de Mello et al., 2017; Seidenstein et al., 2024). Based on the rarefaction analysis of the U1521 samples studied here, the plot approaches a plateau (∼ 20 species) with little additional increase in benthic diversity when at least 48 specimens are present (Fig. 2). Based on these results, only samples containing at least 48 benthic specimens, 40 samples in total, are used to identify benthic biofacies based on a Q-mode (Bray–Curtis) cluster analysis of relative abundance data of benthic foraminifera using PAleontological STatistics program (PAST 4.13; Hammer et al., 2001). We choose the Bray–Curtis method because it is based on abundance data, and the Bray–Curtis method was utilized in Neogene Antarctic foraminiferal records from AND-2A (Patterson and Ishman, 2012). Of these 40 samples, the average number of specimens per sample is 114, and 16 samples have > 100 specimens. Note that 7 of the 40 samples are shipboard core-catcher samples, labeled PAL, which have larger volumes; the PAL samples have some of the highest specimen yields. In defining the clusters, benthic genera that occurred > 20 % of the time within a sample for at least half of the samples in the cluster are considered primary taxa. Any benthic genera occurrences between 15 %–20 % within at least half of the samples within a particular cluster are considered secondary taxa, and genera abundances between 5 %–15 % are considered accessory taxa.

2.2 Age model

The age model for Units IV and III utilizes magnetic reversals, diatom first-appearance datums (FADs), diatom last-appearance datums (LADs), bivalve mollusk $^{87}Sr/^{86}Sr$ dates, and detrital hornblende Ar–Ar dates, as reported by Marschalek et al. (2021) (Fig. 3 and Table S1 in the Supplement). Unit IV (280.72–209.17 m) is constrained between two magnetic reversals (Gradstein et al., 2020), namely C5Cn.1r/C5Cn.2n at 286.3 CSF-A (16.351 Ma) and C5Cn.1n/C5Cn.1r at 207.0 CSF-A (16.261 Ma), with an average sedimentation rate of ∼ 881.11 m Myr^{-1}. Unit III is divided into two intervals; the lowermost interval of Unit III (209.17–207 m; CSF-A) is constrained by magnetic reversal C5Cn.1r/C5Cn.2n at 286.3 CSF-A (16.351 Ma) and C5Br/C5Cn.1n at 105.9 CSF-A (15.994 Ma), with a sedimentation rate of ∼ 378.65 m Myr^{-1}. We assume that the sedimentation rate is continuous through the remainder of Unit III (207–85.34 m). Units III and II are separated by Ross Sea Unconformity 4 (RSU4) at 85.34 m CSF-A (Pérez et al., 2022). The age of the RSU4 erosion is constrained between ∼ 14.6 Ma, based on paleomagnetic evidence, and ∼ 14.2 Ma, based on diatom evidence. The age model for Unit II has been updated since the initial report (McKay et al., 2019) based on diatom biostratigraphy. The lower age of Unit II is constrained between 14.2 and 13.9 Ma by the first appearance of *Denticulopsis simonsenii* (14.2 Ma) in the sample at 84.99 m CSF-A (Core 10-1; 79 cm). The top of Core 8 (Unit II) can be no younger than 13.6 Ma, as indicated by the absence of *Nitzschia denticuloides*, a widespread and common Antarctic diatom with a well-established biostratigraphic range. We consider three potential age ranges (with slopes a, b, and c) for the lower portion of Unit II (Fig. 3). Age model "a" encompasses the entire possible age interval (14.2–13.6 Ma), which is considered unlikely because there is no facies evidence to suggest that the Mi3 glaciation (∼ 13.9–13.8 Ma) is recorded at Site U1521. Therefore, age model "b" (14.2–13.9 Ma) represents a likely maximum age range for the lower part of Unit II. Age model "c" (14.2–14.1 Ma) represents an expanded interval with a sedimentation rate similar to Unit III. Our data are presented using age model "b" for the lower part of Unit II, representing the middle ground of the "a" and "c" age models.

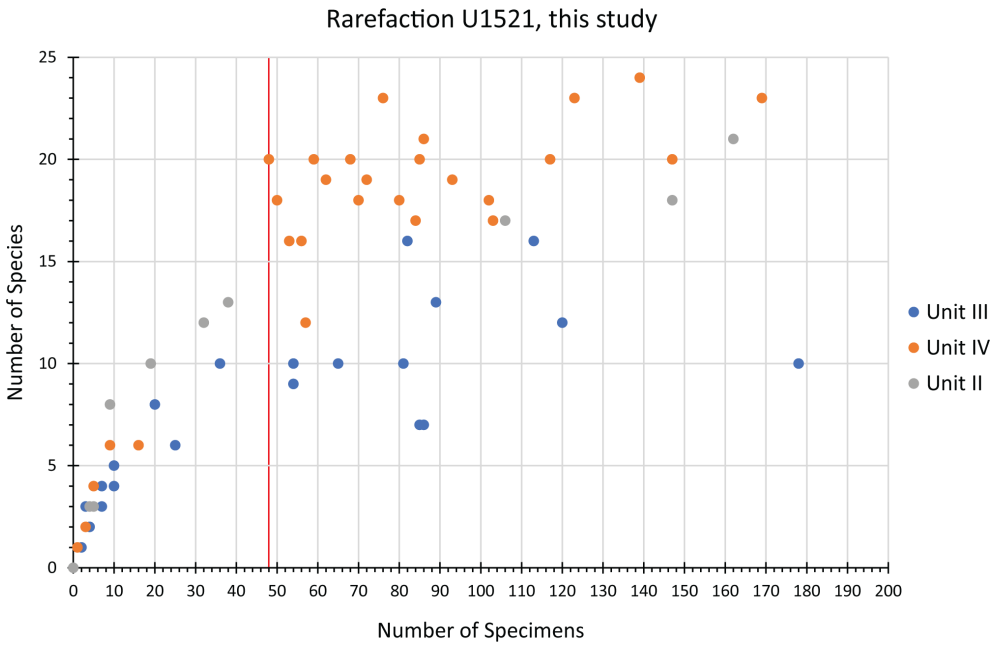

Figure 2. Rarefaction analysis with the number of benthic specimens versus number of species in samples with a maximum of 200 foraminifera (larger samples excluded due to rarity). Samples are categorized based on the lithologic unit, with Unit IV (orange), Unit III (blue), and Unit II (grey). The vertical red line shows the cutoff, with a minimum of 48 specimens, adopted here for inclusion in cluster analyses.

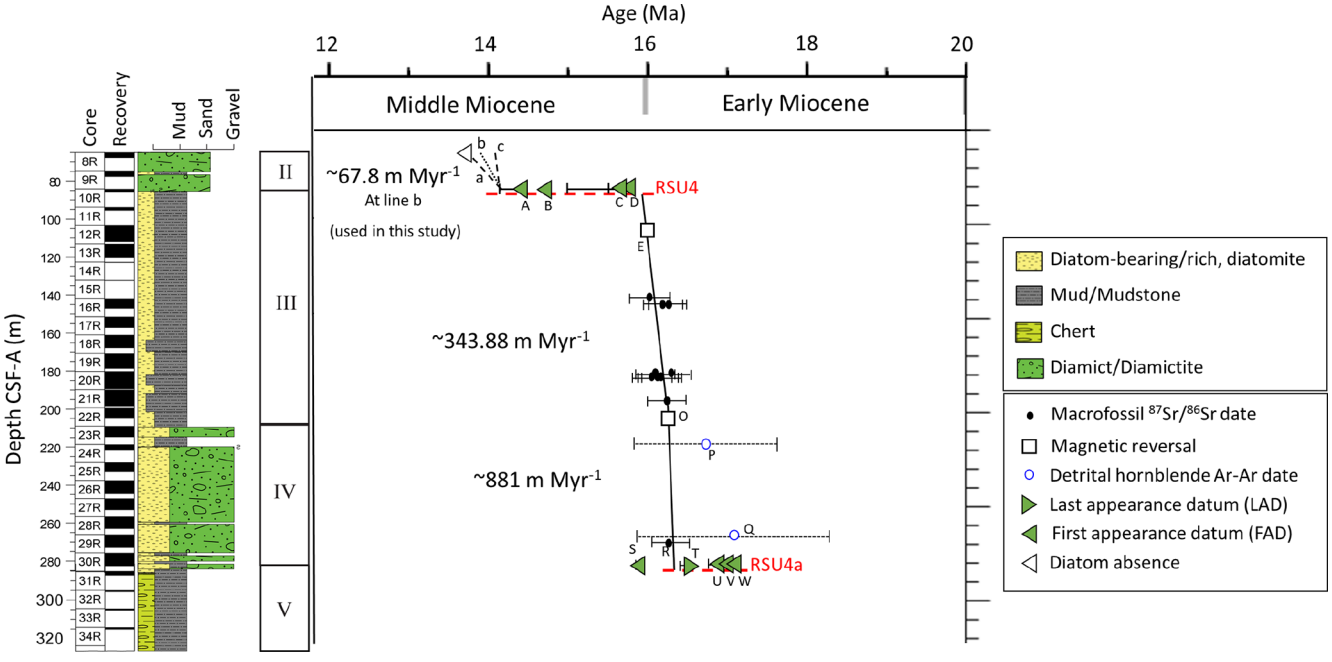

Figure 3. Site U1521 age model. Datum constraints for Units III and IV are from Marschalek et al. (2021). Paleomagnetic reversals C5Cn.1n/C5Cn.1r (16.261 Ma; GTS2020) and C5Br/C5Cn.1n (15.994 Ma; GTS2020) are marked with a square. Unit III shows three options (a–c). Option "a" spans the entirety of the interval constrained by diatom FAD A at 14.2 Ma and diatom absence at 13.6 Ma. Option "b" represents the middle ground between "a" and "c", from 14.2 to 13.9 Ma (used for all plots in this study). Option "c" represents a higher sedimentation rate, similar to Units III and IV, from 14.2 to 14.1 Ma. Dashed red lines are Ross Sea Unconformity 4a (RSU4a) and RSU4.

Table 1. Relative abundance distribution table for the 40 samples with at least 48 benthic specimens used for cluster analysis. Our interpreted benthic biofacies or unique assemblage identification is marked with the respective letter or number.

Lithologic unit	Sample ID	Age	Depth CSF-A (m)	Total foram	Total benthic	Benthic biofacies cluster	*Globocassidulina* %	*Uvigerina* %	*Nonionella* %	*Melonis* %	*Globobulimina* %	*Nodosariidae* %	*Anomalinoides* %	*Astrononion* %	*Elphidium* %	*Ammoelphidiella* %	*Alabaminella* %	*Epistominella* %	*Gyroidina* %	*Gavelinopsis* %	*Rosalina* %	*Sphaeroidina* %	*Miliolids* %	*Fursenkoina* %	*Cibicides* %	*Pullenia* %	Agglutinated %
II	9R-CC, 8–11	14.09	77.63	165	162	E	29.6	6.8	16.0	9.3	0.0	3.7	2.5	0.0	7.4	6.8	1.9	5.6	0.0	0.0	4.3	0.0	0.0	1.2	1.2	0.6	0.6
	9R-CC, 13–16	14.09	77.68	112	106	E	30.2	10.4	14.2	11.3	0.0	0.0	4.7	0.0	4.7	1.9	3.8	5.7	0.0	0.0	7.5	1.9	0.0	0.9	0.9	0.9	0.0
	9R-CC, 16–21 PAL	14.09	77.72	116	147	G	38.1	19.7	5.4	16.3	0.0	3.4	0.0	0.0	4.8	6.8	0.7	1.4	0.0	0.7	0.7	0.0	0.0	0.0	0.7	0.7	0.0
III	10R-CC, 12–17 PAL	15.94	85.70	481	481	G	34.1	18.9	7.1	29.5	0.0	6.0	1.0	0.0	0.0	0.0	0.0	0.0	0.0	0.2	1.9	0.0	0.2	0.0	0.0	0.0	0.0
	12R-CC, 18–23 PAL	16.01	111.97	311	311	X3	30.5	10.0	1.9	17.4	0.6	5.1	1.9	3.2	0.0	0.0	0.3	0.0	16.4	1.9	0.0	9.0	0.3	0.0	0.0	0.0	0.0
	13R-5W, 94–97	16.03	119.57	123	113	B	26.5	5.3	10.6	7.1	5.3	15.9	7.1	0.9	0.0	0.9	3.5	8.0	0.0	0.0	0.0	0.0	0.0	0.9	0.0	1.8	0.0
	13R-6W, 4–7	16.03	119.69	95	89	B	22.5	34.8	1.1	3.4	4.5	9.0	3.4	0.0	0.0	0.0	3.4	13.5	0.0	0.0	0.0	2.2	0.0	1.1	0.0	0.0	0.0
	15R-CC, 0–5 PAL	16.06	132.47	81	81	X2	23.5	22.2	1.2	2.5	39.5	2.5	1.2	0.0	0.0	0.0	0.0	1.2	0.0	3.7	0.0	2.5	0.0	0.0	0.0	0.0	0.0
	16R-CC, 14–19 PAL	16.10	147.05	178	178	A	72.5	0.0	6.7	1.7	0.0	6.7	0.0	0.0	0.0	5.6	0.0	0.0	0.0	0.0	0.0	0.0	2.8	3.9	0.0	0.0	0.0
	17R-1W, 5–8	16.11	151.47	54	54	A	55.6	0.0	18.5	3.7	0.0	11.1	0.0	0.0	0.0	7.4	0.0	0.0	0.0	0.0	0.0	0.0	0.0	1.9	0.0	0.0	0.0
	17R-2W, 9–12	16.12	152.74	66	65	A	43.1	0.0	27.7	1.5	0.0	16.9	0.0	0.0	0.0	7.7	0.0	0.0	0.0	0.0	0.0	0.0	0.0	1.5	0.0	0.0	0.0
	18R-3W, 83–86	16.15	164.00	86	86	X4	3.5	65.1	1.2	0.0	0.0	3.5	0.0	0.0	1.2	0.0	0.0	0.0	0.0	14.0	2.3	0.0	0.0	0.0	0.0	0.0	0.0
	18R-5W, 122–125	16.15	166.13	91	85	A	45.9	0.0	7.1	2.4	3.5	0.0	0.0	0.0	0.0	2.4	0.0	0.0	0.0	0.0	0.0	0.0	0.0	2.4	0.0	0.0	0.0
	18R-6W, 34–37	16.15	166.75	120	120	A	54.2	0.0	1.7	11.7	2.5	10.0	0.0	5.8	0.8	0.0	0.0	0.0	0.0	0.0	0.8	0.0	0.0	12.5	0.0	0.0	0.0
	21R-CC, 12–17 PAL	16.24	198.53	54	54	X1	1.9	18.5	42.6	24.1	0.0	0.0	0.0	0.0	0.0	0.0	0.0	0.0	0.0	1.9	1.9	5.6	0.0	0.0	1.9	0.0	0.0
IV	23R-2W, 20–22	16.27	210.56	90	82	C	34.1	23.2	6.1	4.9	2.4	2.4	4.9	2.4	8.5	2.4	0.0	1.2	0.0	0.0	3.7	0.0	0.0	0.0	0.0	2.4	0.0
	23R-3W, 20–22	16.27	211.67	59	57	A	50.9	7.0	15.8	1.8	0.0	8.8	0.0	0.0	3.5	5.3	0.0	0.0	0.0	1.8	0.0	0.0	0.0	0.0	1.8	0.0	0.0
	23R-5W, 20–22	16.27	214.02	49	48	E	25.0	12.5	16.7	8.3	0.0	4.2	4.2	4.2	4.2	0.0	2.1	2.1	0.0	0.0	4.2	2.1	0.0	2.1	2.1	2.1	0.0
	24R-3W, 20–22	16.28	221.32	77	72	D	15.3	33.3	8.3	6.9	0.0	2.8	5.6	2.8	5.6	1.4	1.4	1.4	0.0	0.0	5.6	0.0	0.0	2.8	4.2	0.0	1.4
	25R-1W, 20–22	16.29	228.31	68	62	D	27.4	21.0	8.1	12.9	0.0	1.6	4.8	1.6	9.7	1.6	0.0	1.6	0.0	0.0	3.2	0.0	1.6	0.0	1.6	1.6	0.0
	25R-2W, 20–22	16.29	229.56	108	102	D	24.5	20.6	10.8	14.7	0.0	2.9	6.9	1.0	4.9	0.0	0.0	0.0	1.0	1.0	2.9	0.0	2.9	0.0	2.0	2.9	0.0
	25R-3W, 20–22	16.29	230.68	153	147	C	30.6	19.7	11.6	8.2	1.4	1.4	8.2	1.4	3.4	2.7	0.0	0.0	1.4	2.0	3.4	0.0	2.0	0.0	0.7	0.7	0.0
	25R-4W, 14–16	16.29	232.08	127	123	D	18.7	25.2	10.6	9.8	1.6	6.5	5.7	0.8	6.5	1.6	0.0	0.8	0.0	0.8	3.3	0.0	3.3	0.8	1.6	0.8	0.0
	26R-1W, 20–22	16.30	237.81	53	50	D	18.0	22.0	16.0	8.0	0.0	4.0	8.0	2.0	2.0	2.0	0.0	4.0	0.0	0.0	4.0	0.0	4.0	4.0	2.0	0.0	0.0
	26R-2W, 23–25	16.30	239.19	120	117	E	29.1	20.5	12.8	6.0	0.9	3.4	0.9	0.0	6.8	0.9	0.0	0.0	0.0	0.0	5.1	0.9	5.1	3.4	2.6	0.9	0.0
	26R-3W, 20–22	16.30	240.65	109	103	E	24.3	16.5	18.4	6.8	0.0	5.8	4.9	4.9	1.9	0.0	1.0	1.0	0.0	0.0	5.8	1.9	1.0	1.9	0.0	1.0	0.0
	26R-4W, 20–22	16.30	242.00	81	70	D	21.4	27.1	12.9	10.0	0.0	2.9	5.7	2.9	5.7	1.4	0.0	0.0	1.4	0.0	4.3	0.0	2.9	0.0	0.0	1.4	0.0
	26R-5W, 20–22	16.30	243.33	89	86	D	23.3	24.4	11.6	7.0	0.0	4.7	3.5	3.5	1.2	1.2	0.0	0.0	1.2	0.0	5.8	0.0	5.8	0.0	0.0	3.5	1.2
	26R-CC, 7–12 PAL	16.30	244.63	56	53	F	20.8	22.6	5.7	15.1	1.9	1.9	17.0	0.0	3.8	1.9	0.0	0.0	0.0	0.0	0.0	0.0	7.5	0.0	0.0	1.9	0.0
	27R-1W, 10–12	16.31	247.21	80	76	D	19.7	23.7	13.2	7.9	0.0	0.0	6.6	2.6	3.9	3.9	0.0	0.0	0.0	0.0	3.9	0.0	7.9	0.0	3.9	0.0	1.3
	27R-2W, 10–12	16.31	248.61	89	85	C	30.6	18.8	8.2	8.2	1.2	1.2	8.2	2.4	12.9	2.4	0.0	0.0	0.0	0.0	0.0	0.0	2.4	0.0	1.2	0.0	0.0
	27R-3W, 10–12	16.31	249.83	148	139	D	22.3	23.0	12.9	15.8	0.0	2.2	2.2	3.6	5.8	0.0	0.7	0.7	0.0	0.7	1.4	1.4	3.6	0.7	0.7	1.4	0.0
	27R-4W, 10–12	16.31	251.09	75	68	D	14.7	22.1	16.2	11.8	1.5	1.5	5.9	2.9	4.4	1.5	0.0	0.0	0.0	1.5	5.9	1.5	0.0	0.0	1.5	0.0	2.9
	27R-5W, 51–54	16.31	252.85	88	84	D	17.9	38.1	9.5	7.1	0.0	0.0	3.6	3.6	3.6	2.4	0.0	0.0	0.0	0.0	2.4	0.0	4.8	0.0	1.2	2.4	1.2
	28R-CC, 9–12	16.32	262.93	84	80	D	18.8	36.3	12.5	10.0	0.0	6.3	5.0	1.3	0.0	1.3	0.0	0.0	0.0	0.0	1.3	1.3	3.8	0.0	0.0	1.3	0.0
	28R-CC, 14–19 PAL	16.32	262.99	57	56	E	19.6	28.6	0.0	16.1	0.0	5.4	10.7	0.0	3.6	0.0	0.0	0.0	0.0	0.0	1.8	3.6	3.6	0.0	1.8	1.8	0.0
	29R-2W, 18–20	16.33	267.50	219	210	E	27.1	21.4	16.7	7.1	1.0	1.9	1.0	1.9	1.0	1.0	2.9	1.0	0.0	0.0	2.9	1.0	3.3	3.3	1.4	0.5	0.5
	29R-6W, 20–22	16.34	272.39	174	169	F	26.0	19.5	16.6	5.3	0.6	1.8	10.1	1.2	1.8	0.0	4.1	2.4	0.0	0.0	1.8	1.8	3.6	1.8	0.6	0.6	0.0
	30R-1W, 10–13	16.34	275.82	61	59	C	32.2	27.1	8.5	3.4	0.0	3.4	3.4	0.0	8.5	1.7	3.4	1.7	0.0	0.0	1.7	1.7	1.7	0.0	1.7	0.0	0.0
	30R-4W, 20–22	16.34	280.12	98	93	C	23.7	22.6	8.6	6.5	3.2	4.3	6.5	0.0	4.3	0.0	0.0	0.0	3.2	0.0	0.0	4.3	1.1	0.0	2.2	7.5	1.1

3 Results

Based on our age model, Units IV and III were deposited during the Miocene Climatic Optimum (MCO), and Unit II was deposited during the Middle Miocene Climate Transition (MMCT) (Fig. 4). The foraminifera vary between and within the lithologic units, with moderate to good preservation overall, with the exception of four samples from Unit III (161.12, 152.74, 151.47, and 147.05 m; CSF-A), and three samples from Unit II (77.72, 77.68, and 77.63 m; CSF-A) that contain orange-stained foraminifera. The most foraminiferal fragments are recorded in Unit III (Fig. 4). Unit IV contains the most consistently abundant and diverse (high simple benthic diversity) assemblages, while Unit III foraminifera are either present or absent, and Unit II has the lowest foraminiferal recovery (Fig. 4). Planktic foraminifera are very rare and sporadic.

3.1 Benthic foraminifer assemblages and biofacies

Benthic foraminiferal assemblages are almost exclusively dominated by calcareous taxa and are highly variable. The tests are moderately to well preserved with very little fragmentation, except in Unit III (Fig. 4). A few intervals contain orange iron-stained specimens that suggest possible reworking or winnowing on the seafloor. Agglutinated taxa such as *Martinottiella communis* and *Ammodiscus* occur very rarely as single specimens. Dominant or co-dominant taxa are *Globocassidulina subglobosa* and *Uvigerina cf. U. fueguina*, with *Nonionella* (*N. iridea*, *N. novozealandica*, and *N. bradii*), *Melonis* (*M. barleeanus* and *M. affinis*) and *Globobulimina* cf. *G. auriculata* being common in some intervals (Fig. 5). Unit IV contains the most persistent, diverse, and abundant specimens. Unit III is characterized by highly variable abundances; samples from muddier intervals (higher NGR values) tend to have more specimens, while samples from diatom-rich intervals (lower NGR values) are barren or contain few individuals. Foraminiferal recovery in Unit II is generally poor.

Based on our Q-mode similarity index derived from the 40 samples containing at least 48 benthic specimens (Table 1), the benthic foraminiferal assemblages are distributed across seven benthic biofacies clusters and an additional four unique samples (Fig. 6). The seven benthic biofacies clusters (A–G) are defined by the abundance of specific primary (abundance greater than 20 % for at least half the samples in the biofacies group), and in some cases secondary (abundance 15 %–20 %), benthic genera and accessory benthic genera (5 %–15 % abundance) (Table 2). In general, the benthic biofacies and unique assemblages are dominated by a combination of *Globocassidulina* (*G. subglobosa*), *Uvigerina* (cf. *U. fueguina*), *Melonis* (*M. affinis* and *M. barleeanus*), *Globobulimina* (cf. *G. auriculata*), and/or *Nonionella* (*N. iridea* and *N. novozealandica*). Lithologic Unit IV records five distinct biofacies in 25 samples, Unit III contains three biofacies (A, B, G) and all four unique assemblages in 12 samples, and Unit II contains two biofacies (E and G) across 3 samples. Benthic biofacies occurrences are not overly repetitive; for example, biofacies D (dominated by *Uvigerina*) only occurs within Unit IV, and all unique assemblages (X samples) are found within Units III.

3.2 Planktic foraminifera

Planktic foraminifera occurrences are sporadic and rare, representing an endemic species and a relatively diverse suite of subpolar to temperate and subtropical species (Fig. 7). The planktic assemblage is primarily composed of rare *Antarcticella antarctica*, a taxon endemic to the Ross Sea and hypothesized to have been planktonic (Leckie and Webb, 1985, 1986), with most occurrences within Unit IV (Fig. 7). In addition to *A. antarctica*, our preliminary investigation of Site U1521 yielded 38 planktic specimens with biogeographic distributions ranging from temperate to subtropical (*Globoturborotalita druryi*, *Trilobatus* cf. *T. quadrilobatus*, *Globoconella* cf. *G. miozea*, and *Dentoglobigerina globosa*), subpolar to temperate (*Globigerinita glutinata*, *Globigerinita uvula*, and *Turborotalita quinqueloba*), and cosmopolitan (*Paragloborotalia continuosa*, *Paragloborotalia* cf. *P. pseudocontinuosa*, *Globorotaloides suteri*, *Tenuitella angustiumblicata*, and *Tenuitella munda*) (Table 3). Additionally, we note an occurrence of Globorotallidae of unknown genus and species (Plate B5 in Appendix B) in Unit III.

These planktic foraminifera are generally moderately to well preserved, occur in very low abundances ranging from one to six specimens within a given sample, and are present in Units IV, III, and II (Fig. 7). All warm planktic occurrences coincide with muddy terrigenous sediment (high NGR) rather than biosiliceous sediment. The sample with the highest abundance of warmer-water planktic specimens is mud-dominated with radiolarians and pteropods at ∼ 16.15 Ma (166.13 m; CSF-A) in Unit III. The youngest occurrences of the subtropical to temperate planktic foraminifera (*T. munda, D.globosa, G. obesa*, and *Globoconella* cf. *G. miozea*) is at ∼ 16.12 Ma in Unit III, the youngest subpolar to temperate taxon (*G. glutinata*) is at ∼ 14.09 Ma in Unit II, and the youngest cosmopolitan planktic foraminiferal species (*T. angustiumblicata*) is at ∼ 14.09 Ma in Unit II.

4 Discussion

4.1 Foraminiferal abundances at Site U1521 and elsewhere in the Ross Sea

Marine sediment core samples from Antarctica typically have low foraminiferal abundances (e.g., Fillon, 1974; Osterman and Kellogg, 1979; Leckie and Webb, 1980, 1983, 1986; D'Agostino and Webb, 1980; Steinhauff and Webb, 1987; Melis and Salvi, 2009; Patterson and Ishman, 2012; Majewski et al., 2018, 2020; Dameron et al., 2024; Seidenstein et

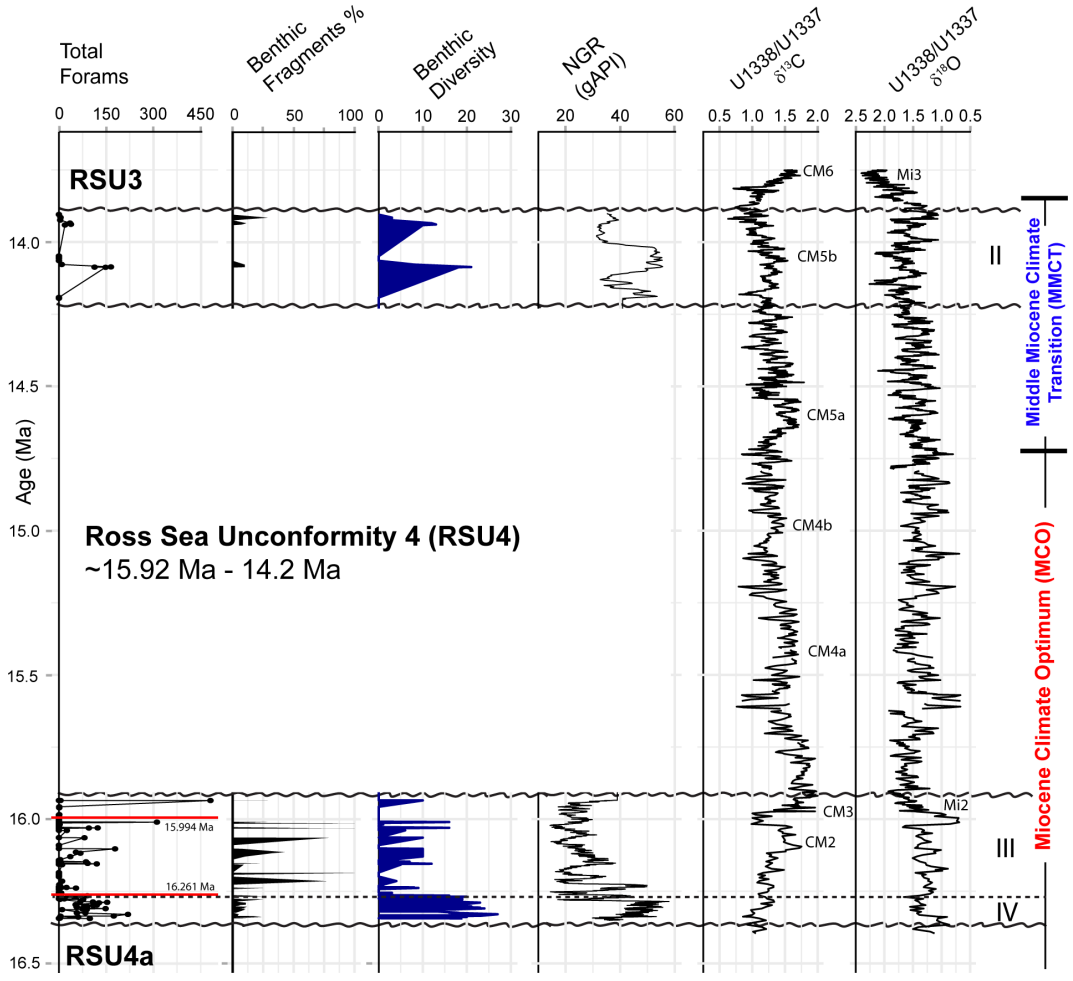

Figure 4. Summary of results comparing (from left to right) the total foraminiferal counts from Site U1521, percent benthic foraminiferal fragments, simple benthic diversity (number of benthic species) to natural gamma ray (NGR) (gAPI) (McKay et al., 2019), and low-latitude Pacific benthic foraminiferal $\delta^{13}C_{bf}$ and $\delta^{18}O_{bf}$ records from Sites U1337 and U1338 (Holbourn et al., 2014, 2015). Dashed black line marks the boundary between Unit IV and III. Paleomagnetic reversals C5Cn.1n/C5Cn.1r (16.261 Ma; GTS2020) and C5Br/C5Cn.1n (15.994 Ma; GTS2020) are marked with a red line in the total forams (foraminifera) plot. Ross Sea Unconformity boundaries (RSU4a, RSU4, and RSU3) are marked with a squiggly black line. The Mi2 and Mi3 glaciations and Carbon Maxima events (Flower and Kennett, 1993; Shevenell et al., 2004; Holbourn et al., 2022) are labeled, along with the lithologic units from Site U1521 and the timing of the MCO and MMCT (e.g., Steinthorsdottir et al., 2021).

al., 2024). At Site U1521, Units IV and III, and lower Unit II, the average foraminiferal abundance is 1.9 specimens g^{-1} of sediment, with as many as 17 specimens g^{-1} (not counting core-catcher samples, which were not weighed). The low abundances of calcareous benthic foraminifera may be an issue related to dissolution, or selective dissolution, as suggested by some of the earlier work on the DSDP Leg 28 sites drilled on the continental shelf. At Site U1521, increased foraminiferal fragmentation is recorded in the biosiliceous (low NGR) intervals of Unit III (Fig. 4). In addition, the overall moderate to good preservation of specimens observed in this study does not indicate the pervasive reworking, transport, or selective preservation of species with thick or resistant tests; i.e., most of the specimens from Site U1521 do not resemble residual assemblages as observed in the Miocene Ross Ice Shelf Project (RISP) cores (Dameron et al., 2024). Rather, the cold, harsh seafloor may limit population sizes due to the low availability of dissolved carbonate ion (CO_3^{2-}) in Antarctic waters for building their tests (Azetsu-Scott et al., 2010; Cummings et al., 2011; Hauck et al., 2012). We do suspect that the more diatom-rich intervals at Site U1521 are corrosive to carbonate because those intervals tend to be barren of foraminifera or contain elevated numbers of foraminiferal fragments and originally may have been more organic-rich and acidic at the seafloor (e.g., Emerson and Bender, 1981; Sachs et al., 2009; Hauck et al., 2013). Carbonate preservation in the uppermost layers of the sediment is a serious syn- to post-deposition problem in diatom-rich

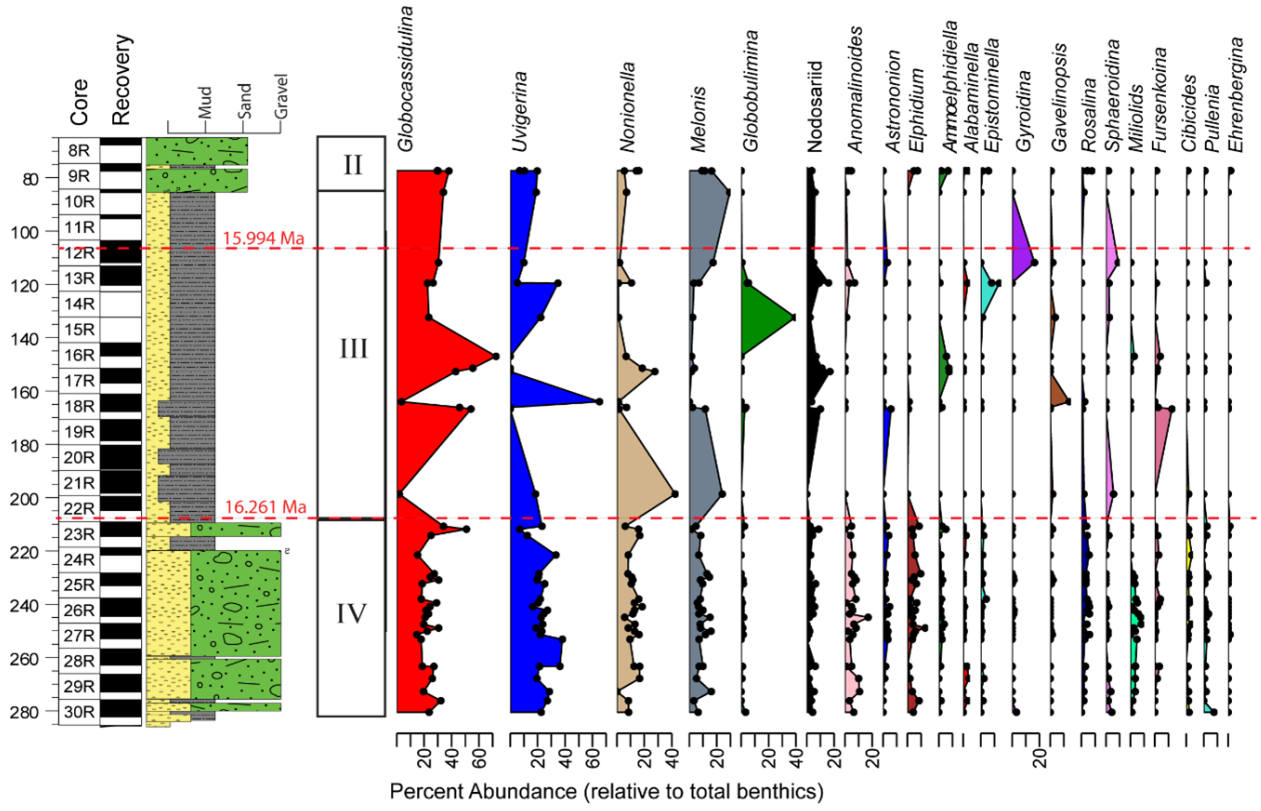

Figure 5. Benthic genera and *Antarcticella antarctica* relative abundances (%) for the 40 samples containing at least 48 benthic specimens to depth CSF-A. Benthic genera percent abundances are relative to total benthics. Paleomagnetic reversals C5Cn.1n/C5Cn.1r (16.261 Ma; GTS2020) and C5Br/C5Cn.1n (15.994 Ma; GTS2020) are marked with a dashed red line (McKay et al., 2019; Marschalek et al., 2021).

sediments of the Ross Sea (Seidenstein et al., 2024). At Site U1521, we can demonstrate that sediments with more terrigenous mud content and less biosiliceous material have better preservation and abundance of calcareous foraminifera.

For comparison with this study, Leckie and Webb (1983, 1986) documented the foraminifera from the upper Oligocene–Lower Miocene glaciomarine sediments of Site 270 in the central Ross Sea, north of the Ross Ice Shelf. In a study of 110 samples, these authors recognized four assemblage zones based on 27 representative samples with the most specimens (∼ 25 % of the total samples examined); of these, the average is 88 specimens per sample, with six samples having more than 100 specimens and six samples having 20–50 specimens. Seidenstein et al. (2024) found a similar issue of low foraminiferal abundances in the Plio-Pleistocene at IODP Site U1523 cored on the shelf break of the Ross Sea, northeast of Pennell Bank. Of the 131 samples examined, 42 (∼ 32 % of the investigated samples) contain at least 40 benthic specimens, with an average of 84 specimens per sample; 12 samples have > 100 specimens, while 36 samples have 50 or more specimens. Additionally, Patterson and Ishman (2012) noted the same challenges from the 163 Lower–Middle Miocene (∼ 125 to 500 m) samples examined from ice proximal site AND-2A. Of the 163 samples, 22 samples (∼ 13.4 %) have 11–50 specimens, and 4 samples (∼ 2.5 %) have greater than 50 specimens; the remaining 137 samples have rare (fewer than 11 specimens) or no foraminifera. Despite the generally low numbers of foraminifera, robust stratigraphic trends with valuable paleoecological implications have emerged from these studies, informed by rarefaction analysis (Sanders, 1968), to identify a reasonable minimum number of specimens for cluster analyses (e.g., Seidenstein et al., 2024; this study), which bear on important issues of water mass, bottom-water circulation activity, productivity, and paleobathymetry of the Ross Sea continental shelf.

An interesting question is why there are so few agglutinated species and specimens in our studied samples. Poor preservation potential of agglutinated tests is one possibility (e.g., Majewski et al., 2018); another is not having the ideal depositional conditions. Leckie and Webb (1983, 1986) reported abundant agglutinated species in two discrete intervals of the upper Oligocene–Lower Miocene at DSDP Site 270 in the central Ross Sea, which suggests that these two intervals had water mass or interstitial pore water characteristics favorable for agglutinated taxa (e.g., low temperature, low pH, and the absence of strong currents). Late Pleistocene- and Holocene-aged sediments of the Ross Sea middle and

Table 2. Primary taxa (> 20 % relative abundance), secondary taxa (15 %–20 %), and accessory taxa (5 %–15 %) of biofacies (A–G) and unique assemblages (X1–X4).

Cluster	Primary Taxa > 20%	Secondary Taxa 15-20%	Accessory Taxa 5-15%
A	*Globocassidulina*	*Nonionella*	Nodosariidae – *Ammoelphidiella*
B	*Globocassidulina* > *Uvigerina*	*Nodosariidae*	*Epistominella* – *Melonis* – *Anomalinoides* – *Globobulimina*
C	*Globocassidulina* > *Uvigerina*		*Nonionella* – *Elphidium* – *Melonis* – *Anomalinoides*
D	*Uvigerina*	*Globocassidulina*	*Nonionella* – *Melonis* – *Anomalinoides* – *Elphidium*
E	*Globocassidulina*	*Uvigerina* > *Nonionella*	*Melonis* – *Rosalina*
F	*Uvigerina* > *Globocassidulina*	*Melonis* > *Anomalinoides*	Milioldes – *Nonionella* – Nodosariidae
G	*Globocassidulina* > *Melonis*	*Uvigerina*	*Nonionella* – Nodosariidae – *Ammoelphidiella*
X1 21R-CC	*Nonionella* > *Melonis*	*Uvigerina*	*Sphaeroidina*
X2 15R-CC	*Globobulimina* > *Globocassidulina* – *Uvigerina*		
X3 12R-CC	*Globocassidulina*	*Melonis* – *Gyroidina*	*Uvigerina* – *Sphaeroidina* – Nodosariidae
X4 18R-3W	*Uvigerina*		*Gavelinopsis*

outer shelf, i.e., biosiliceous muds, are characterized by agglutinated assemblages in open-marine conditions with seasonal sea ice and exposure to corrosive High-Salinity Shelf Water (HSSW) created by brine-rejection processes during annual sea ice formation in polynyas north of the Ross Ice Shelf (e.g., Kennett, 1968; Osterman and Kellogg, 1979; Ishman and Szymcek, 2003; Melis and Salvi, 2009; Majewski et al., 2016, 2018, 2020; Melis et al., 2021). These distinctive agglutinated assemblages, typically dominated by taxa including *Miliammina* and *Portatrochammina*, are not observed in the Miocene samples from Site U1521 that are studied here. Does this imply that HSSW was not being produced during the Miocene, and furthermore, does the absence of these distinctive agglutinated assemblages provide implications about the size of the Antarctic Ice Sheet and the existence of katabatic winds and sea ice polynyas during the MCO and MMCT?

4.2 Benthic biofacies interpretations

Benthic foraminifera from Site U1521 record a history of changing environmental conditions in the Ross Sea in response to the MCO and MMCT. We identified seven benthic biofacies with primary taxa that provide valuable insight into the character of the Ross Sea during the MCO and MMCT. We interpret each of these biofacies as being diagnostic of specific environmental conditions, which allows us to speculate about what the Ross Sea may have looked like when there is an abundance of one or more of these benthic taxa (Table 4). The two most common taxa, *Globocassidulina subglobosa* and *Uvigerina* cf. *U. fueguina* (or *Trifarina earlandi* in the late Neogene and Quaternary), have dominated or co-dominated Ross Sea continental shelf glaciomarine foraminiferal assemblages since the latest Oligocene–Early Miocene, including intervals of DSDP Site 270 (Leckie and Webb, 1980, 1983, 1986); the late Early to Middle Miocene of DSDP Site 273 (D'Agostino and Webb, 1980); and Site 272 (Steinhauff and Webb, 1987); the Late Miocene of RISP Site J-9 (Dameron et al., 2024); and the Plio-Pleistocene of IODP Site U1523 (Seidenstein et al., 2024). We suggest that the mix or alternation of *Globocassidulina* and *Uvigerina/Trifarina* on the Ross Sea continental shelf during the Neogene and Quaternary (today including *G. subglobosa, G. biora, G. crassa rossensis*, and *Trifarina earlandi*; e.g., Melis and Salvi, 2009; Majewski et al., 2018, 2020; Prothro et al.,

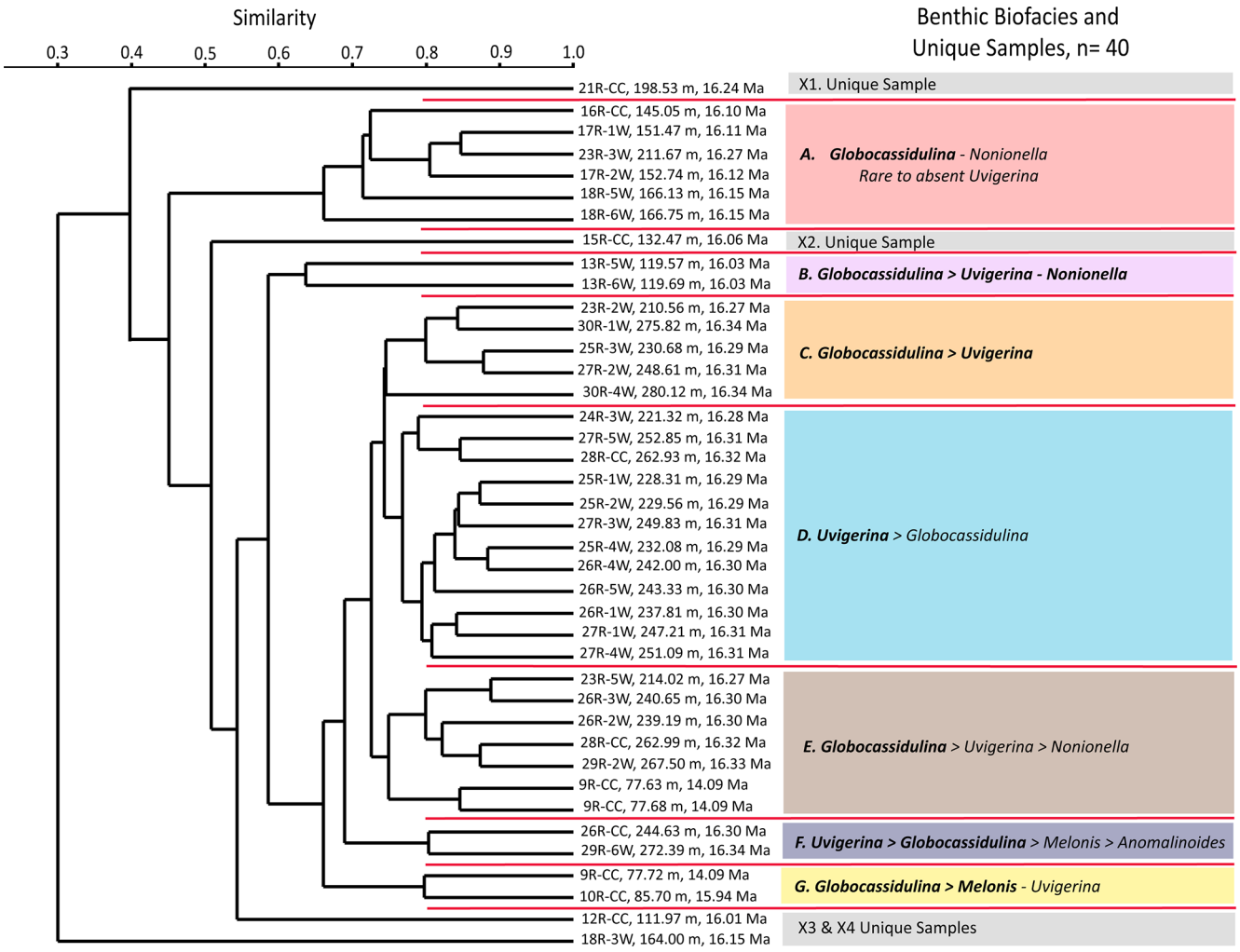

Figure 6. Q-mode similarity plot. Sample ID, depth in CSF-A (m), and age with interpreted biofacies A–G or unique assemblages X1–X4. Genera in bold are the primary taxa. Solid red lines mark the division between the interpreted biofacies.

2018) reflect the dynamics of water mass influence, current activity, and productivity, including the present-day climatic impacts of basal melting by modified Circumpolar Deep Water (mCDW) (e.g., Hillenbrand et al., 2017).

Globocassidulina subglobosa is the most abundant benthic species in the Lower to Middle Miocene of Site U1521. We hypothesize that *G. subglobosa* is a proxy for deep waters that impinge on the continental margin of the Ross Sea from the Southern Ocean, which is here referred to as proto-Circumpolar Deep Water (pCDW). This pCDW differs from late Neogene and Quaternary CDW because relatively warm Northern Component Water, the precursor of North Atlantic Deep Water, was not being produced during the time interval of our study (e.g., Wright et al., 1991), but a Tethyan-sourced warm saline deep-water mass was likely present in the southwest Pacific at this time (Flower and Kennett, 1995; Shevenell and Kennett, 2004). We base this *G. subglobosa*–pCDW connection on the following evidence: (1) *Globocassidulina subglobosa* has been a common, widespread lower-bathyal–abyssal taxon (1500–4000 m; Corliss, 1979, 1983; Peterson and Lohmann, 1982; Peterson, 1984; Mackensen and Berggren, 1992; Schmiedl and Mackensen, 1997) since the Early Eocene (e.g., Mackensen and Berggren, 1992). Today, *G. subglobosa* is associated with CDW in the southwest Atlantic (Hodell et al., 1983) and southwest Pacific (Hayward et al., 2007, 2013). *Globocassidulina subglobosa* invaded the continental shelf of the Ross Sea as Antarctica became increasingly glaciated during the Oligocene and Early Miocene (Leckie and Webb, 1983, 1986; Webb et al., 1986; Coccioni and Galeotti, 1997; Strong and Webb, 2000, 2001; Webb and Strong, 2006; Patterson and Ishman, 2012). (2) In modern Ross Sea sediments, *Globocassidulina* spp. (*G. subglobosa*, *G. biora*, and *G. rossensis*) is the dominant genus in the sub-ice-shelf facies proximal to grounding-zone wedges of the retreating Last Glacial Maximum (LGM) ice sheet in the western and eastern Ross Sea (Melis and Salvi, 2009;

Table 3. Warm planktic species, their geographic distribution, and the age and depth of occurrences at Site U1521.

Species	Geographic distribution	When (Ma) and where present (m; CSF-A)
Globoturborotalita druryi	Subtropical to temperate	16.15 Ma (165.27 and 166.13 m) and 16.30 Ma (244.63 m)
Dentoglobigerina globosa	Subtropical to temperate	16.12 Ma (152.74 m) and 16.23 Ma (194.98 m)
Globoconella cf. *G. miozea*	Subtropical to temperate	16.12 Ma (152.74 m) and 16.24 Ma (197.82 m)
Globigerinella obesa	Subtropical to temperate	16.12 Ma (152.74 m)
Globigerinita glutinata	Subpolar to temperate	14.09 Ma (77.63 m), 16.15 Ma (166.13 m), 16.31 Ma (253.12 m), 16.32 Ma (262.93 m), and 16.34 Ma (275.82 m)
Globigerinita uvula	Subpolar to temperate	16.24 Ma (197.67 m) and 16.34 Ma (272.39 m)
Turborotalita quinqueloba	Subpolar to temperate	15.96 Ma (95.21 m), 15.98 Ma (104.16 m), 16.15 Ma (165.88 m), 16.27 Ma (210.56 m), and 16.30 Ma (240.65 m)
Paragloborotalia continuosa	Cosmopolitan	16.24 Ma (197.67 m)
Paragloborotalia pseudocontinuosa	Cosmopolitan	16.23 Ma (194.98, 195.53, and 195.91 m) and 16.28 Ma (220.19 m)
Globorotaloides suteri	Cosmopolitan	16.30 Ma (244.63 m)
Tenuitella angustiumblicata	Cosmopolitan	14.09 Ma (77.68 m), 16.12 Ma (152.74 m), 16.15 Ma (166.13 m), and 16.24 Ma (197.67 m)
Tenuitella munda	Cosmopolitan	16.12 Ma (152.74 m) and 16.15 Ma (166.13 m)
Trilobatus cf. *T. quadrilobatus*	Cosmopolitan	16.30 Ma (244.63 m)
Globorotallidae		15.96 Ma (93.97 m)

Table 4. Key species and genera with favored environmental conditions and biofacies occurrences.

Taxa	Environmental conditions	References	Biofacies or assemblage primary taxa
Globocassidulina subglobosa	Circumpolar Deep Water; Ross Sea grounding-zone wedges	Schmiedl et al. (1997), Hayward et al. (2007), Melis and Salvi (2009), Hillenbrand et al. (2017), Bart et al. (2016), Prothro et al. (2018), Majewski et al. (2018, 2020), Seidenstein et al. (2024)	A, B, C, E, F, G, X2, and X3 * Rare to absent in X1 and X4
Uvigerina sp.	Enhanced bottom-current activity; high productivity; continental shelf edge	Kellogg et al. (1979), Ishman and Szymcek (2003), Jorissen et al. (2007), Majewski et al. (2018), Seidenstein et al. (2024)	B, C, D, F, X2, and X4
Nonionella spp., *N. iridea*, *N. novozealandica*	Neritic – upper bathyal; high flux of organic carbon; Circumpolar Deep Water?	Gooday (1986), Mackensen et al. (1990), Gooday and Hughes (2002), Duchemin et al. (2008), Gooday (2003), Hillenbrand et al. (2017)	X1
Melonis spp., *M. affinis*, *M. barleeanus*	High productivity	Bornmalm (1997), McCorkle et al. (1997), Schmiedl et al. (1997), Gooday (2003), Jorissen et al. (2007), Knudsen et al. (2012)	G and X1
Globobulimina cf. *G. auriculata*	Low oxygen	McCorkle et al. (1997), Gooday (2003), Bernhard et al. (2012), Knudsen et al. (2012), Woehle et al. (2018, 2022)	X2
Elphidium spp., *E. magellanicum*, *E. excavatum*	Neritic < 150 m	Poag (1981), Hayward et al. (1997a, b), Ward et al. (1987), Leckie and Olson (2003)	Not a primary taxon; key accessory

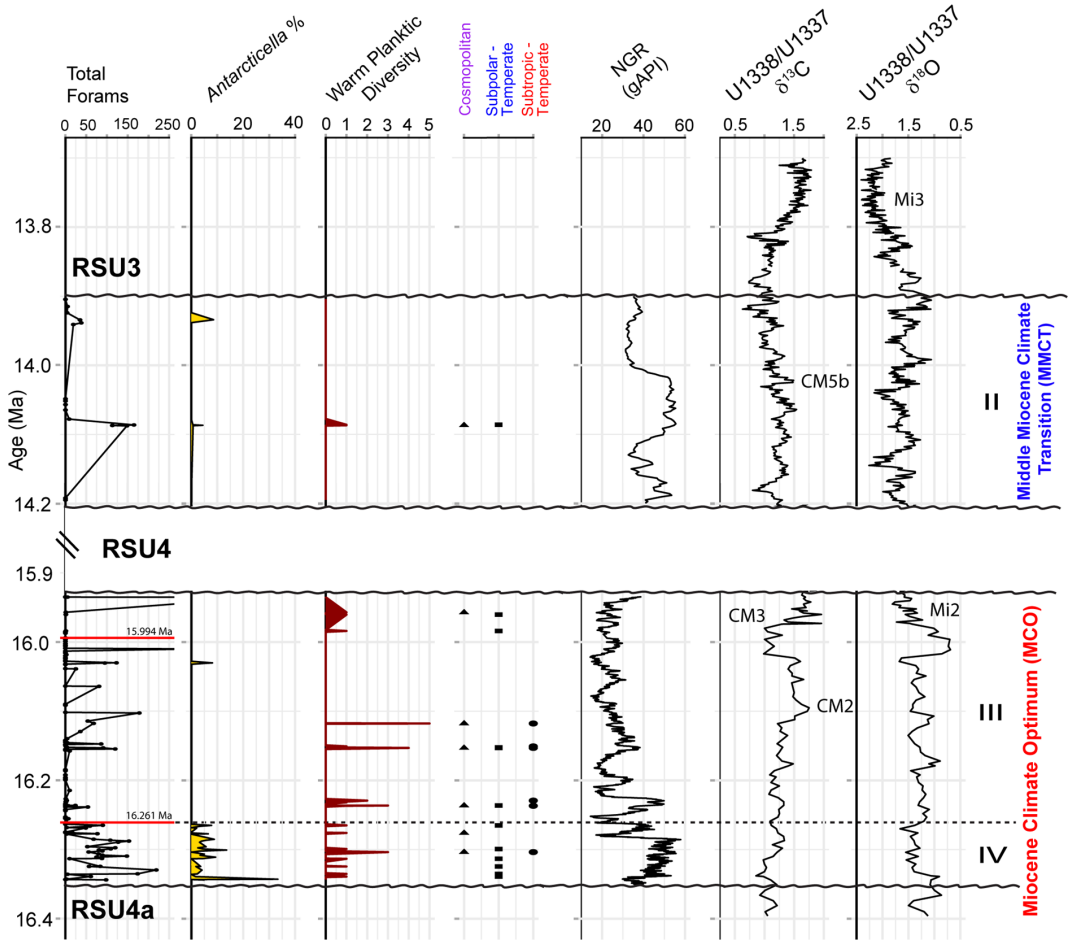

Figure 7. Planktic foraminifera from IODP Site U1521 for Units IV, III, and II. From left to right are the total forams in percent of *Antarcticella antarctica* (a presumed endemic Antarctic planktic species; Leckie and Webb, 1985); warmer-water planktic diversity (number of species within a sample); and the occurrences of cosmopolitan planktics (triangle), subpolar to temperate planktics (square), and subtropical to temperate (circles) compared to NGR (gAPI) (McKay et al., 2019) and the low-latitude Pacific benthic foram $\delta^{13}C_{bf}$ and $\delta^{18}O_{bf}$ record from ODP Sites U1337 and U1338 (Holbourn et al., 2014, 2015). Dashed black line marks the boundary between Unit IV and III. Paleomagnetic reversals C5Cn.1n/C5Cn.1r (16.261 Ma; GTS2020) and C5Br/C5Cn.1n (15.994 Ma; GTS2020) are marked with a red line in the total forams plot. Ross Sea Unconformity boundaries (RSU4a, RSU4, and RSU3) are marked with a squiggly black line. The Mi2 and Mi3 glaciations and Carbon Maxima events (Flower and Kennett, 1993; Shevenell et al., 2004; Holbourn et al., 2022) are labeled, along with the lithologic units from U1521 and the timing of the MCO and MMCT (e.g., Steinthorsdottir et al., 2021).

Bart et al., 2016; Prothro et al., 2018; Majewski et al., 2018, 2020). The grounded LGM ice sheet retreat was facilitated in part by melting caused by incursion of relatively warm CDW/mCDW onto the Ross Sea continental shelf (Prothro et al., 2018; Smith et al., 2019). (3) In a core near the Pine Island Glacier of the West Antarctic Ice Sheet, Hillenbrand et al. (2017) documented dominant *G. subglobosa* and *Nonionella* spp. in an interval with low-$\delta^{13}C_{bf}$ values (higher nutrients) and warm benthic temperatures (Mg/Ca) indicative of CDW during the early Holocene (11.7–7.5 ka) which abruptly changed to *Trifarina earlandi* (reported as *Angulogerina angulosa*) dominance and higher-$\delta^{13}C_{bf}$ (lower nutrients) values and cooler temperatures in the late Holocene. This is strong supporting evidence of an association between *G. subglobosa* and CDW/mCDW. And, (4) incursions of warmer-water planktic foraminifera (temperate to subpolar species) are associated with abundances of *G. subglobosa* in the Pliocene–lower Pleistocene of the Ross Sea shelf edge Site U1523 (Seidenstein et al., 2024), the uppermost Oligocene–Lower Miocene of Site 270 (Leckie and Webb, 1986), and in the Miocene at Site U1521 (this study).

At Site U1521, incursions of pCDW are interpreted to be strongest during occurrences of *G. subglobosa*-rich biofacies samples A, B, C, E, F, G, X2, and X3 (Table 2). *Globocassidulina* is rare to absent in samples X1 and X4, which we suggest represents the diminished influence from pCDW. We hypothesize that the Ross Sea has been bathed by slope waters originating from the Southern Ocean, in this case proto-

CDW, since the continent was first glaciated. We interpret *Globocassidulina subglobosa* and its late Neogene descendants, *G. rossensis* and *G. biora* (Majewski et al., 2021), to be cold-water bathyal invaders and opportunists with CDW affinities that have come to dominate many foraminiferal assemblages of the Ross Sea and Antarctic continental margin (e.g., Seidenstein et al., 2024).

Uvigerina cf. *U. fueguina* is the second most dominant taxon in the Ross Sea in the Lower to Middle Miocene of Site U1521. Based on phylogenetic analyses and genetics, *Uvigerina* and *Trifarina* are closely related genera (Schweizer et al., 2005). During the Plio-Pleistocene, *Trifarina earlandi* is a proxy for enhanced bottom currents, sandy sediment, and high productivity, primarily associated with the continental shelf break (Osterman and Kellogg, 1979; Ishman and Szymcek, 2003; Jorissen et al., 2007; Majewski et al., 2018; Seidenstein et al., 2024). We suggest that *Uvigerina* cf. *U. fueguina* is paleoecologically similar to *Trifarina earlandi*; thus it is likely an indicator of the conditions associated with the continental shelf edge and/or strong bottom-water flow (e.g., residual glaciomarine facies of Prothro et al., 2018). The Ross Sea continental shelf edge is a zone of high productivity, enhanced current activity (i.e., the Antarctic Slope Current), and coarser sediment sizes, where finer diatomaceous mud tends to be winnowed away by the ASC (e.g., Kim et al., 2020; Prothro et al., 2018). At Site U1521, high abundances of *Uvigerina* are characteristic of biofacies B, C, D, and F and unique samples X2 and X4 (Table 2).

Nonionella is a proxy for upper bathyal–outer neritic settings under a high flux of organic carbon. The two dominant *Nonionella* species recorded at Site U1521 are *N. iridea* and *N. novozealandica*, although *N. bradii* is also present. These taxa are interpreted to be opportunistic species that respond positively to phytodetritus (Gooday, 1986; Mackensen et al., 1990; Gooday and Hughes, 2002; Duchemin et al., 2008; Gooday, 2003). At Site U1521, assemblage X1 and one occurrence of biofacies A ($\sim$ 16.12 Ma) are the only assemblages dominated by *Nonionella*. *Nonionella* is often found in association with *Globocassidulina subglobosa* in the Miocene of Site U1521. Hillenbrand et al. (2017) report *Nonionella* spp. in close association with *G. subglobosa* in an early Holocene interval strongly influenced by the CDW/mCDW along the margin of the West Antarctic Ice Sheet. *Melonis* is a moderately deep infaunal taxon and an indicator of refractory organic matter and fine-grained sediment (Bornmalm, 1997; McCorkle et al., 1997; Schmiedl et al., 1997; Gooday, 2003; Jorissen et al., 2007; Knudsen et al., 2012). *Melonis* appears as a primary taxon in biofacies G and unique assemblage X1 (Table 2). Both *Nonionella* and *Melonis* are abundant during intervals of high productivity. *Globobulimina* cf. *G. auriculata*, a deep infaunal and delicate taxon, is a proxy for high productivity and low interstitial oxygen levels (McCorkle et al., 1997; Gooday, 2003; Bernhard et al., 2012; Knudsen et al., 2012; Woehle et al., 2018, 2022). At Site U1521, *Globobulimina* is dominant in sample X2 and occurs as an accessory taxon in biofacies B (Table 2).

4.3 Significance of warmer-water planktic foraminifera

At Site U1521, we note occurrences of planktic foraminifera endemic to Antarctica and species of planktics with a much wider and warmer geographic range. The only endemic and presumed planktic foraminiferal taxon in Antarctica during the Early to Middle Miocene was *Antarcticella antarctica* (Leckie and Webb, 1985, 1986; this study). The presence of *A. antarctica* is still under consideration with respect to whether it was actually planktonic and, if so, whether it preferred open-marine or sea ice conditions. We hypothesize that *A. antarctica* may have thrived in association with sea ice, perhaps becoming benthic-like while grazing diatoms attached to the ice. *Neogloboquadrina pachyderma* is known to be associated with sea ice in the Southern Ocean, including hibernation in brine channels; *N. pachyderma* has been shown to be very tolerant, adaptable, and resilient to the harsh seasonal cycle of the southern high latitudes (Lipps and Krebs, 1974; Spindler and Dieckmann, 1986; Schiebel et al., 2017; Westgard et al., 2023). When *A. antarctica* is present, it is typically in an abundance of 1 to 10 specimens with variable preservation. Three samples of $\sim$ 10 specimens each of *A. antarctica* were collected for isotopic analysis in order to test its planktonic habitat, but unfortunately it failed the quality assurance and quality control (QA–QC) test due to the small sample size.

In addition to *A. antarctica*, we identified Miocene-aged planktic foraminifera that are typically found in subtropical to temperate regions (*Globoturborotalita druryi*, *Trilobatus* cf. *T. quadrilobatus*, *Globoconella* cf. *G. miozea*, and *Dentoglobigerina globosa*), temperate to subpolar regions (*Globigerinita glutinata*, *G. uvula*, and *Turborotalita quinqueloba*), and cosmopolitan taxa that are not normally found near Antarctica (*Paragloborotalia continuosa*, *Paragloborotalia* cf. *P. pseudocontinuosa*, *Globorotaloides suteri*, *Tenuitella angustiumblicata*, and *T. munda*) (Fig. 7; Table 3). Warmer-water planktic species were reported from other Ross Sea drill sites, including the uppermost Oligocene to Lower Miocene of DSDP Site 270 (Leckie and Webb, 1986), the Pliocene and lower Pleistocene IODP Site U1523 (Seidenstein et al., 2024), and in near-surface sediments in McMurdo Sound (Ward et al., 1987). The low abundance of these warmer-water planktic foraminifera, ranging from zero to six specimens, suggests that the species were likely not living in the Ross Sea but rather were transported by ocean currents to the Ross Sea. Their presence may signal times when the Polar Front (PF) was closer to Antarctica, when the sea surface temperature gradient across the PF was weaker, and/or when the Antarctic Circumpolar Current was weaker (Herold et al., 2012; Hill et al., 2013; Evangelinos et al., 2020; Seidenstein et al., 2024). The sporadic occurrences of

warmer-water planktic foraminifera suggest polar amplification in the Ross Sea during the MCO and MMCT.

We propose that the warmer planktic foraminifera found in the Ross Sea were transported either via warm surface water incursions by way of the Ross Gyre and/or by incursions of deep water (e.g., pCDW) originating from the Southern Ocean. According to previous studies, there is evidence to support the presence of warm water (surface and deep water) closer to the Antarctic margin during the Early to Middle Miocene. For example, during the late Oligocene to Middle Miocene, the Subtropical Front (boundary between cool subtropical waters and subantarctic surface waters) was located at ∼ 60° S latitude (Nelson and Cooke, 2001), which is further south than the Antarctic Polar Front is today at ∼ 56° S. Based on dinocyst assemblages at IODP Hole U1356A from the Wilkes Land margin, Sangiorgi et al. (2018) documented the dominance of phototrophic gonyaulacoid taxa during the MCO and described the MCO as a time of inland retreat of the ice sheet, temperate vegetation, and warm oligotrophic waters. Another study from the Wilkes Land margin (DSDP Site 269) found evidence for a shift in the Polar Front during the late Oligocene to Early Miocene (Evangelinos et al., 2020). At 23.23 Ma (Early Miocene), Evangelinos et al. (2020) note a shift in sedimentological (improved carbonate preservation), geochemical (Nd signature resembling modern CDW), and palynological data (increase in G cysts similar to modern temperate and oligotrophic waters) at DSDP Site 269, suggesting a prolonged expansion of proto-CDW closer to the Wilkes Land margin. Evangelinos et al. (2020) concluded that a weaker frontal system and weaker ACC allowed low-latitude warm waters to be present near the Antarctic margin. Numerical modeling studies (e.g., Herold et al., 2012) also indicate a weaker ACC during this time. Our planktic foraminiferal record from Site U1521 further supports the occasional presence of warmer water as far south as the Ross Sea during the MCO and MMCT.

During the MCO there are multiple intervals of warm planktic foraminiferal occurrences. We note the occurrences of cosmopolitan, subpolar–temperate, and subtropical–temperate species throughout Unit IV (Fig. 7). The presence of these warmer-water invaders coincides with peak warmth 3 (∼ 16.351–16.261 Ma) at ice proximal site AND-2A (Levy et al., 2016). Peak warm episodes are intervals during which the AIS grounding-lines retreated inland of the coastal margin with sediments that are rich in terrestrial palynomorphs and surface water temperatures that are 6–10 °C warmer than today (Levy et al., 2016). We suggest the warm planktics were transported into the Ross Sea during peak warmth 3 under a weaker frontal system. Within Unit III, characterized as the warmest interval of the MCO (Browne et al., 2022), there are three distinct intervals of warm planktic occurrences. First, in core 21 (∼ 16.24–16.23 Ma), there are five samples with warm planktics, including *Paragloborotalia pseudocontinuosa* (cosmopolitan) and *Dentoglobigerina globosa* (subtropical to temperate), that coincide with a peak in NGR interpreted as an interglacial interval rich in mud and poor in biosiliceous sediment. The next pulses of warm planktic foraminifera occur within cores 18 (∼ 16.15 Ma) and 17 (∼ 16.12 Ma), coinciding with generally mud-rich and diatom-poor sediments (interglacial conditions) and two pronounced depleted peaks in $\delta^{18}O_{bf}$ from the eastern Pacific (Holbourn et al., 2014, 2015), suggesting that this was a time of warming and less ice (possibly a peak warm episode not captured at AND-2A). The final pulse of warm planktic foraminifera in the MCO interval at Site U1521 is composed of *Turborotalita quinqueloba* and Globorotallidae and occurs near the top of Unit III within cores 12 and 11 (∼ 15.98–15.96 Ma). We suggest that the absence of subpolar-temperate species after ∼ 16.15 Ma was the consequence of either the northward shift in the frontal system (e.g., Sangiorgi et al., 2018), the establishment of a stronger ACC (e.g., Herold et al., 2012; Evangelinos et al., 2020), and or diminished warm-water incursions due to cooling during the Mi2 glaciation (Miocene Isotope event 2, ∼ 16.0 Ma).

After the MCO and RSU4, warm planktic foraminifera briefly reappear in the Ross Sea during the MMCT. In Unit II (MMCT), no subtropical to temperate species were noted; only cosmopolitan and subpolar to temperate taxa are present in two samples from Core 374-U1521-9R-CC. The identification of warmer-water planktics in the Ross Sea during the MMCT is important as their presence suggests occasional incursions of warm water prior to the major Mi3 glaciation (∼ 13.9–13.8 Ma), which is possibly a cause of ice sheet retreat and the end of RSU4 erosion. We speculate that the presence of warmer-water taxa during the MMCT may suggest a weaker frontal system at ∼ 14.09 Ma (Table 3, Fig. 7). Additionally, the planktic foraminiferal specimens are well preserved and white, whereas the benthic specimens are orange. A possible explanation for the preservation differences is that the benthics are reworked from deglaciation melt and that the planktics are in situ. A future study focused on MMCT interval is needed before any further concrete conclusions can be made.

4.4 Unit IV: Miocene Climatic Optimum and continental shelf progradation

Unit IV (∼ 16.34 to ∼ 16.26 Ma; late Early Miocene) is a complex unit deposited during the early stages of the MCO. Prior to the deposition of Unit IV, the ice sheet grounding line was proximal to or north of Site U1521, causing widespread erosion that created RSU4a (Figs. 8, 9; Marschalek et al., 2021; Pérez et al., 2022). After the erosion of RSU4a, the grounding line retreated, allowing for the deposition of Unit IV. Unit IV comprises 45.17 m of the recovered sediment (total thickness 71.55 m) deposited over ∼ 80 000 years. The sequence suggests two progradational cycles based on the pattern of the natural gamma ray (NGR) record, with higher NGR values corresponding to greater terrigenous mud content and lower NGR values corresponding to greater

biosiliceous content (McKay et al., 2019; Christopoulou et al., 2023). Pérez et al. (2022) noted that during the Early Miocene there were periods of localized marine-based ice margin advances identified from the formation of thick sediment wedges that prograded into the basins. This is likely the case for the deposition of Unit IV, a short-lived progradational event, or events, within a shallow embayment. What makes Unit IV particularly interesting is the combination of the high sedimentation rate, the persistence of relatively abundant and diverse benthic foraminiferal assemblages, and multiple occurrences of warmer-water planktic foraminifera. The benthic biofacies from Unit IV suggest three distinct paleoenvironments: a proximal sub-ice shelf with *Globocassidulina* dominance, a distal sub-ice shelf and shelf progradation with *Uvigerina* dominance, and a transitional open-marine setting with alternating *Uvigerina–Globocassidulina* dominance.

The lower interval of Unit IV (∼ 16.35 to 16.34 Ma) is characterized by biofacies C (*Globocassidulina* > *Uvigerina*) (Fig. 8). We hypothesize that intervals with an abundance of *Globocassidulina subglobosa* are associated with incursions of pCDW as the ice sheet retreated from the outer Ross Sea continental shelf after RSU4a. The $\delta^{18}O_{bf}$ records from the low-latitude Pacific (Holbourn et al., 2014, 2015) show a depletion during this interval, suggesting warmer conditions with a lower ice volume (Fig. 8). Incursions of pCDW are enhanced during a warmer climate (e.g., Colleoni et al., 2018). Additionally, the base of Unit IV contains a sharp increase in clasts recording increased meltwater and deposition of ice-rafted debris as the grounded ice sheet retreated during deglacial warming (McKay et al., 2019). Together, the abundance of *G. subglobosa*, the warmer record with a lower ice volume isotope (Holbourn et al., 2014, 2015; Shevenell et al., 2008), and the increased clast abundance of the lowermost interval of Unit IV (McKay et al., 2019) suggest a proximal sub-ice shelf environment from ∼ 16.35–16.34 Ma.

Within the middle and upper Unit IV (∼ 16.34 to 16.28 Ma), the benthic biofacies shift to an increase in *Uvigerina* relative to *Globocassidulina*. Benthic biofacies D (*Uvigerina*) is the dominant biofacies punctuated by occurrences of biofacies C (*Globocassidulina* > *Uvigerina*), biofacies E (*Globocassidulina* > *Uvigerina* > *Nonionella*), and biofacies F (*Globocassidulina* > *Uvigerina* > *Melonis* > *Anomalinoides*) (Fig. 8). The rise in *Uvigerina* suggests increased current activity (e.g., Antarctic Slope Current and/or bottom currents from basal melt) and enhanced productivity associated with the northward progradation of the continental shelf break during rapid deposition of Unit IV. The $\delta^{18}O_{bf}$ record (Shevenell et al., 2008; Holbourn et al., 2014, 2015) indicates a shift to cooler conditions but not necessarily an increase in ice volume (Fig. 8). Under cooler conditions, enhanced winds may have intensified the Antarctic Slope Current (Thompson et al., 2018; Conte et al., 2021), providing the ideal environmental conditions for *Uvigerina*. Within the middle of Unit IV, a sharp decrease in clast abundance, increasing NGR, and magnetic susceptibility (McKay et al., 2019), together with the rise in *Uvigerina*, suggest a prograding continental shelf in a distal sub-ice shelf environment from ∼ 16.34–16.28 Ma (Fig. 8). The end of the first progradational sequence is marked by the sharp reduction in NGR and magnetic susceptibility, an increase in biosiliceous sediments (McKay et al., 2019), and a decrease in foraminifera, suggesting a transitional open-marine environment at ∼ 16.27 Ma (Fig. 9).

The uppermost interval of Unit IV (∼ 16.28 to 16.27 Ma) records a decrease in *Uvigerina* with an increase in *Globocassidulina*, similar to the base of Unit IV. The benthic biofacies clusters include single occurrences of biofacies C (*Globocassidulina* > *Uvigerina*), biofacies A (*Globocassidulina* – *Nonionella*), and biofacies E (*Globocassidulina* > *Uvigerina* > *Nonionella*) (Fig. 8). The Pacific $\delta^{18}O_{bf}$ records (Holbourn et al., 2014, 2015) (Fig. 8) again suggest a shift to warmer conditions with less ice. The increase in *Globocassidulina* may be due to enhanced pCDW incursions during warmer conditions. The return of foraminifera, dominated by *Globocassidulina*, and peak of NGR mark the second progradational cycle in Unit IV.

We interpret Unit IV and the basal part of Unit III to comprise three progradational sequences (obliquity cycles?). The oldest cycle (lower and middle of Unit IV) is a transgression followed by regression with progradation of muddy and increasingly ice-rafted detritus or debris (IRD) clast-poor sediments. It is remarkable that the in situ calcareous benthic foraminiferal assemblages are persistent, moderately diverse, and well preserved throughout Unit IV due to the dominance of mud-rich sediment and the general absence of corrosive biosiliceous sedimentation. The second cycle of Unit IV is transitional with the overlying Unit III (Fig. 8). The third cycle, at the base of Unit III, contains the same NGR architecture as the previous two cycles of Unit IV. These three progradational cycles probably represent deglacial and interglacial conditions characterized by melting, runoff, and rapid terrigenous sedimentation. Progradation is terminated by short-lived glacial events corresponding with less runoff, open-marine conditions, and biosiliceous sedimentation, as indicated by lower NGR values and fewer or absent foraminifera.

4.5 Unit III: Miocene Climatic Optimum and Mi2 glaciation

Unit III (late Early to Early–Middle Miocene) conformably overlies Unit IV and records the deposition of hemipelagic sediment in an open-marine setting (McKay et al., 2019). The primary difference between Units IV and III is the biosiliceous content and lack of IRD clasts (McKay et al., 2019) deposited during the warmest interval of the MCO (Browne et al., 2022). The sedimentary sequence of Unit III

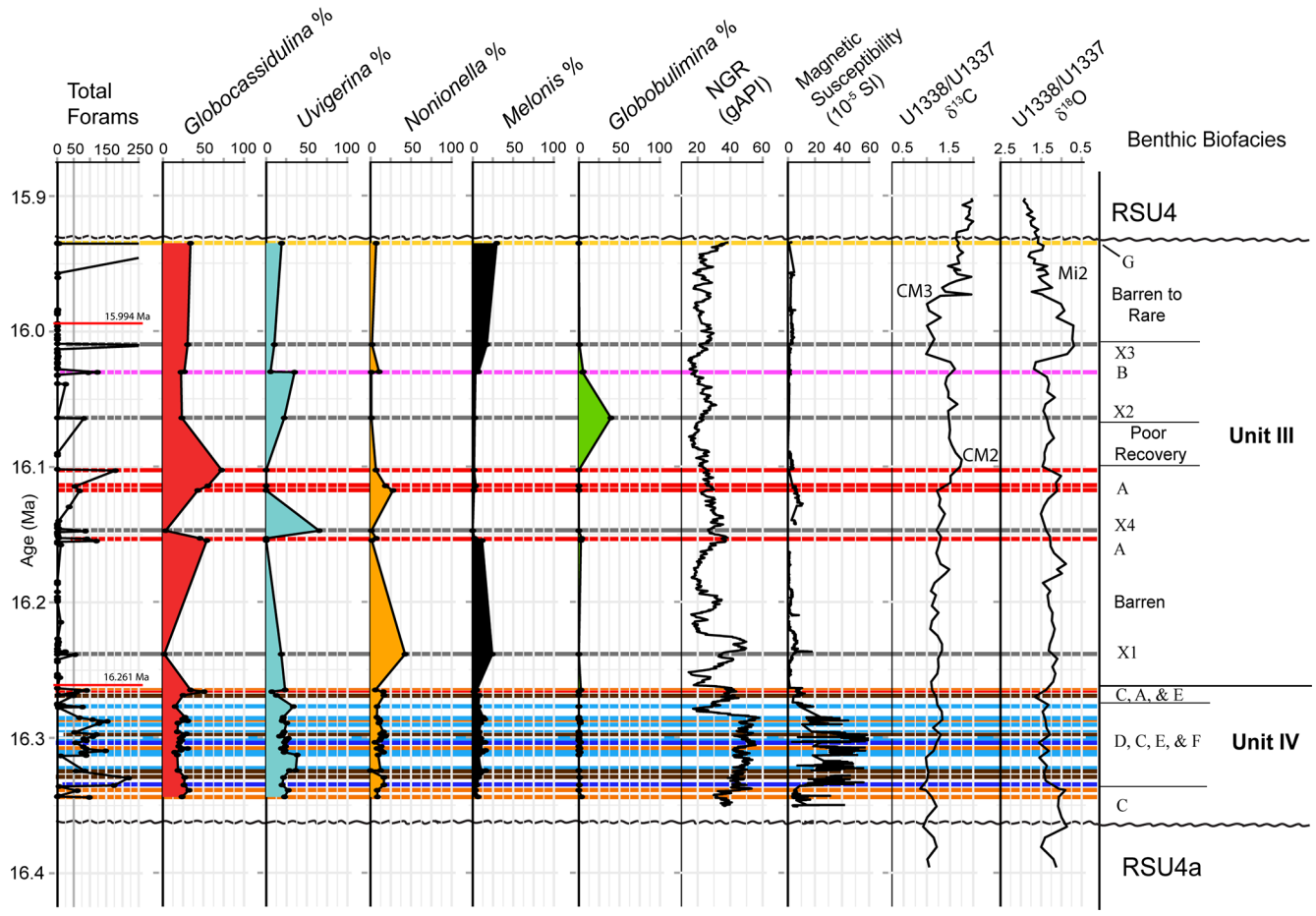

Figure 8. Benthic biofacies of Units IV and III (MCO). From left to right is the total forams; percent of *Globocassidulina, Uvigerina, Nonionella, Melonis*, and *Globobulimina*; NGR (gAPI); and magnetic susceptibility (McKay et al., 2019) compared with low-latitude benthic foraminiferal Pacific $\delta^{13}C_{bf}$ and $\delta^{18}O_{bf}$ records from Sites U1337 and U1338 (Holbourn et al., 2014, 2015). Colored bars represent distinct benthic biofacies, as noted in Figs. 6 and 7. Benthic biofacies are labeled on the right. Paleomagnetic reversals C5Cn.1n/C5Cn.1r (16.261 Ma; GTS2020) and C5Br/C5Cn.1n (15.994 Ma; GTS2020) are marked with a red line in the total forams plot. Ross Sea Unconformity boundaries (RSU4a, RSU4, and RSU3) are marked with squiggly black lines. The Mi2 glaciation and Carbon Maxima events (Flower and Kennett, 1993; Shevenell et al., 2004; Holbourn et al., 2022) are labeled, along with the lithologic units from Site U1521 and interpreted biofacies.

alternates between muds with moderate NGR values, interpreted as interglacial intervals with greater melting and terrigenous runoff, and diatom-rich and diatom-bearing muds with lower NGR values, interpreted as glacial intervals. The sporadic abundances of foraminifera in Unit III are likely due to the corrosive nature of the glacial diatom-rich intervals and better preservation of foraminiferal carbonate in the muddier interglacial intervals of Unit III.

The lower portion of Unit III (~ 16.26 to 16.06 Ma) is dominated by biofacies A (*Globocassidulina* > *Nonionella*) with an occurrence of biofacies X1 (*Nonionella* > *Melonis*) and X4 (*Uvigerina*) (Fig. 8). Biofacies A contains the highest abundances of *Globocassidulina* out of all the biofacies recorded at Site U1521, with *Nonionella* as the secondary taxon (similar to Hillenbrand et al., 2017). The dominance of *Globocassidulina* suggests enhanced incursions of pCDW. Biofacies X1 (~ 16.24 Ma) and X4 (~ 16.15 Ma) are very different from biofacies A due to the near-absence of *Globocassidulina*. We infer the absence of *Globocassidulina* to indicate diminished pCDW incursions onto the Ross Sea continental shelf. In addition to the biofacies, there is an interval at ~ 16.2 Ma during which foraminifera were not present, likely due to dissolution in an open-marine setting.

The middle interval of Unit III (~ 16.06 to 16.0 Ma) records a unique sequence of benthic biofacies characterized by *Globobulimina*. From oldest to youngest are sample X2 (*Globobulimina* > *Globocassidulina* – *Uvigerina*), biofacies B (*Globocassidulina* > *Uvigerina*), and sample X3 (*Globocassidulina*) (Fig. 8). The abundance of *Globobulimina* coincides with higher NGR, with an increase in terrigenous input into the embayment, possibly due to melting. Additionally, this biofacies group correlates to the timing of Carbon Max-

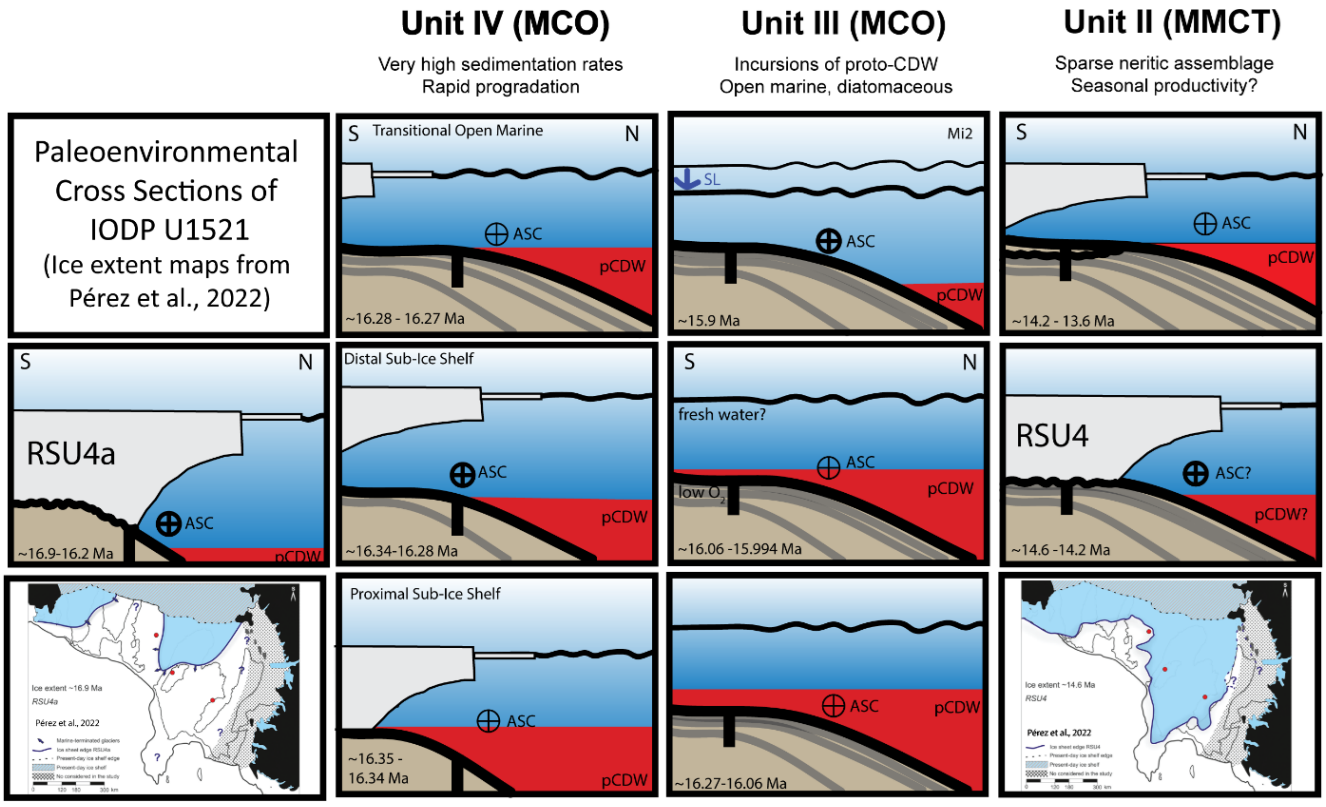

Figure 9. Environmental reconstructions of Units IV, III, and II (age model "b") and RSU4 and RSU4a. Oldest to youngest are shown from the bottom to the top and from left to right. Inset maps at the bottom-left and bottom-right sides are ice sheet edge figures for RSU4a (bottom left) and RSU4 (bottom right) (Pérez et al., 2022). Sea level (SL) is marked with a squiggly black line, proto-Circumpolar Deep water (pCDW) is in red, and the direction and intensity of the Antarctic Slope current (ASC) is noted.

ima 2 (CM2), noted in the isotopic data from Holbourn et al. (2014, 2015, 2022), indicating increased carbon burial. We suggest that the *Globobulimina* interval represents a period of low oxygen within the sediments (elevated refractory organic matter?) and a possible increase in meltwater (water column stratification?) (Fig. 9).

Foraminifera are rare within the upper interval of Unit III (~ 16 to 15.93 Ma). This interval encompasses a decrease in $\delta^{18}O_{bf}$ values that occurs within chron C5Br, often referred to as the Mi2 glaciation (Miller et al., 1991). During Mi2, sea level is estimated to have dropped by ~ 30–40 m (John et al., 2011; Miller et al., 2020). Based on our age model, only one sample, from Core 374-U1521-10R-CC, contains at least 48 benthic specimens for biofacies clustering in the Mi2 interval (Fig. 8). This is the most foraminiferal-rich sample examined from Site U1521 with 481 benthic specimens (no planktics), is characterized by benthic biofacies G (*Globocassidulina* > *Melonis* – *Uvigerina*), and also contains an abundance of echinoderm fragments. The abundance and excellent preservation of benthic foraminifera in this sample suggests low to absent dissolution and pCDW incursions, based on the abundance of *Globocassidulina*. Above this sample, the remainder of the samples in Unit III are barren of foraminifera. Unit III is truncated by the RSU4.

4.6 Unit II: the Middle Miocene Climate Transition and continental shelf aggradation

The Middle Miocene record in Unit II (~ 14.2 to 13.9 Ma; age model "b") was deposited during the Middle Miocene Climate Transition (MMCT) following ice sheet grounding and erosion by RSU4 and before RSU3 (Table 1). By 14.2 Ma, Site U1521 was no longer covered by grounded ice (Fig. 9). Foraminiferal occurrences, including planktics, are in muddy intervals (interglacial); barren samples are in biosiliceous intervals (glacial) (Fig. 4). Our foraminiferal record of the MMCT likely only represents a snapshot of the MMCT during interglacial conditions. Only three samples from Unit II contained enough benthic specimens for biofacies analysis, resulting in one occurrence of biofacies G (*Globocassidulina* > *Melonis*) and two occurrences of biofacies E (*Globocassidulina*) (Figs. 6, 7). Biofacies G and both occurrences of biofacies E are within Core 9 at the base of Unit II. Unit II biofacies are generally characterized by neritic taxa (i.e., *Nonionella* spp., *Melonis* spp., *Epistominella*

vitrea, and *Elphidium* spp.), in addition to *Globocassidulina*, suggesting continued aggradation and shoaling of the shelf with possible pCDW incursions that would have been one of the forcings that ended RSU4.

4.7 Evolution of the Ross Sea continental shelf

Evolution of the Ross Sea continental shelf during the Miocene involved both progradation and aggradation of the shelf edge (Bart, 2003; Chow and Bart, 2003; Bart and De Santis, 2012; Prothro et al., 2018; Anderson et al., 2018; Pérez et al., 2022). Pérez et al. (2022) noted prograding sedimentary wedges from a N–S seismic line (BGR80-008) near Site U1521. The prograding wedges are present before RSU4 and then absent afterwards, indicating that the shelf edge moved northward during deposition of Units IV and III.

Benthic biofacies present in sediments prior to RSU4 (Unit IV and III) are different from the succeeding biofacies (Unit II), as seen by the lower relative abundances of *Uvigerina* and higher relative abundances of *Elphidium* and other taxa characteristic of a neritic paleoenvironment (Table 4). The benthic record of Unit IV, at the base of the study interval, contains the most consistent abundance of *Uvigerina* (Fig. 10). The Unit IV *Uvigerina* interval ($\sim$ 16.34–16.28 Ma) coincides with high magnetic susceptibility (McKay et al., 2019), increasing NGR values (McKay et al., 2019), and more positive low-latitude Pacific $\delta^{18}O_{bf}$ (Holbourn et al., 2014, 2015) and Southern Ocean $\delta^{18}O_{sw}$ values (Shevenell et al., 2008). *Uvigerina* is a shelf-edge-dwelling taxon that thrives under high productivity and enhanced current activity (i.e., Antarctic Slope Current). The seismically imaged prograding wedges (Pérez et al., 2022) suggest that Site U1521 was proximal to the continental shelf edge at the time of the Unit IV deposition, making it an ideal setting for *Uvigerina* to thrive. The high sedimentation rate, in addition to increasing NGR values and high magnetic susceptibility, indicates that terrigenous mud deposition intensified during deglacial conditions following RSU4a, resulting in accelerated progradation (Fig. 8). The bulk of the *Uvigerina* interval may have been deposited within one obliquity cycle. The top of the *Uvigerina*-rich biofacies F coincides with an abrupt decrease in NGR values as the sediment becomes increasingly more biogenic. By $\sim$ 16.27 Ma, *Uvigerina* is no longer the leading primary taxon (except for assemblage X4) as *Globocassidulina* briefly returns to dominance. The massive influx of terrigenous sediment caused the continental shelf break to prograde northward during deposition of Unit IV and the lower part of Unit III (Figs. 9 and 10) and, with it, the environmental conditions favored by *Uvigerina*. Aggradation and shoaling of the continental shelf are supported by the increasing relative abundances of neritic taxa, including *Elphidium*, *Nonionella, Epistominella*, and *Melonis* in Unit III but especially above RSU4 in Unit II.

4.8 Comparison with ANDRILL Site AND-2A

We compare our results from Site U1521 with those from ANDRILL site AND-2A, which has the only published foraminiferal record of the MCO and MMCT in the Ross Sea (Patterson and Ishman, 2012). In addition, extensive work has been done to interpret the paleoenvironment changes during the late Early to Middle Miocene (e.g., Bartek et al., 1991; De Santis et al., 1999; Lewis et al., 2008; Warny et al., 2009; Fielding et al., 2011; Passchier et al., 2011; Gasson et al., 2016; Levy et al., 2016; Halberstadt et al., 2021, 2022). AND-2A is located in the southwestern Ross Sea, $\sim$ 450 km southwest of Site U1521. The foraminiferal record from AND-2A is defined by three benthic assemblage clusters: *Ehrenbergina*, *Ammoelphidiella* subassemblage *Globocassidulina*, *Ammoelphidiella* subassemblage *Nonionella*, and *Cibicides–Cassidulinoides* (Patterson and Ishman, 2012). None of the clusters identified at AND-2A is identified as benthic biofacies at Site U1521. The differing benthic clusters/biofacies between the two sites are due to their locations and paleoenvironmental conditions. AND-2A is ice proximal to the Transantarctic Mountain outlet glaciers draining the East Antarctic Ice Sheet, whereas Site U1521 is an outer continental shelf site of the central Ross Sea, and grounded ice events at this site reflect marine-based ice sheets. Differences in glaciomarine sedimentation, productivity, temperature, and water mass behavior between the two sites would profoundly impact the foraminiferal assemblages. Even though the benthic assemblages differ, paleoenvironmental reconstructions of AND-2A during the Early to Middle Miocene demonstrate parallel changes with those interpreted at Site U1521.

Levy et al. (2016) interpreted a dynamic ice sheet during the Early to Middle Miocene at AND-2A, including three peak warmth events (PW3, PW4, and PW5) (Fig. 10). The peak warming events represent periods when the AIS grounding lines retreated on land (Levy et al., 2016) and correlated to more negative global $\delta^{18}O_{bf}$ values (e.g., Shevenell et al., 2004, 2008; Holbourn et al., 2014, 2015). To compare shelf distal Site U1521 with proximal AND-2A, we followed the paleomagnetic polarity correlation from Marschalek et al. (2021). The correlation is based on chrons C5Cn.1n/C5Cn.1r (16.261 Ma; Gradstein et al., 2020) and C5Br/C5Cn.1n (15.994 Ma; Gradstein et al., 2020) near the base and top of Unit III, respectively. Based on the correlation, PW3 and PW4 are captured at Site U1521, whereas PW5 is lost within Ross Sea Unconformity 4 (RSU4).

Peak warmth event 3 ($\sim$ 16.351 to 16.261 Ma) occurs during the deposition of Unit IV. The sedimentation rate of Unit IV is very high, at $\sim$ 881 m Myr^{-1}, and the lithology is primarily a diamict (McKay et al., 2019). Additionally, the magnetic susceptibility (Fig. 4) and NGR both indicate an increase in terrigenous material input likely from meltwater during deglaciation after RSU4a. Palynological data from Unit IV record an increase in brackish-water algae (i.e., in-

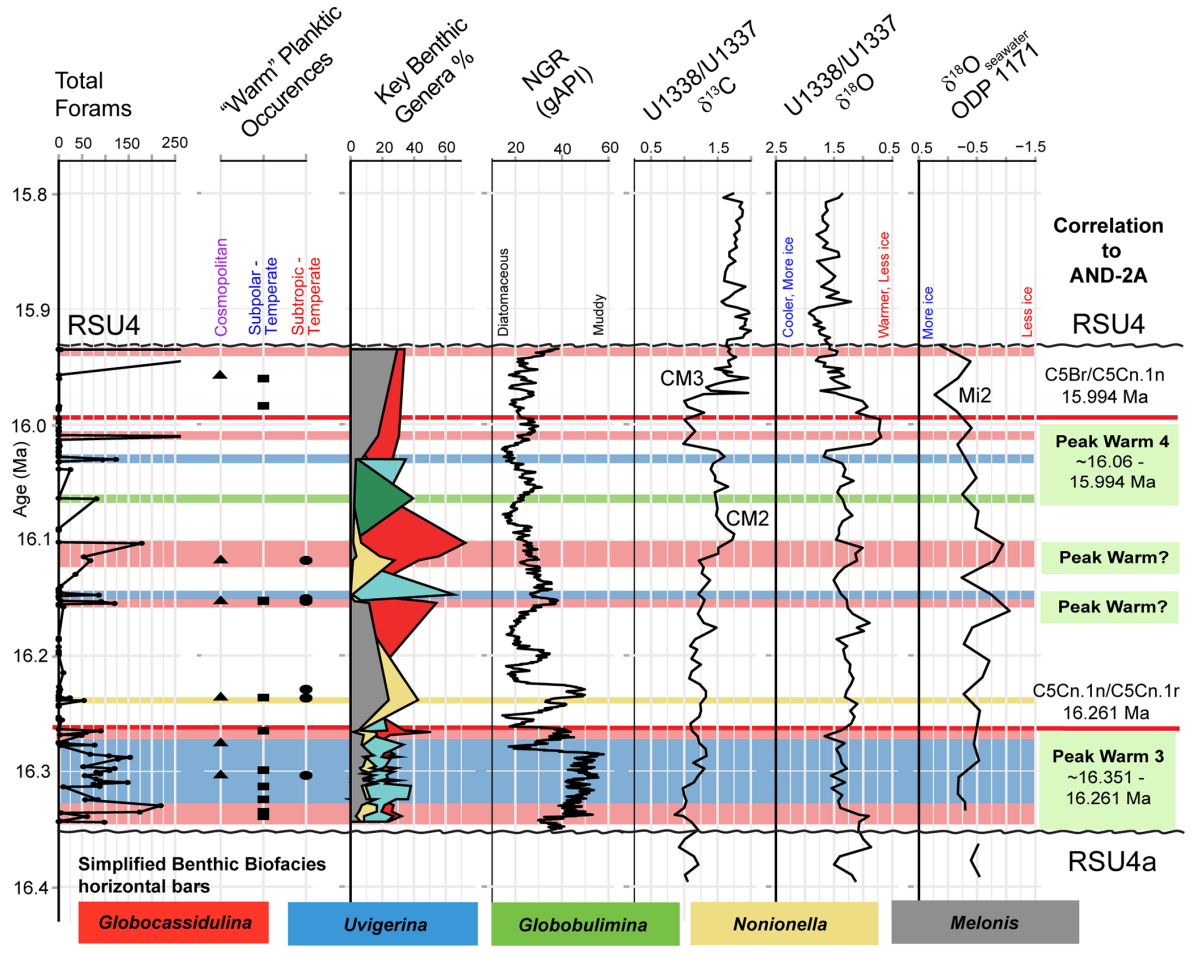

Figure 10. Comparison between IODP Site U1521 data, ODP Site 1171, and AND-2A. From left to right are the total forams; occurrences of warm planktic foraminifera; percent of *Globocassidulina, Uvigerina, Nonionella, Melonis*, and *Globobulimina* samples containing at least 48 specimens of benthic foraminifera; NGR (gAPI) (McKay et al., 2019); $\delta^{13}C_{bf}$ and $\delta^{18}O_{bf}$ records from Sites U1337 and U1338 (Holbourn et al., 2014, 2015, 2022); and $\delta^{18}O_{sw}$ from ODP Site 1171 and the South Tasman Rise (Shevenell et al., 2008). Paleomagnetic datums C5Cn.1n/C5Cn.1r (16.261 Ma; GTS2020) and C5Br/C5Cn.1n (15.994 Ma; GTS2020) used for correlation between Site U1521 and AND-2A are marked with a red line (Marschalek et al., 2021). Peak warm events 4 and 3 from AND-2A (Levy et al., 2016) are noted in green boxes on the right. Colored bars mark benthic biofacies from Site U1521, showing simplified versions with the most abundant taxon only: *Globocassidulina* (red), *Uvigerina* (blue), *Globobulimina* (green), and *Nonionella* (yellow). Ross Sea Unconformity boundaries (RSU4a, RSU4, and RSU3) are marked with squiggly black lines.

creased meltwater) and *Operculodinium* sp., an indicator of warm-water conditions, further suggesting deglaciation during the deposition of Unit IV (Marschalek et al., 2021). A deglaciation interpretation is further supported by the preservation of benthic (*Globocassidulina subglobosa* and *Uvigerina*) and planktic foraminifera (warmer-water invaders). The consistent abundance of *G. subglobosa* suggests that there were pCDW incursions into the Ross Sea embayment during this time. The increase in *Uvigerina* in the middle of Unit IV is likely thriving under a brief cool interval during the PW3 and increased bottom-water currents from meltwater. Last, Unit IV contains warmer-water planktic invaders that were transported into the Ross Sea via pCDW or warm-surface waters (Fig. 10). We suggest Unit IV overall represents a warm interval during the early stages of the MCO with rapid deposition and progradation during deglaciation following RSU4a and driven by warm-water incursions of pCDW and/or warm-surface water.

Between peak warmth events 3 and 4 noted at AND-2A, there is evidence at Site U1521 that suggests the existence of two additional peak warming events at ∼ 16.15 Ma in core 18 and at ∼ 16.12 Ma in core 17. Both of these pulses contain occurrences of warm planktic foraminifera, including subtropical to temperate taxa, that coincide with depleted $\delta^{18}O_{bf}$ values in the Pacific (Holbourn et al., 2014, 2015), as well as depleted $\delta^{18}O_{sw}$ values from Site 1171 (Shevenell et al., 2008), indicating conditions with less ice at this time (Fig. 10). In addition to the presence of warm planktic

foraminifera and supporting isotopic evidence from deep-sea records, the benthic foraminiferal biofacies are dominated by *G. subglobosa*, possibly indicating incursions of pCDW at this time. In contrast, for the interval in between these two warm pulses, there are no warm planktic foraminifera, the benthic biofacies is dominated by *Uvigerina*, and the deep-sea $\delta^{18}O_{bf}$ (Holbourn et al., 2014, 2015) and $\delta^{18}O_{sw}$ (Shevenell et al., 2008) are both enriched, suggesting an increase in ice volume.

Peak warmth event 4 (PW4; ∼ 16.06 to 15.994 Ma) coincides with Cores 15, 14, 13, and 12 in Unit III of Site U1521. Both Cores 15 and 14 have a low recovery of 3% (McKay et al., 2019) and are dominated by *Globobulimina* biofacies (Fig. 10). As previously discussed, *Globobulimina* thrives under low-oxygen conditions that can be produced during warming and stratification (Table 4). In Core 13, *Globobulimina* decreases, while *Globocassidulina* and *Uvigerina* increase, suggesting an increase in pCDW and bottom currents. In Core 12, pCDW incursions become more enhanced, captured by an increase in *Globocassidulina* and the appearance of *Gyroidina* and depleted $\delta^{18}O_{bf}$ values (Holbourn et al., 2014, 2015). All four cores contain evidence supporting a warming event at Site U1521 at the same time as PW4 at AND-2A. PW4 may have helped to trigger the early stages of the Mi2 glaciation captured at the top of Unit III (e.g., Browne et al., 2022).

4.9 Comparison with ODP Site 1171, South Tasman Rise

ODP Site 1171 was cored on the southern tip of the South Tasman Rise (2150 m water depth) beneath the core of the present-day Antarctic Circumpolar Current (Exon et al., 2001). Shevenell et al. (2008) reconstructed the oxygen isotopic composition of seawater ($\delta^{18}O_{sw}$) through the MCO–MMCT interval that was based on a 3 Myr (16.5–13.5 Ma) time series of benthic foraminifer Mg/Ca-derived bottom-water temperatures integrated with benthic $\delta^{18}O$ data from the same samples. Importantly, these $\delta^{18}O_{sw}$ data reveal changes in ice volume that can be compared with Site U1521 data, including the benthic foraminiferal biofacies (Fig. 10).

In our comparison between Site U1521 and ODP Site 1171, we have several key takeaways. First, the *Globocassidulina*-rich intervals (Fig. 10; red intervals) coincide with lower-$\delta^{18}O_{bf}$ values (less ice; Holbourn et al., 2014, 2015). This trend can be seen in the base and at the top of Unit IV, as well as within Unit III. Second, the *Uvigerina*-rich intervals (Fig. 10; blue intervals) coincide with higher-$\delta^{18}O_{bf}$ values (more ice), which are most notable in the middle of Unit IV and in the upper part of Unit III, with the latter coinciding with the Mi2 glaciation (Holbourn et al., 2014, 2015). During the middle of Unit IV, the $\delta^{18}O_{sw}$ values (Shevenell et al., 2008) show a shift from higher to lower values at ∼ 16.3 Ma. We suggest that the change in $\delta^{18}O_{sw}$ values indicates deglaciation and ice sheet retreat associated with a transgression that ultimately truncates the largest Unit IV progradational sequence. Last, we compared the benthic foraminiferal $\delta^{18}O_{bf}$ record from low-latitude Pacific IODP Sites U1337/U1338 (Holbourn et al., 2014, 2015) with the seawater $\delta^{18}O_{sw}$ from ODP Site 1171 (Shevenell et al., 2008). In general, enriched $\delta^{18}O_{sw}$ from Site 1171 coincide with enriched $\delta^{18}O_{bf}$ trends from U1337/U1338 (e.g., see Mi2; Fig. 10), and depleted $\delta^{18}O_{sw}$ from Site 1171 coincides with depleted $\delta^{18}O_{bf}$ trends from U1337/U1338. There is good correspondence between the reconstructed MCO–MMCT seawater $\delta^{18}O_{sw}$ record from the Southern Ocean Site 1171 and glacial–interglacial cyclicity interpreted from the gamma ray and foraminiferal records of Site U1521.

5 Conclusions

The Early to Middle Miocene foraminiferal record from IODP Site U1521 provides key insights into the nature of the Ross Sea during the Miocene Climatic Optimum (MCO; ∼ 16.9–14.7 Ma), as recorded by Units IV and III, and the Middle Miocene Climate Transition (MMCT; ∼ 14.7–13.8 Ma), as recorded by the lower part of Unit II. Our key findings are as follows:

- Foraminifera are not overly abundant at Site U1521; only 46% of the 135 examined samples contain foraminifera. This is not a unique situation in Antarctic marine sediments. Low foraminiferal abundances are the consequence of cold temperatures, low carbonate ion availability in Antarctic waters, and the dissolution of carbonate in biosiliceous-rich sediment.

- A total of 40 samples with at least 48 benthic foraminiferal specimens (average of 114 specimens per sample) reveal seven benthic biofacies clusters dominated by abundant *Globocassidulina* and/or *Uvigerina*, with *Nonionella* and/or *Melonis* as important secondary taxa, based on a Q-mode cluster analysis to develop preliminary interpretations about the environment.

- We hypothesize that *Globocassidulina*, specifically *G. subglobosa*, is a proxy for incursions of waters into the Ross Sea from the Southern Ocean, here referred to as a proto-Circumpolar Deep Water (pCDW). Our hypothesis is supported by the association of *G. subglobosa* with CDW at bathyal to abyssal depths in the Southern Ocean (e.g., Hayward et al., 2007, 2013) and other studies in the Ross Sea showing that *G. subglobosa* is abundant and widespread in distal sub-ice shelf and proximal grounding-zone environments during LGM deglacial and interglacial regimes (Melis and Salvi, 2009; Bart et al., 2016; Prothro et al., 2018; Smith et al., 2019; Majewski et al., 2020), as well as its association with warm nutrient-rich CDW/mCDW in the Amundsen Sea during the early Holocene (Hillenbrand et al., 2017).

- *Uvigerina* is a proxy for conditions common to the continental shelf break, including high productivity and enhanced bottom-current activity (i.e., Antarctic Slope Current). Seismic evidence and the changing relative abundance of *Uvigerina* suggest northward progradation of the continental shelf edge in the area of Site U1521 during the late Early Miocene and Middle Miocene.

- *Globobulimina* is a deep infaunal taxon that thrives on reworked refractory organics and low oxygen. We interpret the increase in *Globobulimina* and in NGR at Site U1521 to be related to meltwater input and stratification during the time of CM2 and peak warmth 4 at AND-2A.

- The presence of neritic benthic foraminifera, including *Elphidium magellanicum*, *Epistominella vitrea*, *Melonis* spp., *Nonionella iridea*, *Ammoelphidiella uniforamina*, and *Rosalina globularis*, suggests that the shelf was much shallower during the Early and Middle Miocene compared with the modern shelf depth. This shallow shelf facilitated the growth and expansion of marine-based ice sheets responsible for widespread unconformities on the Ross Sea continental shelf.

- The presence of sporadic and rare subtropical, temperate, and subpolar planktic foraminifera suggests there were episodic incursions of warm waters into the Ross Sea. The very low abundances of these species indicate that they were likely not living in the Ross Sea. Occurrences of warmer-water planktic foraminiferal species are known in Ross Sea shelf sites spanning the uppermost Oligocene to lower Pleistocene (Leckie and Webb, 1986; Seidenstein et al., 2024; this study), likely corresponding with times warmer than the present when the Antarctic Circumpolar Current was weaker and/or the Polar Front was weaker and further south (Nelson and Cooke, 2001; Herold et al., 2012; Hill et al., 2013; Sangiorgi et al., 2018; Evangelinos et al., 2020). The record of occasional warm-water taxa provide evidence for polar amplification during the MCO and MMCT in the Ross Sea.

- Based on NGR data, Unit IV and the basal part of Unit III are strongly dominated by mud (terrigenous sedimentation) as the continental shelf prograded northward. These mud-dominated sediments record the most persistently abundant and diverse foraminiferal assemblages recovered at Site U1521. The benthic assemblages shift in dominance between *Globocassidulina* and *Uvigerina*, suggesting changes in pCDW relative to productivity and/or current activity.

- Unit IV is characterized by two progradational sequences, perhaps driven by obliquity climate forcing. Together with the basal part of Unit III, these three progradational cycles likely represent deglacial and interglacial conditions characterized by increased melting, runoff, and rapid terrigenous sedimentation. Each progradational cycle was terminated by short-lived glacial events corresponding with less runoff, open-marine conditions, and biosiliceous sedimentation, as revealed by NGR data.

- Unit III was deposited in an open-marine setting. The high variability in the foraminiferal record of Unit III is likely due to the corrosive conditions and carbonate dissolution in diatom-rich sediments, as evidenced by increased foraminiferal fragmentation. The succession of benthic biofacies indicates a dynamic change in dominance, from *Globocassidulina* to *Globobulimina*, caused by a warming event (PW4).

- Moderate NGR values (McKay et al., 2019) in Unit III coincide with interglacial meltwater and terrigenous runoff (muddy) sedimentation, higher foraminiferal abundances, and better preservation. Warmer-water planktic foraminifera also occur in these muddier intervals. Low NGR values coincide with glacial biosiliceous sedimentation and poor foraminiferal abundances and/or preservation.

- Unit II represents the interval between RSU4 erosion and the Mi3 glaciation during the MMCT. The benthic biofacies composition shows a further increase in neritic taxa, including *Elphidium magellanicum*, *Nonionella* spp., *Melonis* spp., and *Epistominella vitrea*, suggesting continued shoaling and aggradation of the Ross Sea continental shelf.

- The presence of warmer-water planktics in the Ross Sea during the MMCT (Unit II) suggests incursions of warm water prior to the major Mi3 glaciation ($\sim$ 13.9–13.8 Ma) and may have contributed to ice sheet retreat and end of RSU4 erosion.

- Site U1521 data correlate well with the peak warming events PW3 and PW4 recorded at the ANDRILL AND-2A site (Levy et al., 2016) and with the $\delta^{18}O_{sw}$ ice volume record generated at the South Tasman Rise ODP Site 1171 (Shevenell et al., 2008).

Appendix A

A1 Abbreviated taxonomy

Taxon lists for most benthic and planktic foraminiferal species found in the Lower and Middle Miocene of the IODP Site U1521 are presented below. Taxa not identified to species level are labeled "sp."; others are labeled "cf." (from Latin, meaning to confer or to be compared with). Key species references with illustrations are cited. For benthic foraminifera, key references focus on the upper Oligocene, Neogene, Quaternary, and Holocene studies

from Antarctica and the Southern Ocean. Additional information about planktic foraminiferal species can be found online at Mikrotax (https://www.mikrotax.org/pforams/index.php?dir=pf_cenozoic, last access: 24 July 2024). Taxa illustrated in this study are in bold.

A2 Benthic foraminiferal taxon list

Alabaminella weddellensis (Earland).

McKnight (1962), p. 126, pl. 21, fig. 137; Hayward et al. (2013), fig. 6.31, 32; Seidenstein et al. (2024), pl. 2, figs. 11a–11b.

Ammodiscus Reuss, sp.

Ammoelphidiella pustulosa (Leckie and Webb).

Leckie and Webb (1986), pp. 1113–1114, pl. 8, figs. 1–12, 14, 15; pl. 21, figs. 14–19; Strong and Webb (2000), pl. 1, fig. 1.

***Ammoelphidiella uniforamina* (D'Agostino)**.
Plate B2, figs. 7a, 7b, 8.

Leckie and Webb (1986), p. 1114, pl. 9, figs. 1–12; pl. 21, figs. 8–13; Strong and Webb (2000), pl. 1, fig. 2.

Ammoelpihidiella Conato and Segre, sp.

***Anomalinoides* cf. *A. macraglabra* (Finlay)**.
Plate B1, figs. 10, 11.

Hornibrook (1961), p. 155, pl. 24, figs. 473–475; Hayward and Buzas (1979), p. 40, pl. 5, figs. 52, 53; Leckie and Webb (1986), p. 1116, pl. 14, figs. 8, 9.

Astrononion echolsi Kennett.

Fillon (1974), pl. 6, figs. 1–3; Ward and Webb (1986), p. 198, pl. 7, fig. 3; Ishman and Domack (1994), pl. II, fig. 3; Majewski (2005), fig. 25.6, 25-7; Majewski (2013), fig. 10.7; Majewski et al. (2018), fig. 4.1; Seidenstein et al. (2024), pl. 2, fig. 10.

Astrononion Cushman and Edwards, sp.

Bolivina d'Orbigny, sp.

Buccella Andersen, sp.

Bulimina d'Orbigny, sp.

Cibicides lobatulus (Walker and Jacob).

Hayward and Buzas (1979), p. 48, pl. 10, figs. 124–126; Osterman and Kellogg (1979), pl. 1, figs. 1–3; Leckie and Webb (1986), p. 1115, pl. 11, figs. 10–12; Ward and Webb (1986), p. 194, pl. 6, figs. 6, 7; Majewski (2005), fig. 24.7, 8; Majewski (2013), fig. 11.5; Majewski et al. (2017), fig. 4.7; fig. 7.8; Strong and Webb (2000), pl. 1, figs. 9,10; Seidenstein et al. (2024), pl. 2, fig. 12.

Cibicides refulgens Montfort.

Hayward and Buzas (1979), p. 48, pl. 10, figs. 130, 131; Osterman and Kellogg (1979), pl. 1, figs. 4, 5; Leckie Leckie and Webb (1986), p. 1115, pl. 11, figs. 13–15; Majewski (2005), fig. 25.1; Majewski (2013), fig. 11.4.

Cibicides temperatus Vella.

Hornibrook (1961), p. 162, pl. 24, figs. 476, 477, 482; Hayward and Buzas (1979), p. 48, pl. 11, figs. 135–137; Leckie and Webb (1986), p. 1115, pl. 11, figs. 1–9; pl. 22, figs. 1–3.

Cibicides Montfort, sp.

Cruciloculina d'Orbigny, sp.

Dentalina d'Orbigny, sp.

Ehrenbergina glabra Cushman.

McKnight (1962), p. 127, pl. 22, fig. 142; Fillon (1974), pl. 5, figs. 9, 10; Osterman and Kellogg (1979), pl. 2, fig. 4; Ward and Webb (1986), p. 194, pl. 6, figs. 9–11; Majewski (2013), fig. 10.13; Seidenstein et al. (2024), pl. 2, fig. 8.

Elphidium cf. *E. excavatum* (Terquem).

Leckie and Webb (1986), pl. 7, fig. 7; Ward and Webb (1986), p. 194, pl. 6, figs. 4, 5; Hayward et al. (1997b), p. 77, pl. 9, figs. 9–18; Hayward et al. (1999), pl. 17, figs. 13–14.

***Elphidium magellanicum* Heron-Allen and Earland**.
Plate B2, figs. 4a, 4b.

Leckie and Webb (1986), p. 1113, pl. 7, figs. 1–4, 6, 8; Strong and Webb (2000), pl. 1, figs. 13, 14.

Elphidium Montfort, sp.

***Epistominella vitrea* Parker**.
Plate B1, figs. 9a, 9b.

Leckie and Webb (1986), p. 1113, pl. 6, figs. 1–5; Ward and Webb (1986), p. 190, pl. 4, figs. 15, 16; Hayward et al. (1999), p. 150, pl. 13, figs. 14–16; Seidenstein et al. (2024), pl. 2, figs. 14a–14b.

Fursenkoina fusiformis (Cushman).

Ishman and Domack (1994), pl. II, fig. 7; Majewski (2005), fig. 23.9–12; Majewski et al. (2017), fig. 7.5, 6.

***Gavelinopsis praegeri* (Heron-Allen and Earland)**.
Plate B1, figs. 12a, 12b.

Hayward et al. (2010), p. 230, pl. 31, figs. 14–21.

***Globobulimina* cf. *G. auriculata* (Bailey)**.
Plate B1, fig. 3.

Leckie and Webb (1986), p. 1112, pl. 5, figs. 15–16.

***Globocassidulina crassa rossensis* Kennett**.
Plate B1, fig. 7.

Fillon (1974), pl. 1, figs. 1-7; Osterman and Kellogg (1979), pl. 2, fig. 2; Leckie and Webb (1986), p. 1115, pl. 12, figs. 7–9.

***Globocassidulina subglobosa* (Brady)**.
Plate B1, figs. 5, 6.

Hayward and Buzas (1979), p. 59, pl. 17, figs. 219, 220; Leckie and Webb (1986), p. 1115, pl. 12, figs. 4–6; Ward and Webb (1986), p. 190, pl. 4, figs. 15, 16; Ward and Webb (1986), p. 198, pl. 4, figs. 10; Majewski et al. (2017), fig.4.4; Majewski et al. (2018), fig. 4.5; Strong and Webb (2001), pl. 1, fig. 18; Hayward et al. (2013), fig. 6.16; Seidenstein et al. (2024), pl. 2, fig. 3.

Globocassidulina Voloshinova, sp.

***Gyroidina danvillensis* Howe and Wallace**.
Plate B2, figs. 10a–10c.

Hayward and Buzas (1979), pp. 59–60, pl. 18, figs. 224, 225; Hayward et al. (2010), p. 218, pl. 26, figs. 13–15; Seidenstein et al. (2024), pl. 3, fig. 15.

Martinotiella communis (d'Orbigny).

Hayward and Buzas (1979), p. 34, pl. 1, figs. 9, 10.

***Melonis affinis* (Reuss)**.
Plate B2, figs. 3, 5a, 5b.

Leckie and Webb (1986), p. 1116, pl. 14, figs. 5–7.

***Melonis barleeanus* (Williamson)**.
Plate B2, figs. 1a, 1b, 2.

Leckie and Webb (1986), p. 1116, pl. 14, figs. 1–4; Strong and Webb (2000), pl. 2, fig. 4; Seidenstein et al. (2024), pl. 3, fig. 7.

Miliolidae Ehrenberg.

Nodosariidae Ehrenberg.

Nonion Montfort, sp.

Nonionella bradii (Chapman).

Fillon (1974), pl. 5, figs. 12, 13; Leckie and Webb (1986), p. 1115, pl. 13, fig. 6; pl. 23, figs. 1, 2 Ishman and Domack (1994), pl. II, figs. 10, 12; Majewski (2005), fig. 25.4, 5; Majewski et al. (2018), fig. 4.3; Strong and Webb (2000), pl. 2, fig. 6; Seidenstein et al. (2024), pl. 2, fig. 5.

***Nonionella iridea* Heron-Allen and Earland**.
Plate B2, fig. 6.

Fillon (1974), pl. 5, figs. 11, 14; Leckie and Webb (1986), p. 1115, pl. 13, figs. 3–4; pl. 23, figs. 5–7; Ward and Webb (1986), p. 198, pl. 7, fig. 4; Ishman and Domack (1994), pl. II, fig. 11; Majewski (2005), fig. 25.2, 3; Majewski (2013), fig. 10.8, 9; Majewski et al. (2018), fig. 4.4; Strong and Webb (2000), pl. 2, 7, 8; Seidenstein et al. (2024), pl. 2, fig. 6.

***Nonionella novozealandica* Cushman**.
Plate B2, fig. 9.

Hornibrook (1961), p. 94, pl. 11, figs. 217, 221; Hayward and Buzas (1979), p. 67, pl. 21, figs. 266–271.

Nonionella Cushman, sp.

Polymorphina sp. d'Orbigny, sp.

Pullenia bulloides (d'Orbigny).

McKnight (1962), p. 128, pl. 22, fig. 143; Hayward and Buzas (1979), p. 72, pl. 24, figs. 303, 304; Leckie and Webb (1986), p. 1115, pl. 13, fig. 10.

Pullenia subcarinata (d'Orbigny).

McKnight (1962), p. 128, pl. 22, fig. 144; Fillon (1974), pl. 6, figs. 7, 8; Leckie and Webb (1986), p. 1116, pl. 13, figs. 7–9; Ward and Webb (1986), p. 198, pl. 7, figs. 5–7; Majewski (2005), fig. 26.1; Strong and Webb (2000), pl. 2, figs. 13, 14; Seidenstein et al. (2024), pl. 3, fig. 10.

Pyrgo Defrance, sp.

Quinqueloculina d'Orbigny, sp.
Plate B1, fig. 4.

Reophax Montfort, sp.

Robertina d'Orbigny, sp.

***Rosalina globularis* d'Orbigny**.
Plate B1, figs. 13a, 13b.

Leckie and Webb (1986), p. 1113, pl. 6, figs. 6–7; Ward and Webb (1986), p. 190, pl. 5, figs. 1–4; Majewski (2005), fig. 24.1–4; Majewski (2013), fig. 11.1; Majewski et al. (2017), fig. 7.1–4; Majewski et al. (2018), fig. 4.14; Strong and Webb (2000), pl. 2, fig. 18; Seidenstein et al. (2024), pl. 2, fig. 7.

***Sphaeroidina bulloides* d'Orbigny**.
Plate B1, fig. 8.

Leckie and Webb (1986), p. 1112, pl. 5, figs. 1–4.

Textularia Defrance, sp.

Triloculina d'Orbigny, sp.

***Uvigerina* cf. *U. fueguina* (Malumián)**.
Plate B1, figs. 1. 2.

Leckie and Webb (1986), p. 1113, pl. 6, figs. 10–12.

Uvigerina d'Orbigny, sp.

A3 Planktic foraminiferal taxon list

***Antarcticella antarctica* (Leckie and Webb)**.
Plate B3, figs. 1a, 1b, 2a, 2b.

Leckie and Webb (1985), p. 66, pl. 1, figs. 1–17, pl. 2, figs. 1–9, pl. 3, figs. 3, 6, 8.

***Dentoglobigerina globosa* (Bolli)**.
Plate B4, figs. 1a–1c, 2.

Chaisson and Leckie (1993), p. 155, pl. 9, fig. 8; Wade et al. (2018), p. 348–350, pl. 11.6, figs. 1–16.

***Globigerinella obesa* (Bolli)**.
Plate B4, figs. 4a, 4b.

Spezzaferri et al. (2018a), pp. 198–200, pl. 6.8, figs. 1–23.

***Globigerinita glutinata* (Egger)**.
Plate B3, figs. 7–10.

Pearson et al. (2018), pp. 436–442, pl. 16.2, figs. 1–16, pl. 16.3, figs. 1–13.

***Globigerinita uvula* (Ehrenberg)**.
Plate B3, fig. 6.

Chaisson and Leckie (1993), p. 157, pl. 10, figs. 1, 7; Pearson et al. (2018), pp. 442–443, pl. 16.3, figs. 14, 15.

***Globoconella* cf. *G. miozea* (Finlay)**.
Plate B4, figs. 8a, 8b, Pl. B5, figs. 1a–1c.

Hornibrook (1961), p. 144, pl. 22, figs. 450, 453, 454; Chaisson and Leckie (1993), p. 162, pl. 4, figs. 12, 17, 18; Lam and Leckie (2020), p. 201, pl. 13, figs. 1–4, pl. 20, figs. 9, 10.

***Globorotaloides suteri* Bolli**.
Plate B5, figs. 3a, 3b.

Chaisson and Leckie (1993), p. 164, pl. 9, fig. 2; Coxall and Spezzaferri (2018), pp. 107–111, pl. 4.9, figs. 1–16, pl. 4.10, figs. 1–16.

***Globoturborotalita druryi* (Akers)**.
Plate B5, figs. 2, 4a, 4b.

Chaisson and Leckie (1993), p. 156, pl. 1, figs. 10, 11; Lam and Leckie (2020), pp. 195–196, pl. 7, figs. 12–19.

***Paragloborotalia* cf. *P. continuosa* (Blow)**.
Plate B4, figs. 7a, 7b.

Leckie et al. (2018), p. 137–138, pl. 5.4, figs. 1–4, 8; Lam and Leckie (2020), p. 197, pl. 9, figs. 12, 15–16.

***Paragloborotalia pseudocontinuosa* (Jenkins)**.
Plate B4, figs. 5a, 5b, 6a, 6b.

Leckie et al. (2018), pp. 157–159, pl. 5.4, figs. 9–16.

***Tenuitella angustiumbilicata* (Bolli)**.
Plate B3, figs. 3, 4.

Chaisson and Leckie (1993), p. 166, pl. 1, fig. 9; Pearson et al. (2018), pp. 443–447, pl. 16.4, figs. 1–16.

***Tenuitella munda* (Jenkins)**.
Plate B3, fig. 5.

Chaisson and Leckie (1993), p. 166, pl. 1, fig. 5; Pearson et al. (2018), pp. 451–454, pl. 16.6, figs. 1–16.

***Trilobatus* cf. *T. quadrilobatus* (d'Orbigny)**.
Plate B4, figs. 3a, 3b.

Spezzaferri et al. (2018b), p. 296, pl. 9.12, figs. 1–20.

***Turborotalita quinqueloba* (Natland)**.
Plate B3, figs. 11a, 11b, 12a, 12b.

Pearson and Kucera (2018), p. 388, pl. 12.2, figs. 1–17; Lam and Leckie (2020), p. 199, pl. 12, figs. 4, 8; Seidenstein et al. (2024), pl. 1, figs. 9, 1

Appendix B

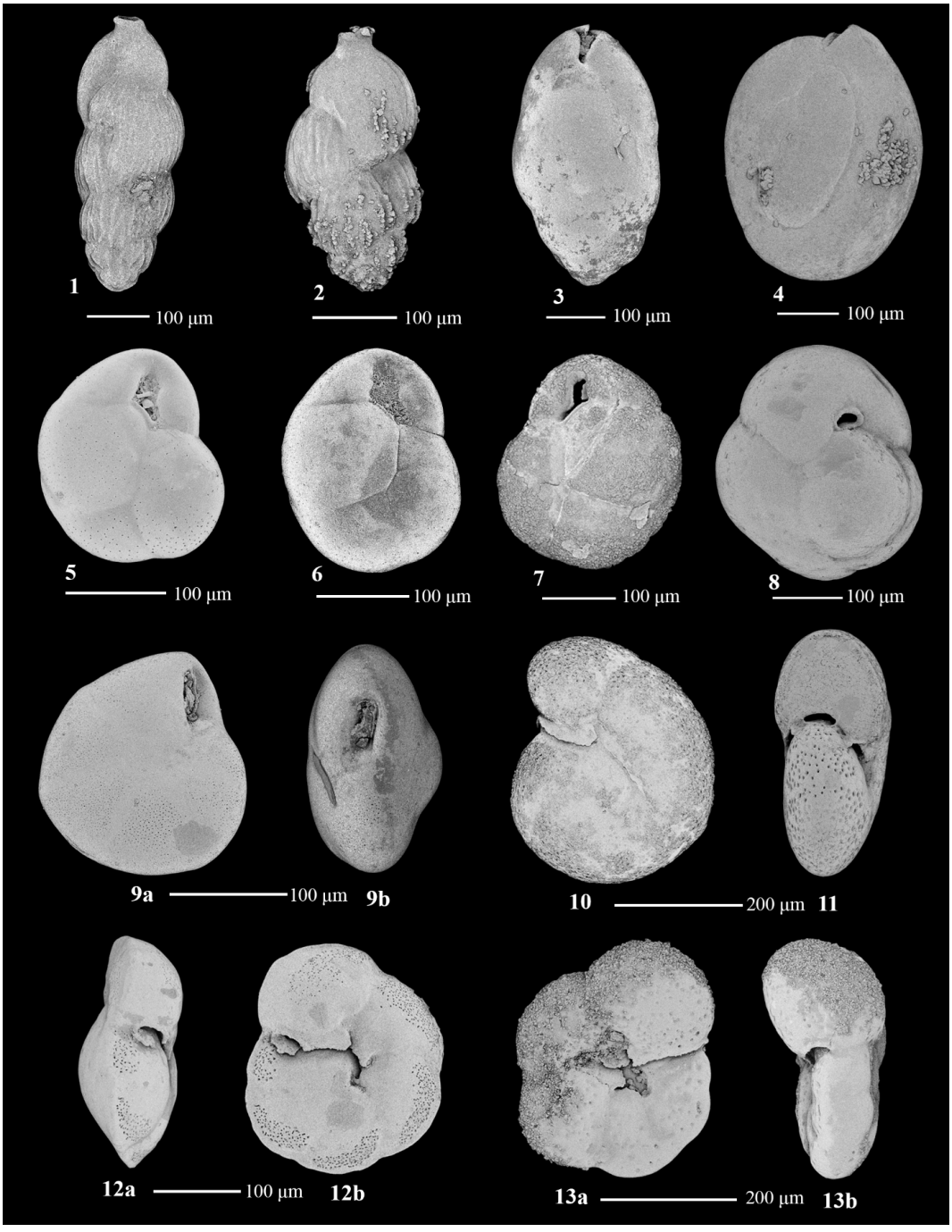

Plate B1. **(1–2)** *Uvigerina* cf. *U. fuegina* (Malumián), U1521A-27R-2W, 10–12 cm. **(3)** *Globobulimina* cf. *G. auriculata* (Bailey), U1521A-14RCC, 0–7 cm. **(4)** *Quinqueloculina* sp. d'Orbigny, U1521A-27R-3W, 10–12 cm. **(5–6)** *Globocassidulina subglobosa* (Brady), U1521-26RCC, 7–12 cm, and U1521A-18R-6W, 34–37 cm. (7) *Globocassidulina crassa rossensis* Kennett, U1521A-27R-2W, 18–20 cm. **(8)** *Sphaeroidina bulloides* d'Orbigny, U1521A-12RCC, 18–23 cm. **(9)** *Epistominella vitrea* Parker, U1521A-13R-6W, 4–7 cm. **(10–11)** *Anomalinoides* cf. *A. macraglabra* (Finlay), U1521A-27R-2W, 10–12 cm, and U1521A-30R-4W, 20–22 cm. **(12)** *Gavelinopsis praegeri* (Heron-Allen and Earland), U1521A-12RCC, 18–23 cm. **(13)** *Rosalina globularis* d'Orbigny, U1521A-27A-3W, 10–12 cm.

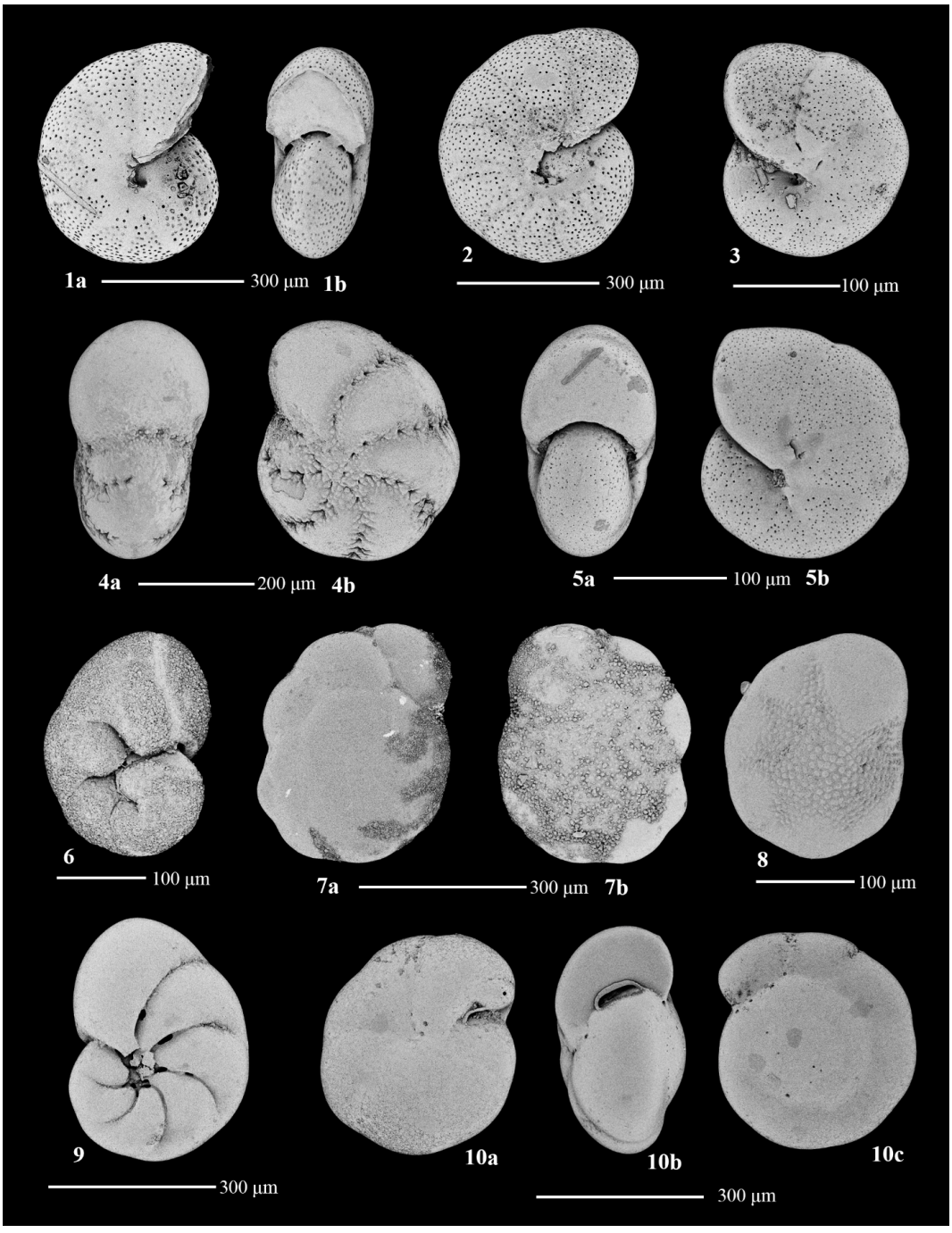

Plate B2. **(1–2)** *Melonis barleeanus* (Williamson), U1521A-12RCC, 18–23 cm. **(3, 5)** *Melonis affinis* (Reuss), U1521A-12RCC, 18–23 cm. **(4)** *Elphidium magellanicum* Heron-Allen and Earland, U1521A-14RCC, 0–7 cm. **(6)** *Nonionella iridea* Heron-Allen and Earland, U1521A-28RCC, 9–12 cm. **(7–8)** *Ammoelphidiella uniforamina* (D'Agostino), U1521A-27R-3W, 10–12 cm, and U1521A-9RCC, 16–20 cm. **(9)** *Nonionella novozealandica* Cushman, U1521A-21RCC, 12–17 cm. **(10)** *Gyroidina danvillensis* Howe and Wallace, U1521A-12RCC, 18–23 cm.

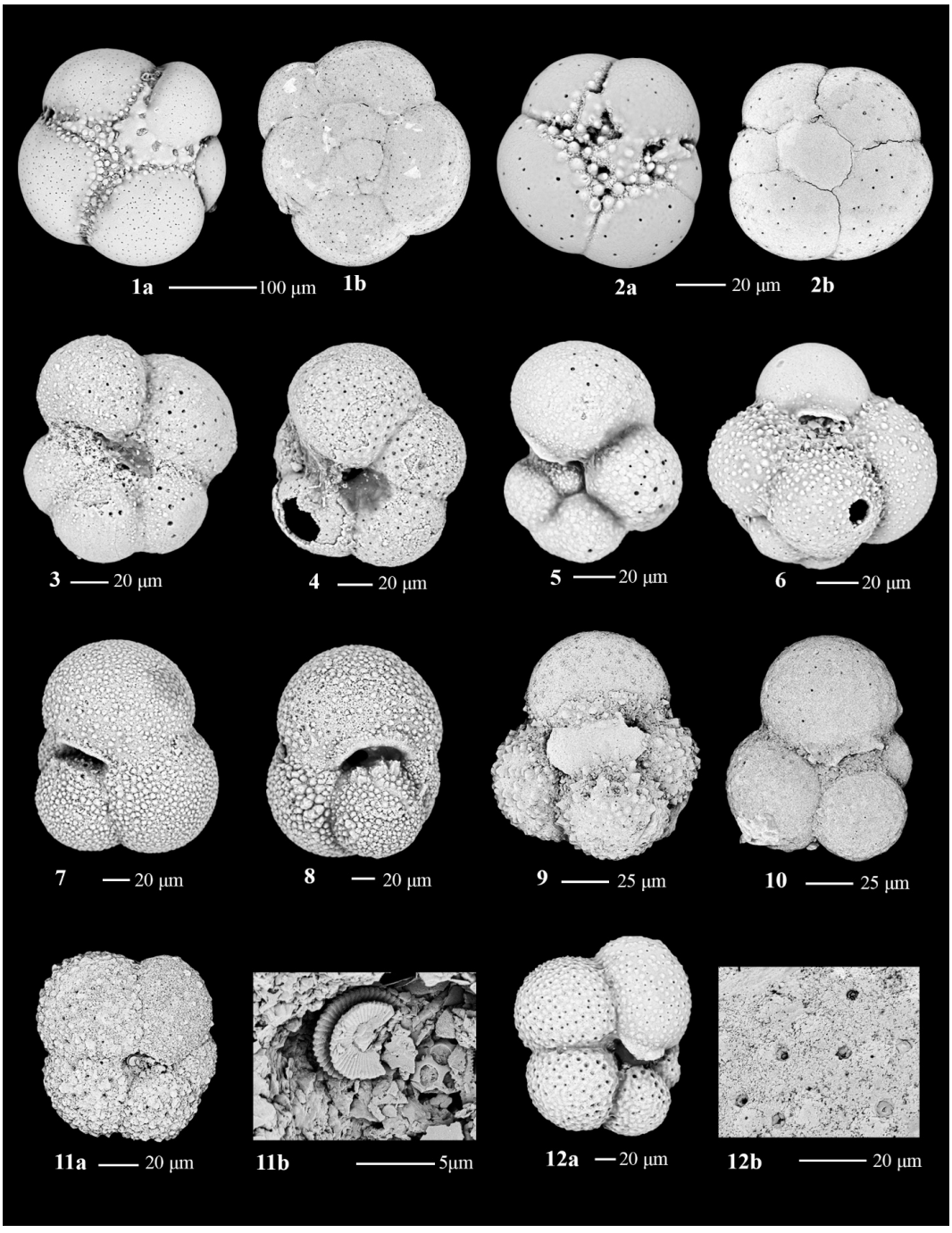

Plate B3. **(1–2)** *Antarcticella antarctica* (Leckie and Webb), U1521A-23R-2W, 20–22 cm, U1521A-9RCC, 8–11 cm. **(3–4)** *Tenuitella angustiumblicata* (Bolli), U1521A-18R-5W, 122–125 cm. **(5)** *Tenuitella munda* (Jenkins), U1521A-18R-5W, 122–125 cm. **(6)** *Globigerinita uvula* (Ehrenberg),U1521A-29R-6W, 20–22 cm. **(7–10)** *Globigerinita glutinata* (Egger), U1521A-18R-5W, 122–125 cm, and U1521A-9RCC, 8–11 cm. **(11–12)** *Turborotalita quinqueloba* (Natland), U1521A-11R-2W, 38–41 cm, and U1521A-12R-1W, 74–77 cm.

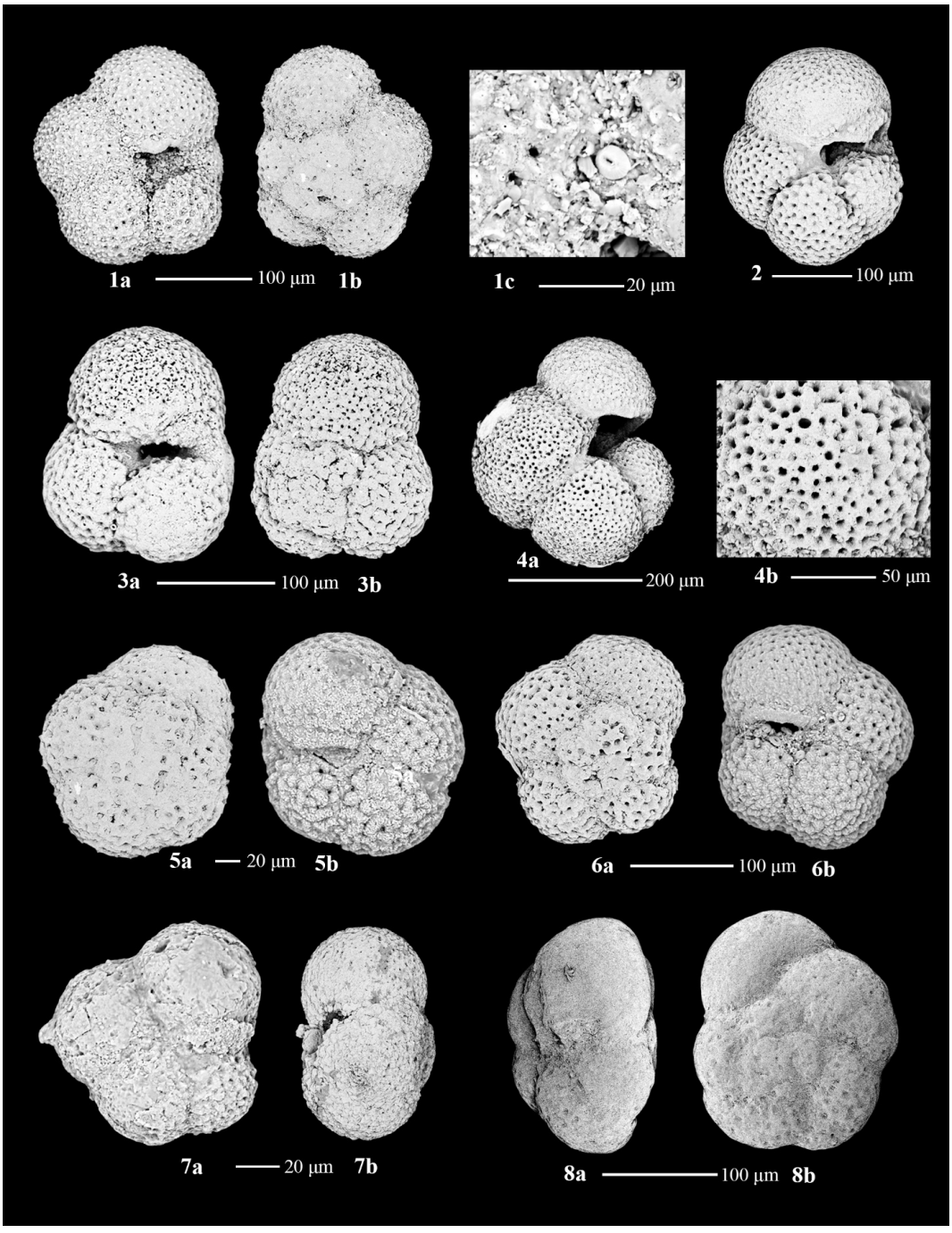

Plate B4. **(1–2)** *Dentoglobigerina globosa* (Bolli), U1521A-21R4W, 89–92 cm, and U1521A-17R-2W, 9–12 cm. **(3)** *Trilobatus* cf. *T. quadrilobatus* d'Orbigny, U1521A-26RCC, 7–12 cm. **(4)** *Globigerinella obesa* (Bolli), U1521A-17R-2W, 9–12 cm. **(5–6)** *Paragloborotalia pseudocontinuosa* (Jenkins). **(7)** *Paragloborotalia* cf. *P. continuosa* (Blow), U1521A-24R2W, 20–22 cm, and U1521A-21R-4W, 89–92 cm. **(8)** *Globoconella* cf. *G. miozea* (Finlay), U1521A-21R-6W, 71–74 cm.

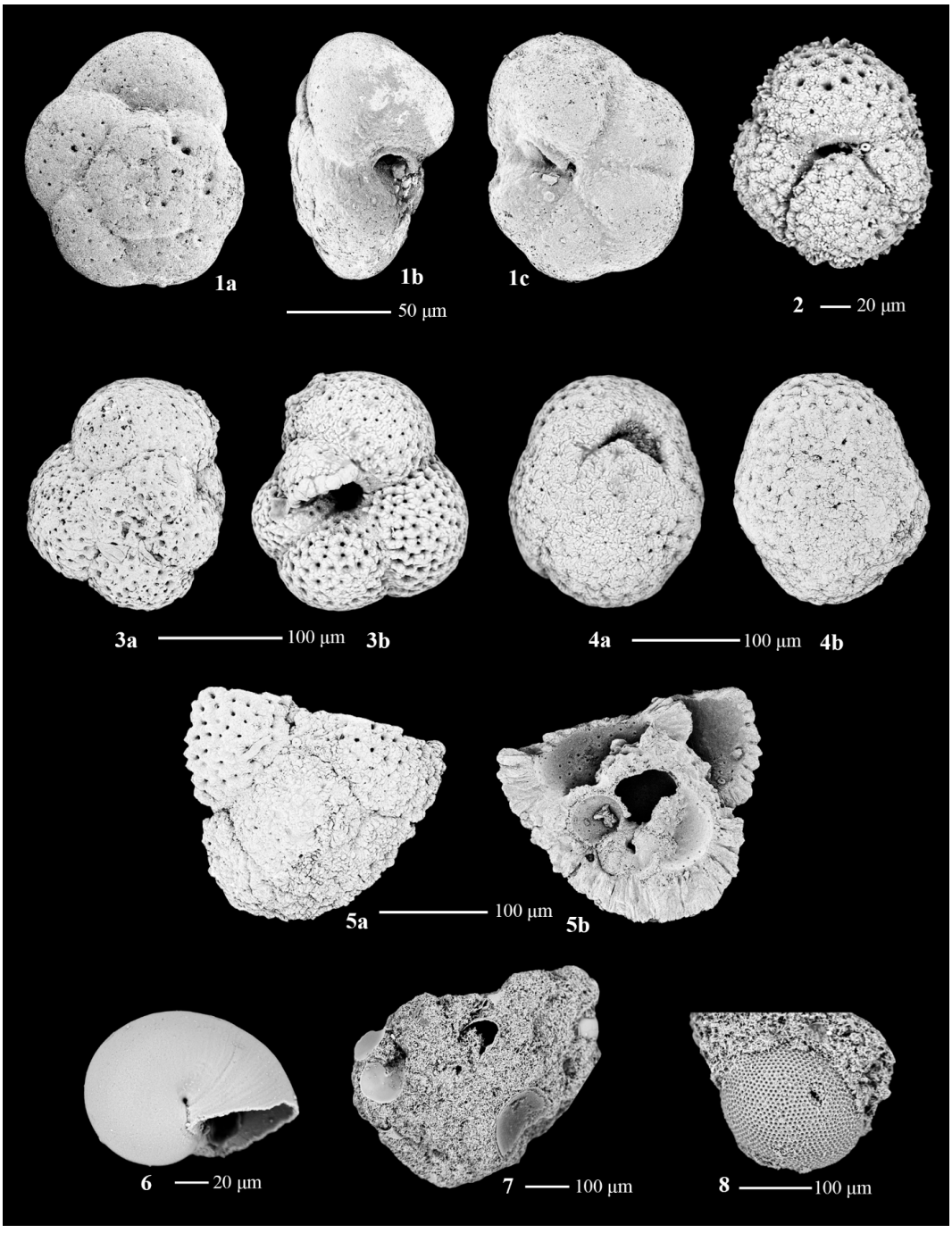

Plate B5. **(1)** *Globoconella* cf. *G. miozea* (Finlay), U1521A-17R-2W, 9–12 cm. **(2, 4)** *Globoturborotalita druryi* (Akers), U1521A-18R-5W, 36–39 cm, and U1521A-26RCC, 7–12 cm. **(3)** *Globorotaloides suteri* (Bolli), U1521A-26RCC, 7–12 cm. **(5)** Unidentified Globorotallidae, U1521A-11R-1W, 15–18 cm. **(6)** Pteropod, U151A-18R-5W, 122–125 cm. **(7)** Clast with pteropods and radiolarians, U151A-18R-5W, 122–125 cm. **(8)** Radiolarian, U151A-18R-5W, 122–125 cm.

Data availability. Data will be published on PANGAEA, the Data Publisher for Earth and Environmental Science online data repository. The data are available upon request to the corresponding author.

Sample availability. Microfossil specimens from this study are stored at the University of Massachusetts Amherst Micropaleontology Lab.

Supplement. The supplement related to this article is available online at: https://doi.org/10.5194/jm-43-383-2024-supplement.

Team list. Jeanine Ash (Department of Earth, Environmental and Planetary Sciences, Rice University, Houston, TX, USA), François Beny (Laboratoire d'Océanologie et de Géosciences, Université de Lille I, Villeneuve d'Ascq, France), Imogen M. Browne (College of Marine Science, University of South Florida, St. Petersburg, FL, USA), Giuseppe Cortese (GNS Science, Lower Hutt, Aotearoa / New Zealand), Laura De Santis (Instituto Nazionale di Oceanografia e di Geofisica Sperimentale (OGS), Trieste, Italy), Justin P. Dodd (Department of Earth, Atmosphere and Environmental Geosciences, Northern Illinois University, DeKalb, IL, USA), Oliver M. Esper (Alfred Wegener Institute, Bremerhaven, Germany), Jenny A. Gales (School of Biological and Marine Sciences, University of Plymouth, Plymouth, UK), David M. Harwood (Earth and Atmospheric Sciences, University of Nebraska, Lincoln, NE, USA), Saki Ishino (Department of Earth and Planetary Sciences, Nagoya University, Nagoya, Japan), Benjamin A. Keisling (Department of Earth, Geographic, and Climate Science, University of Massachusetts, Amherst, MA, USA), Sookwan Kim (Ocean Climate Response and Ecosystem Research Department, Korea Institute of Ocean Science and Technology, Busan, Republic of Korea), Sunghan Kim (Division of Polar Paleoenvironment, Korea Polar Research Institute, Republic of Korea), Denise K. Kulhanek (Institute of Geosciences, Christian Albrecht University of Kiel, Kiel, Germany), Jan Sverre Laberg (Department of Geosciences, UIT – The Arctic University of Norway, Tromsø, Norway), R. Mark Leckie (Department of Earth, Geographic, and Climate Science, University of Massachusetts, Amherst, MA, USA), Robert M. McKay (Antarctic Research Centre, Victoria University of Wellington, Wellington, Aotearoa / New Zealand), Juliane Müller (Alfred Wegener Institute, Bremerhaven, Germany), Molly O. Patterson (Department of Earth Sciences, Binghamton University, State University of New York, Binghamton, NY, USA), Brian W. Romans (Geosciences, Virginia Tech, Blacksburg, VA, USA), Oscar E. Romero (MARUM, University of Bremen, Bremen, Germany), Francesca Sangiorgi (Earth Sciences, University of Utrecht, Utrecht, the Netherlands), Osamu Seki (Institute of Low Temperature Science, Hokkaido University, Sapporo, Hokkaido, Japan), Amelia E. Shevenell (College of Marine Science, University of South Florida, St. Petersburg, FL, USA), Shiv M. Singh (Polar Biology Lab, National Centre for Antarctic and Ocean Research (NCAOR), Goa, India), Isabela M. Cordeiro de Sousa (Instituto de Geociencias, Universidade de Brasília, Brasilia, Brazil), Saiko T. Sugisaki (Marine Geology Research Group, Geological Survey of Japan, Tsukuba, Ibaraki, Japan), Tina van de Flierdt (Department of Earth Science and Engineering, Imperial College London, London, UK), Tim E. van Peer (National Oceanography Centre Southampton, University of Southampton, Southampton, UK), Whenshen Xiao (State Key Laboratory of Marine Geology, Tongji University, Shanghai, China), and Zhifang Xiong (First Institute of Oceanography, State Oceanic Administration, Qingdao, China).

Author contributions. RML came up with the concept for this study and aided in collecting the cores and analyzing some of the samples during IODP Expedition 374. SEB completed the foraminiferal lab work for this study and analyzed the data with help from RML. IMB and AES provided impactful feedback and ran the stable isotopes on *Antarcticella antarctica*. RMM provided valuable feedback and comments on our comparison with ANDRILL AND-2A. DMH provided key information related to the age model.

Competing interests. The contact author has declared that none of the authors has any competing interests.

Disclaimer. Any use of trade, firm, or product names is for descriptive purposes only and does not imply endorsement by the US Government.

Publisher's note: Copernicus Publications remains neutral with regard to jurisdictional claims made in the text, published maps, institutional affiliations, or any other geographical representation in this paper. While Copernicus Publications makes every effort to include appropriate place names, the final responsibility lies with the authors.

Special issue statement. This article is part of the special issue "Advances in Antarctic chronology, paleoenvironment, and paleoclimate using microfossils: Results from recent coring campaigns". It is not associated with a conference.

Acknowledgements. The authors extend their thanks to the IODP Expedition 374 Scientists, crew, and staff for making this study possible. Furthermore, we thank the National Science Foundation (NSF) Graduate Research Fellowship Program for the grant to Samantha E. Bombard. This study has been supported by NSF Collaborative Research: Miocene Climate Extremes, A Ross Sea Perspective (grant no. 1947558 to R. Mark Leckie). We would like to thank Dipa Desai for the initial processing and characterization of many of the samples used in this study. We also thank our two anonymous reviewers, who helped us further sculpt our work. We extend our special gratitude to Francesca Sangiorgi and the editorial staff of the *Journal of Micropalaeontology* (Copernicus Publications) for their assistance and to our University of Massachusetts Amherst (UMass) Micropaleo Lab mates and associates Serena Dameron, Erin Kim, and Julia Seidenstein for their input, feedback, and support. We thank Justin Dodd and Marialena Christopoulou for providing an additional perspective during discussions and Paul Pearson and Bridget Wade for consulting with planktic identification. We thank Michael Jercinovic, Alexan-

der Ribbe, and Zaw Lin for aiding in the scanning electron microscope preparations and imaging.

Financial support. This research has been supported by the National Science Foundation Division of Ocean Sciences (NSF OCE; 14-50528) grant to R. Mark Leckie (grant no. 19747558).

Review statement. This paper was edited by Francesca Sangiorgi and Masao Iwai and reviewed by two anonymous referees.

References

Ainley, D. G. and Jacobs, S. S.: Sea-bird affinities for ocean and ice boundaries in the Antarctic, Deep-Sea Res. Pt. A, 28, 1173–1185, 1981.

Anderson, J. B., Simkins, L. M., Bart, P. J., De Santis, L., Halberstadt, A. R. W., Olivo, E., and Greenwood, S. L.: Seismic and geomorphic records of Antarctic Ice Sheet evolution in the Ross Sea and controlling factors in its behaviour, Geol. Soc. Spec. Publ., 475, 223–240, https://doi.org/10.1144/SP475.5, 2018.

Azetsu-Scott, K., Clarke, A., Falkner, K., Hamilton, J., Jones, E. P., Lee, C., Petrie, B., Prinsenberg, S., Starr, M., and Yeats, P.: Calcium carbonate saturation states in the waters of the Canadian Arctic Archipelago and the Labrador Sea, J. Geophys. Res.-Oceans, 115, C11021, https://doi.org/10.1029/2009JC005917, 2010.

Barrett, P. J. (Ed.): Antarctic Cenozoic history from the MSSTS-1 drillhole, McMurdo Sound: New Zealand Department of Scientific and Industrial Research Miscellaneous Bulletin No. 237, 174 pp., 1986.

Barrett, P. J., Hambrey, M. J., and Robinson, P. R.: Cenozoic glacial and tectonic history from CIROS-1, McMurdo Sound, Int. Symp. Antarct. Earth Sci., 5, 651–656, 1991.

Bart, P. J.: Were West Antarctic Ice Sheet grounding events in the Ross Sea a consequence of East Antarctic Ice Sheet expansion during the middle Miocene?, Earth Planet. Sc. Lett., 216, 93–107, https://doi.org/10.1016/S0012-821X(03)00509-0, 2003.

Bart, P. J. and De Santis, L.: Glacial intensification during the Neogene a review of seismic Stratigraphic evidence from the Ross Sea, Antarctica, continental shelf, Oceanography, 25, 166–183, https://doi.org/10.5670/oceanog.2012.92, 2012.

Bart, P. J., Coquereau, L., Warny, S., and Majewski, W.: *In situ* foraminifera in grounding zone diamict: A working hypothesis, Antarct. Sci., 28, 313–321, https://doi.org/10.1017/S0954102016000055, 2016.

Bartek, L. R., Vail, P. R., Anderson, J. B., Emmet, P. A., and Wu, S.: The effect of Cenozoic Ice Sheet fluctuations on the stratigraphic signature of the Neogene, J. Geophys. Res., 96, 6753–6778, 1991.

Bernhard, J. M., Casciotti, K. L., McIlvin, M. R., Beaudoin, D. J., Visscher, P. T., and Edgcomb, V. P.: Potential importance of physiologically diverse benthic foraminifera in sedimentary nitrate storage and respiration, J. Geophys. Res., 117, G03002, https://doi.org/10.1029/2012JG001949, 2012.

Bornmalm, L.: Taxonomy and paleoecology of late Neogene benthic foraminifera from the Caribbean Sea and eastern equatorial Pacific Ocean, Fossils and Strata, 41, 1–96, 1997.

Browne, I. M., Shevenell, A., Leckie, R. M., Dodd, J. P., Christopoulou, M.-P., Sangiorgi, F., Wubben, E., Prebble, J., Ash, J., van Peer, T. M., Harwood, D. M., Levy, R. H., McKay, R. M., De Santis, L., Kulhanek, D. K., and IODP Expedition 374 Scientists: Antarctic Ice Sheet growth during the Miocene Climatic Optimum, Am. Geophys. Un., Fall Meeting, Chicago, IL, 2022.

Budillon, G., Pacciaroni, M., Cozzi, S., Rivaro, P., Catalano, G., Ianni, C., and Cantoni, C.: An optimum multiparameter mixing analysis of the shelf waters in the Ross Sea, Antarct. Sci., 15, 105–118, https://doi.org/10.1017/S095410200300110X, 2003.

Capotondi, L., Bergami, C., Giglio, F., Langone, L., and Ravaioli, M.: Benthic foraminifera distribution in the Ross Sea (Antarctica) and its relationship to oceanography, B. Soc. Paleontol. Ital., 57, 187–202, https://doi.org/10.4435/BSPI.2018.12, 2018.

Castagno, P., Falco, P., Dinniman, M. S., Spezie, G., and Budillon, G.: Temporal variability of the Circumpolar Deep Water inflow onto the Ross Sea continental shelf, J. Marine Syst., 166, 37–49, https://doi.org/10.1016/j.jmarsys.2016.06.009, 2017.

Chaisson, W. and Leckie, R. M.: High-resolution Neogene planktonic foraminiferal biostratigraphy of Site 806, Ontong Java Plateau (western equatorial Pacific), in: Proceedings of the Ocean Drilling Program, Scientific Results, Vol. 130: College Station, TX (Ocean Drilling Program), edited by: Berger, W., Kroenke, Mayer, L. A., et al., 137–178, 1993.

Chow, J. M. and Bart, P. J.: West Antarctic Ice Sheet grounding events on the Ross Sea outer continental shelf during the middle Miocene, Palaeogeogr. Palaeocl., 198, 169–186, https://doi.org/10.1016/S0031-0182(03)00400-0, 2003.

Christopoulou, M. E., Dodd, J. P., Cassarino, L., Harwood, D. M., Marschalek, J., van de Flierdt, T., Sangiorgi, F., Shevenell, A., McKay, R. M., and De Santis, L.: The Role of the Ice Sheet Dynamics and Ocean Circulation in Nutrient Supply and Diatom Productivity during the Miocene Climatic Optimum in the Ross Sea, Antarctica: Evidence from IODP Site U1521, in: AGU Fall Meeting Abstracts, San Francisco, CA, Vol. 2023, PP24A-07, 2023.

Coccioni, R. and Galeotti, S.: Foraminiferal biostratigraphy and paleoecology of the CIROS-1 Core from McMurdo Sound (Ross Sea, Antarctica), Terra Antarctica, 4, 103–117, 1997.

Colleoni, F., De Santis, L., Siddoway, C. S., Bergamasco, A., Golledge, N. R., Lohmann, G., Passchier, S., and Siegert, M. J.: Spatio-temporal variability of processes across Antarctic ice-bed-ocean interfaces, Nat. Commun., 9, 2289, https://doi.org/10.1038/s41467-018-04583-0, 2018.

Conte, R., Rebesco, M., De Santis, L., Colleoni, F., Bensi, M., Bergamasco, A., Kovacevic, V., Gales, J., Zgur, F., and Accettella, D.: Bottom current control on sediment deposition between the Iselin Bank and the Hillary Canyon (Antarctica) since the late Miocene: an integrated seismic-oceanographic approach, Deep-Sea Res. Pt. I, 176, 103606, https://doi.org/10.1016/j.dsr.2021.103606, 2021.

Corliss, B. H.: Taxonomy of Recent deep-sea benthonic foraminifera from the southeast Indian Ocean, Micropaleontology, 25, 1–19, 1979.

Corliss, B. H.: Distribution of Holocene deep-sea benthonic foraminifera in the southwest Indian Ocean, Deep-Sea Res. Pt. A, 30, 95–117, 1983.

Coxall, H. K. and Spezzaferri, S.: Taxonomy, biostratigraphy, and phylogeny of Oligocene *Catapsydrax, Globorotaloides*, and *Protentelloides*, in: Wade, B. S., Olsson, R. K., Pearson, P. N., Huber, B. T., and Berggren, W. A., Atlas of Oligocene Planktonic Foraminifera, Cushman Foundation Special Publication, 46, 79–124, 2018.

Cummings, V., Hewitt, J., Van Rooyen, A., Currie, K., Beard, S., Thrush, S., Norkko, J., Barr, N., Heath, P., and Halliday, N. J.: Ocean acidification at high latitudes: potential effects on functioning of the Antarctic bivalve *Laternula elliptica*, PLoS One, 6, e16069, https://doi.org/10.1371/journal.pone.0016069, 2011.

D'Agostino, A. and Webb, P.-N.: Interpretation of mid-Miocene to Recent lithostratigraphy and biostratigraphy at DSDP Site 273, Ross Sea, Antarct. J. US, 155, 118–120, 1980.

Dameron, S. N., Leckie, R. M., Harwood, D., Scherer, R., and Webb, P.-N.: Return to the Ross Ice Shelf Project (RISP), Site J-9 (1977–1979): perspectives of West Antarctic Ice Sheet history from Miocene and Holocene benthic foraminifera, J. Micropalaeontol., 43, 187–209, https://doi.org/10.5194/jm-43-187-2024, 2024.

DeConto, R. M. and Pollard, D.: Contribution of Antarctica to past and future sea-level rise, Nature, 531, 591–597, https://doi.org/10.1038/nature17145, 2016.

de Mello, R., Leckie, R. M., Fraass, A. J., and Thomas, E.: Upper Maastrichtian-Eocene benthic foraminiferal biofacies of the Brazilian margin, western South Atlantic, in: Proceedings of the Ninth International Workshop on Agglutinated Foraminifera, edited by: Kaminski, M. and Alegret, L., Grzybowski Foundation Special Publication, 22, 119–161, 2017.

De Santis, L., Prato, S., Brancolini, G., Lovo, M., and Torelli, L.: The Eastern Ross Sea continental shelf during the Cenozoic: Implications for the West Antarctic ice sheet development, Global Planet. Change, 23, 173–196, https://doi.org/10.1016/S0921-8181(99)00056-9, 1999.

Dinniman, M. S., Klinck, J. M., and Smith Jr., W. O.: A model study of Circumpolar Deep Water on the West Antarctic Peninsula and Ross Sea continental shelves, Deep-Sea Res. Pt. II, 28, 1508–1523, https://doi.org/10.1016/j.dsr2.2010.11.013, 2011.

Duchemin, G., Jorissen, F. J., Le Loc'h, F., Andrieux-Loyer, F., Hily, C., and Thouzeau, G.: Seasonal variability of living benthic foraminifera from the outer continental shelf of the Bay of Biscay, J. Sea Res., 59, 297–319, https://doi.org/10.1016/j.seares.2008.03.006, 2008.

Emerson, S. and Bender, M.: Carbon fluxes at the sediment-water interface of the deep-sea: Calcium carbonate preservation, J. Marine Res., 39, 139–162, 1981.

Evangelinos, D., Escutia, C., Etourneau, J., Hoem, F., Bijl, P., Boterblom, W., van de Flierdt, T., Valero, L., Flores, J. A., Rodriguez-Tovar, F. J., Jimenez-Espejo, F. J., Salabarnada, A., and López-Quirós, A.: Late Oligocene-Miocene proto-Antarctic Circumpolar Current dynamics off the Wilkes Land margin, East Antarctica, Global Planet. Change, 191, 103221, https://doi.org/10.1016/j.gloplacha.2020.103221, 2020.

Exon, N. F., Kennett, J. P., Malone, M. J., and the Leg 189 Shipboard Scientific Party: Proceedings of Ocean Drilling Program Initial Report, Vol. 189, Ocean Drill. Program, College Station, TX, https://doi.org/10.2973/odp.proc.ir.189.2001, 2001.

Fielding, C. R., Browne, G. H., Field, B., Florindo, F., Harwood, D. M., Krissek, L. A., Levy, R. H., Panter, K. S., Passchier, S., and Pekar, S. F.: Sequence stratigraphy of the ANDRILL AND-2A drillcore, Antarctica: A long-term, ice-proximal record of Early to Mid-Miocene climate, sea-level, and glacial dynamism, Palaeogeogr. Palaeocl., 305, 337–351, https://doi.org/10.1016/j.palaeo.2011.03.026, 2011.

Fillon, R. H.: Late Cenozoic foraminiferal paleoecology of the Ross Sea, Antarctica, Micropaleontology, 20, 129–151, 1974.

Flower, B. P. and Kennett, J. P.: The middle Miocene ocean/climate transition: H igh-resolution oxygen and carbon isotopic records from DSDP Site 588A, southwest Pacific, Paleoceanography, 8, 811–843, 1993.

Flower, B. P. and Kennett, J. P.: The middle Miocene climatic transition: East Antarctic ice sheet development, deep ocean circulation and global carbon cycling, Palaeogeogr. Palaeocl., 108, 537–555, https://doi.org/10.1016/0031-0182(94)90251-8, 1994.

Flower, B. P. and Kennett, J. P.: Middle Miocene deepwater paleoceanography in the southwest Pacific: Relations with East Antarctic Ice Sheet development, Paleoceanography, 10, 1095–1112, 1995.

Gasson, E., DeConto, R. M., Pollard, D., and Levy, R. H.: Dynamic Antarctic ice sheet during the early to mid-Miocene, P. Natl. Acad. Sci. USA, 113, 3459–3464, https://doi.org/10.1073/pnas.1516130113, 2016.

Gooday, A. J.: Meiofaunal foraminiferans from the bathyal Porcupine Seabight (northeast Atlantic): size structure, standing stock, taxonomic composition, species diversity and vertical distribution in the sediment, Deep-Sea Res. Pt. A, 33, 1345–1373, 1986.

Gooday, A. J.: Benthic foraminifera (Protista) as tools in deep-water palaeoceanography: environmental influences on faunal characteristics, in: Adv. Mar. Biol., edited by: Southward, A. J., Tyler, P. A., Young, C. M., and Fuiman, L. A., 46, 3–90, 2003.

Gooday, A. J. and Hughes, J. A.: Foraminifera associated with phytodetritus deposits at a bathyal site in the northern Rockall Trough (NE Atlantic): seasonal contrasts and a comparison of stained and dead assemblages, Mar. Micropaleontol., 46, 83–110, 2002.

Gradstein, F. M., Ogg, J. G., Schmitz, M. D. and Ogg, G. M. (Eds.): Geologic time scale 2020, Elsevier, https://doi.org/10.1016/C2020-1-02369-3, 2020.

Halberstadt, A. R. W., Chorley, H., Levy, R. H., Naish, T., DeConto, R. M., Gasson, E., and Kowalewski, D. E.: CO_2 and tectonic controls on Antarctic climate and ice-sheet evolution in the mid-Miocene, Earth Planet. Sc. Lett., 564, 116908, https://doi.org/10.1016/j.epsl.2021.116908, 2021.

Halberstadt, A. R. W., Kowalewski, D. E., and DeConto, R. M.: Reconciling persistent sub-zero temperatures in the McMurdo Dry Valleys, Antarctica, with Neogene dynamic marine ice-sheet fluctuations, Geology, 50, 557–561, https://doi.org/10.1130/G49664.1, 2022.

Hammer, Ø., Harper, D. A. T., and Ryan, P. D.: PAST: Paleontological Statistics Software Package for Education and Data Analysis, Palaeontol. Electron., 4, 1–9, http://palaeo-electronica.org/2001_1/past/issue1_01.htm (last access: 8 September 2024), 2001.

Hauck, J., Gerdes, D., Hillenbrand, C.-D., Hoppema, M., Kuhn, G., Nehrke, G., Völker, C. and Wolf-Gladrow, D. A.: Distribution

and mineralogy of carbonate sediments on Antarctic shelves, J. Marine Syst., 90, 77–87, 2012.

Hauck, J., Arrigo, K. R., Hoppema, M., van Dijken, G. L., Völker, C., and Wolf-Gladrow, D. A.: Insignificant buffering capacity of Antarctic shelf carbonates, Global Biogeochem. Cy., 27, 1–10, https://doi.org/10.1029/2011GB004211, 2013.

Hayes, D. E., Frakes, L. A., Barrett, P. J., Burns, D. A., Chen, P.-H., Ford, A. B., Kaneps, A. G., Kemp, E. M., McCollum, D. W., Piper, D. J. W., Wall, R. E., and Webb, P. N.: Initial Reports of the Deep Sea Drilling Project, 28, U.S. Government Printing Office, Washington, 1007 pp., https://doi.org/10.2973/dsdp.proc.28.1975, 1975.

Hayward, B. W. and Buzas, M. A.: Taxonomy and paleoecology of early Miocene benthic foraminifera of northern New Zealand and the North Tasman Sea, Sm. C. Paleob., 36, 154 pp., 1979.

Hayward, B. W., Grenfell, H. R., Pullin, A. D., Reid, C., and Hollis, C. J.: Foraminiferal associations in the upper Waitemata Harbour, Auckland, New Zealand, J. Roy. Soc. New Zeal., 27, 21–51, 1997a.

Hayward, B. W., Hollis, C. J., and Grenfell, H. R.: Recent Elphidiidae (Foraminiferida) of the Southwest Pacific and fossil Elphidiidae of New Zealand, Institute of Geological and Nuclear Sciences Monograph, 16, 166 pp., https://doi.org/10.2113/gsjfr.29.1.90, 1997b.

Hayward, B. W., Grenfell, H. R., Reid, C. M., Hayward, K. A.: Recent New Zealand shallow-water benthic Foraminifera: Taxonomy, ecologic distribution, biogeography, and use in paleoenvironmental assessment, Institute of Geological and Nuclear Sciences Monograph, 21, 258 pp., 1999.

Hayward, B. W., Grenfell, H. R., Sabaa, A. T., and Daymond-King, R.: Biogeography and ecological distribution of shallow-water benthic foraminifera from the Auckland and Campbell Islands, subantarctic southwest Pacific, J. Micropalaeontol., 26, 127–143, https://doi.org/10.1144/jm.26.2.127, 2007.

Hayward, B. W., Grenfell, H. R., Sabaa, A. T., Neil, H. L., and Buzas, M. A.: Recent New Zealand deep-water benthic foraminifera: Taxonomy, ecologic distribution, biogeography, and use in paleoenvironmental assessment, GNS Science Monograph 26, NZ Geological Survey Paleontological Bulletin, 77, 371 pp., ISBN 978-0-478-19777-8, 2010.

Hayward, B. W., Sabaa, A. T., Grenfell, H. R., Neil, H., and Bostock, H.: Ecological distribution of Recent deep-water foraminifera around New Zealand, J. Foramin. Res., 43, 415–442, 2013.

Herold, N., Huber, M., Müller, R. D., and Seton, M.: Modeling the Miocene climatic optimum: Ocean circulation, Paleoceanography, 27, 1–22, https://doi.org/10.1029/2010PA002041, 2012.

Hill, D. J., Haywood, A. M., Valdes, P. J., Francis, J. E., Lunt, D. J., Wade, B. S., and Bowman, V. C.: Paleogeographic controls on the onset of the Antarctic circumpolar current, Geophys. Res. Lett., 40, 5199–5204, https://doi.org/10.1002/grl.50941, 2013.

Hillenbrand, C.-D., Smith, J. A., Hodell, D. A., Greaves, M., Poole, C. R., Kender, S., Williams, M., Andersen, T. J., Jernas, P. E., Elderfield, H., Klages, J. P., Roberts, S. J., Gohl, K., Larter, R. D., and Kuhn, G.: West Antarctic Ice Sheet retreat driven by Holocene warm water incursions, Nature, 547, 43–48, https://doi.org/10.1038/nature22995, 2017.

Hodell, D. A., Kennett, J. P., and Leonard, K. A.: Climatically induced changes in vertical water mass structure of the Vema Channel during the Pliocene: Evidence from DSDP Holes 516A, 517, and 518, in: Initial Reports of the Deep Sea Drilling Project, edited by: Barker, P. F., Carlson, R. L., and Johnson, D. A., National Science Foundation, 72, 907–919, 1983.

Holbourn, A., Kuhnt, W., Lyle, M., Schneider, L., Romero, O., and Andersen, N.: Middle Miocene climate cooling linked to intensification of eastern equatorial Pacific upwelling, Geology, 42, 19–22, https://doi.org/10.1130/G34890.1, 2014.

Holbourn, A., Kuhnt, W., Kochhann, K. G. D., Andersen, N., and Sebastian Meier, K. J.: Global perturbation of the carbon cycle at the onset of the Miocene Climatic Optimum, Geology, 43, 123–126, https://doi.org/10.1130/G36317.1, 2015.

Holbourn, A., Kuhnt, W., Kochhann, K. G. D., Matsuzaki, K. M., and Andersen, N.: Middle Miocene climate–carbon cycle dynamics: Keys for understanding future trends on a warmer Earth?, Underst. Monterey Form. Similar Biosiliceous Units across Sp. Time, 2556, 93–111, https://doi.org/10.1130/2022.2556(05), 2022.

Hönisch, B., Royer, D. L., Breecker, D. O., Polissar, P. J., Bowen, G. J., Ridgwell, A., and The Cenozoic CO_2 Proxy Integration Project (CenCO2PIP) Consortium: Toward a Cenozoic history of atmospheric CO_2, Science, 382, eadi5177, https://doi.org/10.1126/science.adi5177, 2023.

Hornibrook, N. de B.: Tertiary foraminifera from Oamaru district (N.Z.). Part 1 – Systematics and distribution, Paleontol. Bull. N. Z. Geol. Surv., 34, 192 pp., 1961.

Ishman, S. E. and Domack, E. W.: Oceanographic controls on benthic foraminifers from the Bellingshausen margin of the Antarctic Peninsula, Mar. Micropaleontol., 24, 119–155, 1994.

Ishman, S. E. and Szymcek, P.: Foraminiferal Distributions in the Former Larsen-A Ice Shelf and Prince Gustav Channel Region, Eastern Antarctic Peninsula Margin: A Baseline for Holocene Paleoenvironmental Change, Antarct. Penins. Clim. Var. Hist. Paleoenviron. Perspect., 79, 239–260, 2003.

Jacobs, S. S., Gordon, A. L., and Ardai Jr., J. L.: Circulation and melting beneath the Ross Ice Shelf, Science, 203, 439–443, 1979.

John, C. M., Karner, G. D., and Mutti, M.: $\delta^{18}O$ and Marion Plateau backstripping: Combining two approaches to constrain late middle Miocene eustatic amplitude, Geology, 32, 829–832, https://doi.org/10.1130/G20580.1, 2004.

John, C. M., Karner, G. D., Browning, E., Leckie, R. M., Mateo, Z., Carson, B., and Lowery, C.: Timing and magnitude of Miocene eustasy derived from the mixed siliciclastic-carbonate stratigraphic record of the northeastern Australian margin, Earth Planet. Sc. Lett., 304, 455–467, https://doi.org/10.1016/j.epsl.2011.02.013, 2011.

Jorissen, F. J., Fontanier, C., and Thomas, E.: Chapter seven paleoceanographical proxies based on deep-sea benthic foraminiferal assemblage characteristics, Dev. Mar. Geol., 1, 263–325, 2007.

Kellogg, T. B., Truesdale, R. S., and Osterman, L. E.: Late Quaternary extent of the West Antarctic ice sheet: new evidence from Ross Sea Cores, Geology, 7, 249–253, 1979.

Kennett, J. P.: Foraminiferal evidence of a shallow calcium carbonate solution boundary, Ross Sea, Antarctica, Science, 153, 191–193, https://doi.org/10.1126/science.153.3732.191, 1966.

Kennett, J. P.: The Fauna of the Ross Sea: Ecology and Distribution of Foraminifera, New Zealand Department of Scientific and Industrial Research, 186, 1–47, 1968.

Kennett, J. P.: Cenozoic evolution of Antarctic glaciation, the Circum-Antarctic Ocean, and their impact on paleoceanography, J. Geophys. Res., 82, 3843–3860, 1977.

Kim, S., Lee, J. I., McKay, R. M., Yoo, K. C., Bak, Y. S., Lee, M. K., Roh, Y. H., Yoon, H. I., Moon, H. S., and Hyun, C. U.: Late Pleistocene paleoceanographic changes in the Ross Sea: Glacial-interglacial variations in paleoproductivity, nutrient utilization, and deep-water formation, Quaternary Sci. Rev., 239, 10356, https://doi.org/10.1016/j.quascirev.2020.106356, 2020.

Knudsen, K. L., Eiríksson, J., and Bartels-Jónsdóttir, H. B.: Oceanographic changes through the last millennium off North Iceland: Temperature and salinity reconstructions based on foraminifera and stable isotopes, Mar. Micropaleontol., 84, 54–73, 2012.

Kulhanek, D. K., Levy, R. H., Clowes, C. D., Prebble, J. G., Rodelli, D., Jovane, L., Morgans, H. E. G., Kraus, C., Zwingmann, H., Griffith, E. M., Scher, H. D., McKay, R. M., and Naish, T. R.: Revised chronostratigraphy of DSDP Site 270 and late Oligocene to early Miocene paleoecology of the Ross Sea sector of Antarctica, Global Planet. Change, 178, 46–64, https://doi.org/10.1016/j.gloplacha.2019.04.002, 2019.

Lam, A. R. and Leckie, R. M.: Late Neogene and Quaternary diversity and taxonomy of subtropical to temperate planktic foraminifera across the Kuroshio Current Extension, northwest Pacific Ocean, Micropaleontology, 66, 177–268, 2020.

Leckie, R. M. and Olson, H. C.: Foraminifera as proxies for sea-level change on siliciclastic margins, in: Micropaleontologic Proxies for Sea-Level Change and Stratigraphic Discontinuities, edited by: Olson, H. C. and Leckie, R. M., SEPM Society for Sedimentary Geology Special Publication No. 75, 5–19, https://doi.org/10.2110/pec.03.75.0005, 2003.

Leckie, R. M. and Webb, P.-N.: Foraminifera of DSDP Site 270 as indicators of the evolving Ross Sea in the late Oligocene/early Miocene, Antarct. J. US, 15, 117–118, 1980.

Leckie, R. M. and Webb, P.-N.: Late Oligocene-Early Miocene glacial record of the Ross Sea, Antarctica: Evidence from DSDP Site 270, Geology, 11, 578–582, 1983.

Leckie, R. M. and Webb, P.-N.: *Candeina antarctica*, n. sp., and the phylogenetic history and distribution of *Candeina* spp. in the Paleogene-early Neogene of the Southern Ocean, J. Foramin. Res., 15, 65–78, 1985.

Leckie, R. M. and Webb, P.-N.: Late Paleogene and Early Neogene foraminifers of Deep Sea Drilling Project Site 270, Ross Sea, Initial Reports DSDP 90: 1093-1142, Washington, DC, US Government Printing Office, 1986.

Leckie, R. M., Wade, B. S., Pearson, P. N., Fraass, A. J., King, D. J., Olsson, R. K., Premoli Silva, I., Spezzaferri, S., and Berggren, W. A.: Taxonomy, biostratigraphy, and phylogeny of Oligocene and early Miocene *Paragloborotalia* and *Parasubbotina*, in: Atlas of Oligocene Planktonic Foraminifera, edited by: Wade, B. S., Olsson, R. K., Pearson, P. N., Huber, B. T., and Berggren, W. A., Cushman Foundation Special Publication, 46, 125–178, 2018.

Levy, R., Harwood, D., Florindo, F., Sangiorgi, F., Tripati, R., von Eynatten, H., Gasson, E., Kuhn, G., Tripati, A., Deconto, R., Fielding, C., Field, B., Golledge, N., McKay, R., Naish, T., Olney, M., Pollard, D., Schouten, S., Talarico, F., Warny, S., Willmott, V., Acton, G., Panter, K., Paulsen, T., Taviani, M., Askin, R., Atkins, C., Bassett, K., Beu, A., Blackstone, B., Browne, G., Ceregato, A., Cody, R., Cornamusini, G., Corrado, S., Del Carlo, P., Di Vincenzo, G., Dunbar, G., Falk, C., Frank, T., Giorgetti, G., Grelle, T., Gui, Z., Handwerger, D., Hannah, M., Harwood, D. M., Hauptvogel, D., Hayden, T., Henrys, S., Hoffmann, S., Iacoviello, F., Ishman, S., Jarrard, R., Johnson, K., Jovane, L., Judge, S., Kominz, M., Konfirst, M., Krissek, L., Lacy, L., Maffioli, P., Magens, D., Marcano, M. C., Millan, C., Mohr, B., Montone, P., Mukasa, S., Niessen, F., Ohneiser, C., Passchier, S., Patterson, M., Pekar, S., Pierdominici, S., Raine, I., Reed, J., Reichelt, L., Riesselman, C., Rocchi, S., Sagnotti, L., Sandroni, S., Schmitt, D., Speece, M., Storey, B., Strada, E., Tuzzi, E., Verosub, K., Wilson, G., Wilson, T., Wonik, T., and Zattin, M.: Antarctic ice sheet sensitivity to atmospheric CO_2 variations in the early to mid-Miocene, P. Natl. Acad. Sci. USA, 113, 3453–3458, https://doi.org/10.1073/pnas.1516030113, 2016.

Lewis, A. R., Marchant, D. R., Ashworth, A. C., Hedenäs, L., Hemming, S. R., Johnson, J. V., Leng, M. J., Machlus, M. L., Newton, A. E., Raine, J. I., Willenbring, J. K., Williams, M., and Wolfe, A. P.: Mid-Miocene cooling and the extinction of tundra in continental Antarctica, P. Natl. Acad. Sci. USA, 105, 10676–10680, https://doi.org/10.1073/pnas.0802501105, 2008.

Lipps, J. H. and Krebs, W. N.: Planktonic foraminifera associated with Antarctic sea ice, J. Foramin. Res., 4, 80–85, 1974.

Mackensen, A. and Berggren, W. A.: Paleogene benthic foraminifers from the southern Indian Ocean (Kerguelen Plateau): Biostratigraphy and paleoecology, in: Proceedings of the Ocean Drilling Program, edited by: Wise Jr., S. W. and Schlich, R., 120, 603–630, 1992.

Mackensen, A., Grobe, H., Kuhn, G., and Fu, D. K.: Benthic foraminiferal assemblages from the eastern Weddell Sea between 68 and 73 S: Distribution, ecology and fossilization potential, Mar. Micropaleontol., 16, 241–283, 1990.

Majewski, W.: Benthic foraminiferal communities: Distribution and ecology in Admiralty Bay, King George Island, West Antarctica, Pol. Polar Res., 26, 159–214, 2005.

Majewski, W.: Benthic foraminifera from Pine Island and Ferrero bays, Amundsen Sea, Pol. Polar Res., 34, 169–200, 2013.

Majewski, W., Wellner, J. S., and Anderson, J. B.: Environmental connotations of benthic foraminiferal assemblages from coastal West Antarctica, Mar. Micropaleontol., 124, 1–15, https://doi.org/10.1016/j.marmicro.2016.01.002, 2016.

Majewski, W., Tatur, A., Witkowski, J., and Gazdzicki, A.: Rich shallow-water benthic ecosystem in Late Miocene East Antarctica (Fisher Bench Fm, Prince Charles Mountains), Mar. Micropaleontol., 133, 40–49, https://doi.org/10.1016/j.marmicro.2017.06.002, 2017.

Majewski, W., Bart, P. J., and McGlannan, A. J.: Foraminiferal assemblages from ice-proximal paleo-settings in the Whales Deep Basin, eastern Ross Sea, Antarctica, Palaeogeogr. Palaeocl., 493, 64–81, https://doi.org/10.1016/j.palaeo.2017.12.041, 2018.

Majewski, W., Prothro, L. O., Simkins, L. M., Demianiuk, E. J., and Anderson, J. B.: Foraminiferal patterns in deglacial sediment in the western Ross Sea, Antarctica: Life near grounding lines, Paleoceanogr. Paleocl., 35, 1–24, https://doi.org/10.1029/2019PA003716, 2020.

Majewski, W., Holzmann, M., Gooday, A. J., Majda, A., Mamos, T., and Pawlowski, J.: Cenozoic climatic changes drive evolution and dispersal of coastal benthic foraminifera in the Southern Ocean, Sci. Rep., 11, 19869, https://doi.org/10.1038/s41598-021-99155-6, 2021.

Marschalek, J. W., Zurli, L., Talarico, F., van de Flierdt, T., Vermeesch, P., Carter, A., Beny, F., Bout-Roumazeilles, V., Sangiorgi, F., Hemming, S. R., Pérez, L. F., Colleoni, F., Prebble, J. G., van Peer, T. E., Perotti, M., Shevenell, A. E., Browne, I., Kulhanek, D. K., Levy, R., Harwood, D., Sullivan, N. B., Meyers, S. R., Griffith, E. M., Hillenbrand, C.-D., Gasson, E., Siegert, M. J., Keisling, B., Licht, K. J., Kuhn, G., Dodd, J. P., Boshuis, C., De Santis, L., McKay, R. M., and IODP Expedition 374 Scientists: A large West Antarctic Ice Sheet explains early Neogene sea-level amplitude, Nature, 600, 450–455, https://doi.org/10.1038/s41586-021-04148-0, 2021.

McCorkle, D. C., Corliss, B. H., and Farnham, C. A.: Vertical distributions and stable isotopic compositions of live (stained) benthic foraminifera from the North Carolina and California continental margins, Deep-Sea Res. Pt. I, 44, 983–1024, 1997.

McKay, R. M., De Santis, L., Kulhanek, D. K., Ash, J. L., Beny, F., Browne, I. M., Cortese, G., Cordeiro de Sousa, I. M., Dodd, J. P., Esper, O. M., Gales, J. A., Harwood, D. M., Ishino, S., Keisling, B. A., Kim, S., Kim, S., Laberg, J. S., Leckie, R. M., Müller, J., Patterson, M. O., Romans, B. W., Romero, O. E., Sangiorgi, F., Seki, O., Shevenell, A. E., Singh, S. M., Sugisaki, S. T., van de Flierdt, T., van Peer, T. E., Xiao, W., and Xiong, Z.: Ross Sea West Antarctic Ice Sheet History, Proceedings of the International Ocean Discovery Program, 374, College Station, TX (International Ocean Discovery Program), https://doi.org/10.14379/iodp.proc.374.2019, 2019.

McKay, R. M., Escutia, C., De Santis, L., Donda, F., Duncan, B., Gohl, K., Gulick, S., Hernández-Molina, J., Hillenbrand, C.-D., and Hochmuth, K.: Cenozoic history of Antarctic glaciation and climate from onshore and offshore studies, in: Antarctic Climate Evolution, edited by: Florindo, F., Siegert, M., De Santis, L., and Naish, T., 41–164, Elsevier, https://doi.org/10.1016/B978-0-12-819109-5.00008-6, 2022.

McKnight Jr., W. M.: The distribution of foraminifera off parts of the Antarctic coast, Bulletins of American Paleontology, 44, 65–158, 1962.

Melis, R. and Salvi, G.: Late Quaternary foraminiferal assemblages from western Ross Sea (Antarctica) in relation to the main glacial and marine lithofacies, Mar. Micropaleontol., 70, 39–53, https://doi.org/10.1016/j.marmicro.2008.10.003, 2009.

Melis, R., Capotondi, L., Torricella, F., Ferretti, P., Geniram, A., Hong, J. K., Kuhn, G., Khim, B.-K., Kim, S., Malinverno, E., Yoo, K. C., and Colizza, E.: Last Glacial Maximum to Holocene paleoceanography of the northwestern Ross Sea inferred from sediment core geochemistry and micropaleontology at Hallett Ridge, J. Micropalaeontol., 40, 15–35, https://doi.org/10.5194/jm-40-15-2021, 2021.

Miller, K. G., Fairbanks, R. G., and Mountain, G. S.: Tertiary oxygen isotope synthesis, sea level history, and continental margin erosion, Paleoceanography, 2, 1–19, 1987.

Miller, K. G., Wright, J. D., and Fairbanks, R. G.: Unlocking the ice house: Oligocene-Miocene oxygen isotopes, eustasy, and margin erosion, J. Geophys. Res., 96, 6829–6848, https://doi.org/10.1029/90JB02015, 1991.

Miller, K. G., Browning, J. V., John Schmelz, W., Kopp, R. E., Mountain, G. S. and Wright, J. D.: Cenozoic sea-level and cryospheric evolution from deep-sea geochemical and continental margin records, Sci. Adv., 6, eaaz1346, https://doi.org/10.1126/sciadv.aaz1346, 2020.

Nelson, C. S. and Cooke, P. J.: History of oceanic front development in the New Zealand sector of the Southern Ocean during the Cenozoic – A synthesis, New Zeal. J. Geol. Geop., 44, 535–553, https://doi.org/10.1080/00288306.2001.9514954, 2001.

Orsi, A. H. and Wiederwohl, C. L.: A recount of Ross Sea waters, Deep-Sea Res. Pt. II, 56, 778–795, https://doi.org/10.1016/j.dsr2.2008.10.033, 2009.

Osterman, L. E. and Kellogg, T. B.: Recent benthic foraminiferal distributions from the Ross Sea, Antarctica; relation to ecologic and oceanographic conditions, J. Foramin. Res., 9, 250–269, https://doi.org/10.2113/gsjfr.9.3.250, 1979.

Passchier, S., Browne, G., Field, B., Fielding, C. R., Krissek, L. A., Panter, K., and Pekar, S. F.: Early and middle Miocene Antarctic glacial history from the sedimentary facies distribution in the AND-2A drill hole, Ross Sea, Antarctica, Geol. Soc. Am. Bull., 123, 2352–2365, https://doi.org/10.1130/B30334.1, 2011.

Patterson, M. O. and Ishman, S. E.: Neogene benthic foraminiferal assemblages and paleoenvironmental record for McMurdo Sound, Antarctica, Geosphere, 8, 1331–1341, https://doi.org/10.1130/GES00771.1, 2012.

Pearson, P. N. and Kucera, M.: Taxonomy, biostratigraphy, and phylogeny of Oligocene *Turborotalita*, in: Atlas of Oligocene Planktonic Foraminifera, edited by: Wade, B. S., Olsson, R. K., Pearson, P. N., Huber, B. T., and Berggren, W. A., Cushman Foundation Special Publication, 46, 385–392, 2018.

Pearson, P. N., Wade, B. S., and Huber, B. T.: Taxonomy, biostratigraphy, and phylogeny of Oligocene Globigerinitidae (*Dipsidripella, Globigerinita*, and *Tenuitella*), in: Atlas of Oligocene Planktonic Foraminifera, edited by: Wade, B. S., Olsson, R. K., Pearson, P. N., Huber, B. T., and Berggren, W. A., Cushman Foundation Special Publication, 46, 429–458, 2018.

Pérez, L. F., Santis, L. De, McKay, R. M., Larter, R. D., Ash, J., Phil, J., Böhm, G., Brancatelli, G., Browne, I., Colleoni, F., Dodd, J. P., Geletti, R., Harwood, D. M., Kuhn, G., Laberg, J. S., Leckie, R. M., Levy, R. H., Marschalek, J., Mateo, Z., Naish, T. R., Sangiorgi, F., Shevenell, A. E., Sorlien, C. C., Van De Flierdt, T., and Discovery, I. O.: Early and middle Miocene ice sheet dynamics in the Ross Sea: Results from integrated core-log-seismic interpretation, GSA Bull., 348–370, https://doi.org/10.1130/B35814.1, 2022.

Peterson, L. C.: Recent abyssal benthic foraminiferal biofacies of the eastern equatorial Indian Ocean, Mar. Micropaleontol., 8, 479–519, 1984.

Peterson, L. C. and Lohmann, G. P.: Major change in Atlantic dee and bottom waters 700,000 yr ago: Benthonic foraminiferal evidence from the South Atlantic, Quaternary Res., 17, 26–38, 1982.

Poag, C. W.: Ecologic atlas of benthic foraminifera of the Gulf of Mexico, Hutchinson Ross Publishing Co., 174 pp., 1981.

Pritchard, H., Ligtenberg, S. R. M., Fricker, H. A., Vaughan, D. G., Van den Broeke, M. R., and Padman, L.: Antarctic ice-sheet loss driven by basal melting of ice shelves, Nature, 484, 502, https://doi.org/10.1038/nature10968, 2012.

Prothro, L. O., Simkins, L. M., Majewski, W., and Anderson, J. B.: Glacial retreat patterns and processes determined from integrated sedimentology and geomorphology records, Mar. Geol., 395, 104–119, https://doi.org/10.1016/j.margeo.2017.09.012, 2018.

Roberts, A. P., Wilson, G. S., Harwood, D. M., and Verosub, K. L.: Glaciation across the Oligocene–Miocene boundary in southern

McMurdo Sound, Antarctica: new chronology from the CIROS-1 drill hole, Palaeogeogr. Palaeoclimatol., 198, 113–130, 2003.

Sachs, O., Sauter, E. J., Schlüter, M., Rutgers van der Loeff, M. M., Jerosch, K., and Holby, O.: Benthic organic carbon flux and oxygen penetration reflect different plankton provinces in the Southern Ocean, Deep Sea Res. Pt. I, 56, 1319–1335, https://doi.org/10.1016/j.dsr.2009.02.003, 2009.

Sanders, H. L.: Marine benthic diversity: A comparative study, Am. Nat., 102, 243–282, 1968.

Sangiorgi, F., Bijl, P. K., Passchier, S., Salzmann, U., Schouten, S., McKay, R., Cody, R. D., Pross, J., Van De Flierdt, T., Bohaty, S. M., Levy, R., Williams, T., Escutia, C., and Brinkhuis, H.: Southern Ocean warming and Wilkes Land ice sheet retreat during the mid-Miocene, Nat. Commun., 9, 1–11, https://doi.org/10.1038/s41467-017-02609-7, 2018.

Schiebel, R., Spielhagen, R. F., Garnier, J., Hagemann, J., Howa, H., Jentzen, A., Martinez-Garcia, A., Meilland, J., Michel, E., Repschlaeger, J., Salter, I., Yamasaki, M., and Haug, G.: Modern planktic foraminifers in the high-latitude ocean, Mar. Micropaleontol., 136, 1–13, https://doi.org/10.1016/j.marmicro.2017.08.004, 2017.

Schmiedl, G., Mackensen, A., and Müller, P. J.: Recent benthic foraminifera from the eastern South Atlantic Ocean: dependence on food supply and water masses, Mar. Micropaleontol., 32, 249–287, 1997.

Schweizer, M., Pawlowski, J., Duijnstee, I. A. P., Kouwenhoven, T. J., and Van der Zwaan, G. J.: Molecular phylogeny of the foraminiferal genus *Uvigerina* based on ribosomal DNA sequences, Mar. Micropaleontol., 57, 51–67, 2005.

Scotese, C. R.: An atlas of Phanerozoic paleogeographic maps: the seas come in and the seas go out, Annu. Rev. Earth Planet. Sc., 49, 679–728, 2021.

Seidenstein, J. L., Leckie, R. M., McKay, R., De Santis, L., Harwood, D., and IODP Expedition 374 Scientists: Pliocene–Pleistocene warm-water incursions and water mass changes on the Ross Sea continental shelf (Antarctica) based on foraminifera from IODP Expedition 374, J. Micropalaeontol., 43, 211–238, https://doi.org/10.5194/jm-43-211-2024, 2024.

Shackleton, N. J. and Kennett, J. P.: Paleotemperature history of the Cenozoic and the initiation of Antarctic glaciation: oxygen and carbon isotope analyses in DSDP Sites 277, 279, and 281, Initial Reports Deep Sea Drill. Proj., 29, 743–755, 1975.

Shepherd, A., Fricker, H. A., and Farrell, S. L.: Trends and connections across the Antarctic cryosphere, Nature, 558, 223–232, 2018.

Shevenell, A. E. and Kennett, J. P.: Paleoceanographic change during the middle Miocene climate revolution: an Antarctic stable isotope perspective, Cenozoic South. Ocean Tectonics, Sedimentation, Clim. Chang. Between Aust. Antarct. Geophys. Monogr. Ser, 151, 235–252, 2004.

Shevenell, A. E., Kennett, J. P., and Lea, D. W.: Middle Miocene Southern Ocean cooling and Antarctic cryosphere expansion, Science, 305, 1766–1770, 2004.

Shevenell, A. E., Kennett, J. P., and Lea, D. W.: Middle Miocene ice sheet dynamics, deep-sea temperatures, and carbon cycling: A Southern Ocean perspective, Geochem. Geophy. Geosy., 9, Q02006, https://doi.org/10.1029/2007GC001736, 2008.

Smith, J. A., Graham, A. G. C., Post, A. L., Hillenbrand, C.-D., Bart, P. J., and Powell, R. D.: The marine geological imprint of Antarctic ice shelves, Nat. Commun., 10, 5635, https://doi.org/10.1038/s41467-019-13496-5, 2019.

Smith Jr., W. O., Sedwick, P. N., Arrigo, K. R., Ainley, D. G., and Orsi, A. H.: The Ross Sea in a sea of change, Oceanography, 25, 90–103, https://doi.org/10.5670/oceanog.2012.80, 2012.

Spezzaferri, S., Coxall, H. K., Olsson, R. K., and Hemleben, C.: Taxonomy, biostratigraphy, and phylogeny of Oligocene *Globigerina, Globigerinella*, and *Quiltyella* n. gen., in: Atlas of Oligocene Planktonic Foraminifera, edited by: Wade, B. S., Olsson, R. K., Pearson, P. N., Huber, B. T., and Berggren, W. A., Cushman Foundation Special Publication, 46, 179–214, 2018a.

Spezzaferri, S., Olsson, R. K., and Hemleben, C.: Taxonomy, biostratigraphy, and phylogeny of Oligocene to lower Miocene *Globigerinoides* and *Trilobatus*, in: Atlas of Oligocene Planktonic Foraminifera, edited by: Wade, B. S., Olsson, R. K., Pearson, P. N., Huber, B. T., and Berggren, W. A., Cushman Foundation Special Publication, 46, 269–306, 2018b.

Spindler, M. and Dieckmann, G. S.: Distribution and abundance of the planktic foraminifer *Neogloboquadrina pachyderma* in sea ice of the Weddell Sea, Antarctica, Polar Biol., 5, 185–191, 1986.

Steinhauff, D. M. and Webb, P.-N.: Miocene foraminifera from DSDP site 272, Ross Sea, Geology, 11, 578–582, 1987.

Steinthorsdottir, M., Coxall, H. K., de Boer, A. M., Huber, M., Barbolini, N., Bradshaw, C. D., Burls, N. J., Feakins, S. J., Gasson, E., Henderiks, J., Holbourn, A. E., Kiel, S., Kohn, M. J., Knorr, G., Kürschner, W. M., Lear, C. H., Liebrand, D., Lunt, D. J., Mörs, T., Pearson, P. N., Pound, M. J., Stoll, H., and Strömberg, C. A. E.: The Miocene: The Future of the Past, Paleoceanogr. Paleocl., 36, e2020PA004037, https://doi.org/10.1029/2020PA004037, 2021.

Strong, C. P. and Webb, P.-N.: Oligocene and Miocene foraminifera from CRP-2/2A, Victoria Land Basin, Antarctica, Terra Antarctica, 7, 461–472, 2000.

Strong, C. P. and Webb, P.-N.: Lower Oligocene foraminiferal fauna from CRP-3 Drillhole, Victoria Land Basin, Antarctica, Terra Antarctica, 8, 347–358, 2001.

Thompson, A. F., Stewart, A. L., Spence, P., and Heywood, K. J.: The Antarctic Slope Current in a changing climate, Rev. Geophys., 56, 741–770, 2018.

Vincent, E. and Berger, W. H.: Carbon dioxide and polar cooling in the Miocene: the Monterey hypothesis, in: The Carbon Cycle and Atmospheric CO, edited by: Sundquist, E. T. and Broeker, W. S., AGU, 455–468, 1985.

Wade, B. S., Pearson, P. N., Olsson, R. K., Fraass, A. J., Leckie, R. M., and Hemleben, C.: Taxonomy, biostratigraphy, and phylogeny of Oligocene and lower Miocene *Dentoglobigerina* and *Globoquadrina*, in: Atlas of Oligocene Planktonic Foraminifera, edited by: Wade, B. S., Olsson, R. K., Pearson, P. N., Huber, B. T., and Berggren, W. A., Cushman Foundation Special Publication, 46, 331–384, 2018.

Wang, Y., Zhou, M., Zhang, Z., and Dinniman, M. S.: Seasonal variations in Circumpolar Deep Water intrusions into the Ross Sea continental shelf, Frontiers in Marine Science, 10, 1020791, https://doi.org/10.3389/fmars.2023.1020791, 2023.

Ward, B. L. and Webb, P.-N.: Late Quaternary foraminifera from raised deposits of the Cape Royds-Cape Barne area, Ross Island, Antarctica, J. Foramin. Res., 16, 176–200, 1986.

Ward, B. L., Barrett, P. J., and Vella, P.: Distribution and ecology of benthic foraminifera in McMurdo Sound, Antarctica, Palaeo-

geogr. Palaeocl., 58, 139–153, https://doi.org/10.1016/0031-0182(87)90057-5, 1987.

Warny, S., Askin, R. A., Hannah, M. J., Mohr, B. A. R., Raine, J. I., Harwood, D. M., Florindo, F., and the SMS Science Team: Palynomorphs from a sediment core reveal a sudden remarkably warm Antarctica during the middle Miocene, Geology, 37, 955–958, https://doi.org/10.1130/G30139A.1, 2009.

Webb, P.-N.: Benthic foraminifera, in: Antarctic Cenozoic history from the CIROS-1 Drillhole, edited by: Barrett, P. J., McMurdo Sound, DSIR Bulletin, 245, 99–118, 1989.

Webb, P.-N. and Strong, C. P.: Pliocene benthic foraminifera from CRP-2 (lithostratigraphic unit 2.2), Victoria Land Basin, Antarctica, Terra Antartica, 7, 453–459, 2000.

Webb, P.-N. and Strong, C. P.: Foraminiferal biostratigraphy and palaecology in Upper Oligocene-Lower Miocene glacial marine sequences 9, 10, and 11, CRP-2/2A drill hole, Victoria Land Basin, Antarctica, Palaeogeography Palaeoclimatology, Palaeoecology, 231, 71–100, https://doi.org/10.1016/j.palaeo.2005.07.036, 2006.

Webb, P.-N., Leckie, R. M., and Ward, B. L.: Foraminifera (Late Oligocene), in: Antarctic Cenozoic history from the MSSTS-1 Drillhole, edited by: Barrett, P. J., McMurdo Sound, DSIR Bulletin, 237, 115–125, 1986.

Westgard, A., Ezat, M. M., Chalk, T. B., Chierici, M., Foster, G., and Meilland, J.: Large-scale culturing of Neogloboquadrina pachyderma, its growth in, and tolerance of, variable environmental conditions, J. Plankton Res., 45, 732–745, https://doi.org/10.1093/plankt/fbad034, 2023.

Whitworth III, T., Orsi, A. H., Kim, S.-J., Nowlin Jr., W. D., and Locarnini, R. A.: Water masses and mixing near the Antarctic Circumpolar Front, in: Ocean, Ice, and Atmosphere: Interactions at the Antarctic Continental Margin, Antarct. Res. Ser., Vol. 75, edited by: Jacobs, S. S. and Weiss, R. F., AGU, Washington, D.C., 1998.

Woehle, C., Roy, A.-S., Glock, N., Wein, T., Weissenbach, J., Rosenthiel, C., Michels, J., Schönfeld, J., and Dagan, T.: A novel eukaryotic denitrification pathway in foraminifera, Curr. Biol., 28, 2536–2543, https://doi.org/10.1016/j.cub.2018.06.027, 2018.

Woehle, C., Roy, A.-S., Glock, N., Michels, J., Wein, T., Weissenbach, J., Romero, D., Hiebenthal, C., Gorb, S. N., Schönfeld, J., and Dagan, T.: Denitrification in foraminifera has an ancient origin and is complemented by associated bacteria, P. Natl. Acad. Sci. USA, 119, e2200198119, https://doi.org/10.1073/pnas.2200198119, 2022.

Wright, J. D., Miller, K. G., and Fairbanks, R. G.: Evolution of Modern Deepwater Circulation: Evidence from the Late Miocene Southern Ocean, Paleoceanography, 6, 275–290, https://doi.org/10.1029/90PA02498, 1991.

Zachos, J. C., Shackleton, N. J., Revenaugh, J. S., Pälike, H., and Flower, B. P.: Climate response to orbital forcing across the Oligocene-Miocene boundary, Science, 292, 274–278, https://doi.org/10.1126/science.1058288, 2001.